Mechanistic Studies of the Methanol-to-olefin Process on Acidic Zeolite Catalysts by *In Situ* Solid-state NMR-UV/Vis Spectroscopy

Von der Fakultät Chemie der Universität Stuttgart
zur Erlangung der Würde eines
Doktors der Naturwissenschaften (Dr. rer. nat.)
genehmigte Abhandlung

vorgelegt von

Yijiao Jiang
aus Zhe'jiang, V.R. China

Hauptberichter: Prof. Dr. Michael Hunger
Mitberichter: Prof. Dr. Emil Roduner

Tag der mündlichen Prüfung: 05.10.2007

Institut für Technische Chemie
der Universität Stuttgart
2007

Dedicated to my parents.

Acknowledgment

I would first like to acknowledge the Graduate College “Modern Methods of Magnetic Resonance in Materials Science” for passing on to me numerous fascinating aspects of spectroscopic techniques as well as for the very instructional lectures, seminars and workshops with their unforgettable, pleasant, and very promotional atmosphere.

I would like to express my deepest gratitude to my supervisor Prof. Dr. Michael Hunger for his scientific insights and trustworthy advice during the work during the work with this thesis. Sincerest thanks are also given to Prof. Dr. Wei Wang and Dr. Aswin Verhoeven for their fruitful discussions and comments throughout my PhD study.

I am also grateful to Prof. Dr. Emil Roduner and Prof. Dr. Thomas Schleid for their readiness to be my co-examiners.

I would like to take this opportunity to express my sincere thanks to our institute leader Prof. Dr.-Ing. Jens Weitkamp for his encouragement and support of my work.

My special thanks are given to Mrs. Ute Albrecht and Mrs. Inge Blankenship who helped me a lot in all kinds of administration problems and contributed to a pleasant atmosphere in my institute and the Graduate College, respectively. I wish also to thank all the colleagues: Dr. R. Gläser, Dr. Y. Traa, Dr. T. Donauer, Dr. S. Altwasser, Dr. C. Berger, Dr. P. De Cola, Dr. S. Laha, Dr. J. Jiao, F. Demir, D. Singer, T. Schreiber, V.R.R Marthala, S. Rabl, E. Rezaei, I. Nägele, A. Stieber, B. Gehring, H. Fingerle, L. Valiente, A. Telfah, and so on, for their help and friendship during these years, without which could have made the completion of this degree more difficult.

Last but not least I would like to thank my dear husband Jun and my family for their continuous encouragement and support.

1 Abbreviations and Symbols

1.1 Abbreviations

ICP-AES	Inductively Coupled Plasma Atomic Emission Spectroscopy
ATI	Aluminiumtriisopropylate
BFW	Boiler Feed Water
CHA	Chabazite
CF	Continuous-flow
CP	Cross Polarization
CSA	Chemical Shift Anistropy
DME	Dimethyl Ether
DMA	Dimethylanthracene
DRS	Diffuse Reflectance Spectroscopy
EPR	Electron Paramagnetic Resonance
ERI	Erionite
FCC	Fluid Catalytic Cracking
FID	Free Induction Decay
FT-IR	Fourier Transform Infrared Spectroscopy
GC	Gas Chromatography
GTG	Gas-to-gasoline
HGT	Heavy Gasoline Treatment
HPDEC	High Power Decoupling
IZA	International Zeolite Association
LAB	Laboratory Frame
MAS	Magic Angle Spinning
MS	Mössbauer Spectroscopy

	Mass Spectroscopy
MTHC	Methanol-to-hydrocarbons
MTG	Methanol-to-gasoline
MTO	Methanol-to-olefin
NMR	Nuclear Magnetic Resonance
PAS	Principal Axis System
rf	Radio Frequency
RS	Raman Spectroscopy
SF	Stopped-flow
SS	Solid-state
TEAOH	Tetraethyl Ammonium Hydroxide
TGA	Thermogravimetric Analysis
TMS	Tetramethylsilane
TPAOH	Tetrapropylammonium Hydroxide
TPD	Temperature-programmed Desorption
TPRS	Temperature-programmed Reaction Spectroscopy
UV/Vis	Ultraviolet and Visible Spectroscopy
XRD	X-ray Powder Diffraction

1.2 Symbols

A	$m^{-2} \cdot g^{-1}$	Specific Surface Area
$\boldsymbol{B}$	T	Magnetic Induction
c	$mol \cdot l^{-1}$	Concentration
d	m	Diameter
e	C	Elementary Charge, (1.602176×10^{-19} C)
E	J	Energy

h	J·s	Planck Constant, (6.626068×10^{-34} J.s)
$\hat{H}$	-	Hamiltonian Operator
$\hat{I}$	-	Angular Momentum Operator
I	-	Nuclear Spin
$\boldsymbol{M}$	$A\cdot m^{-1}$	Magnetization
m	-	Magnetic Quantum Number
n_m	mol	Monolayer Capacity
p	Pa	Pressure
q	$V\cdot m^{-2}$	Field Gradient
$\boldsymbol{r}$	m	Internuclear Vector
S	-	Electronegativity
t	-	Statistical Thickness
t	s, min, h	Time
V	V	Electric Potential
α	-	Adiabacity Parameter
γ	$s^{-1}\cdot A^{-1}\cdot m$	Magnetogyric Ratio
Δ	-	Difference
δ	ppm	Chemical Shift
η	-	Asymmetry Parameter
ν	s^{-1}	Frequency
μ	$J\cdot m\cdot A^{-1}$	Magnetic Momentum
σ	-	Chemical Shielding Tensor
τ_{CP}	s	Contact Time
ω	s^{-1}	Angular Frequency

2 Zusammenfassung

Seit den ersten Veröffentlichungen zur Umsetzung von Methanol zu Kohlenwasserstoffen (methanol-to-hydrocarbons: MTHC) an sauren Zeolith-Katalysatoren durch Chang und Silvestri im Jahr 1977 wurde diese Reaktion von einer großen Zahl von Gruppen untersucht. Wegen der innerhalb der letzten zehn Jahre stark angewachsenen Nachfrage nach leichten Olefinen, wie z.B. nach Ethen und Propen, konzentrieren sich die gegenwärtigen Forschungen auf die Untersuchung des MTO-Prozesses, d.h. auf die Umwandlung von Methanol zu Olefinen (methanol-to-olefin: MTO).

Der Reaktionsweg des MTO-Prozesses wird wie folgt beschrieben: Der erste Schritt ist die Dehydratisierung des Methanols an den sauren Oberflächenzentren des Zeolith-Katalysators zu Dimethylether (DME). Das hierbei gebildete Gleichgewichtsgemisch aus Methanol, DME und Wasser wird nach einer Induktionsperiode, während der es zur Bildung der ersten Kohlenwasserstoffe kommt, in leichte Olefine umgesetzt. Diese leichten Olefine bilden im weiteren verzweigte Olefine, Aromaten und Naphthene. Es entsteht ein Kohlenwasserstoff-Pool in den Poren und Hohlräumen des Zeolith-Katalysators. Hierbei laufen Wasserstofftransfer-, Alkylierungs-, Isomerisierungs-, Polykondensations- und andere Sekundärreaktionen ab. Gegenwärtig ist allgemein anerkannt, dass unter stationären Bedingungen des MTO-Prozesses der so genannte “Kohlenwasserstoff-Pool-Mechanismus” der dominierende Reaktionsweg ist. Nach diesem Mechanismus wird das Methanol direkt an reaktiven organischen Spezies addiert, wie z.B. an Methylbenzol, zyklischen Carbeniumionen und Methylbenzeniumkationen. Danach erfolgt die Bildung leichter Olefine durch Abspaltung von Alkylgruppen von den Komponenten des o.g. Kohlenwasserstoff-Pools. In der letzten Phase des MTO-Prozesses kommt es zur Desaktivierung des arbeitenden Katalysators aufgrund der Bildung von harten Koks.

Der detaillierte Reaktionsmechanismus der ersten C-C-Verknüpfungen bei der Umsetzung von Methanol zu Kohlenwasserstoffen während der Induktionsperiode ist bisher noch nicht vollständig geklärt. Mehr als 20 verschiedene Mechanismen wurden für die ersten C-C-Verknüpfungsreaktionen in der Literatur vorgeschlagen. Einige dieser Mechanismen basieren auf der Mitwirkung reaktiver Alkoxy-Spezies, Oxoniumylide-Spezies, Carbenen, Carbokationen und freier Radikale. Festkörper-^{13}C-MAS-NMR-Untersuchungen ergaben, dass die chemische Umsetzung von Oberflächen-Methoxy-Spezies an sauren

Zeolith-Katalysatoren zur Bildung primärer Kohlenwasserstoffe führen kann. Weiterhin wurde gezeigt, dass Oberflächen-Methoxy-Spezies an der Methylierung von Aromaten beteiligt sind, die wiederum reaktive Komponenten des Kohlenwasserstoff-Pools sind. Von anderen Gruppen wurde eine Initiierung der Methanol-Umsetzung an sauren Zeolith-Katalysatores durch Verunreinigungen im Methanol-Feed vorgeschlagen.

Eine sehr neue Entwicklung ist die Kombination verschiedener spektroskopischer Methoden in einem *In-situ*-Messkopf, insbesondere von spektroskopischen Methoden, die komplementäre Informationen zu den Eigenschaften von Feststoffkatalysatoren oder zu den Mechanismen heterogen katalysierter Reaktionen liefern. Die erste Kombination der *In-situ*-MAS-NMR-Spektroskopie mit einer weiteren spektroskopischen Methode führte in den Gruppen von Hunger zur Entwicklung der *In-situ*-MAS-NMR-UV/Vis-Technik. Mit dieser neuartigen spektroskopischen Technik ist eine direkte Untersuchung der Bildung und Transformation von Komplexen an den Oberflächen von Feststoffkatalysatoren unter Gleichgewichtsbedingungen mit hoher Auflösung mittels Festkörper-NMR-Spektroskopie und, in einigen Fällen, mit einer gleichzeitigen gas-chromatographischen Analyse der Reaktionsprodukte möglich. Anderseits ist es möglich geworden, gleichzeitig Olefine mit konjugierten Doppelbindungen, Aromaten und ungesättigte Carbeniumionen mit hoher Empfindlichkeit mittels UV/Vis-Spektroskopie zu untersuchen. Diese neue Technik verknüpft die Vorteile zweier sehr unterschiedlicher spektroskopischer Methoden und eröffnet damit neue Wege zur Identifizierung und Untersuchung von reaktiven Zwischenprodukten und Koksdepositen auf den Oberflächen arbeitender Feststoffkatalysatoren.

Durch die Einführung und Entwicklung der Kombination verschiedener spektroskopischer Methoden ist es möglich geworden, offene Fragestellungen zum MTO-Prozess zu bearbeiten: (1) Einfluss von organischen Verunreinigungen im Methanol-Feed auf die Bildung von Kohlenwasserstoffen durch die chemische Umsetzung von Oberflächen-Methoxy-Spezies; (2) Reaktivität von Oberflächen-Methoxy-Spezies als Voraussetzung für ihren Beitrag zur Bildung des Kohlenwasserstoff-Pool an sauren Zeolith-Katalysatoren; (3) Zusammensetzung des Kohlenwasserstoff-Pools und des während der stationären Phase des MTO-Prozesses gebildeten Kokses; (4) Mechanismus der Desaktivierung des arbeitenden Katalysators und Natur des Kokses.

Einfluss von organischen Verunreinigungen im Methanol-Feed auf die Bildung von Kohlenwasserstoffen durch die chemische Umsetzung von Oberflächen-Methoxy-Gruppen an sauren Zeolith-Katalysatoren

Spuren von organischen Verunreinigungen sind generell in allen kommerziellen Methanol-Produkten enthalten. Um zu klären, ob diese organischen Verunreinigungen auch die Reaktion von Oberflächen-Methoxy-Spezies beeinflussen, wurde in den hier beschriebenen Experimenten die Bildung von primären Kohlenwasserstoffen an methylierten Zeolith-Katalysatoren untersucht, die mit ^{13}C-angereichertem Methanol (^{13}C-Anreicherung von 99%, chemische Verunreinigungen von ca. 1000 ppm) und mit hochreinem Methanol (nicht ^{13}C-angereichert, organische Verunreinigungen < 30 ppm) präpariert worden waren. Hierzu wurden ein Zeolith H-Y und ein Silicoalumophosphat H-SAPO-34 als Katalysatoren verwendet. Um zu überprüfen, ob die Bildung der Oberflächen-Methoxy-Spezies aus ^{13}C-angereichertem oder hochreinem, aber nicht angereichertem Methanol in gleicher Weise erfolgt, wurden die methylierten Katalysatoren mittels ^{1}H-MAS-NMR-Spektroskopie charakterisiert. Für einige Experimente wurde der dehydratisierte H-SAPO-34 mit ^{13}C-1-Ethanol bzw. ^{13}C-2-Aceton beladen und in Glasröhrchen eingeschmolzen. Diese Moleküle sind die im kommerziellen Methanol-Feed am häufigsten auftretenden Verunreinigungen. Die mit Ethanol und Aceton beladenen Proben wurden nach thermischen Behandlungen bei 473 bis 673 K für 20 Minuten unter Schutzgas in luftdichte 7 mm-MAS-NMR-UV/Vis-Rotoren umgefüllt.

Die chemische Umsetzung der Oberflächen-Methoxy-Gruppen nach thermischen Behandlungen bei 473 bis 673 K wurde mittels ^{13}C-MAS-NMR- und UV/Vis-Spektroskopie verfolgt. Es konnte festgestellt werden, dass die Bildung von primären Aromaten und Carbeniumionen an den mit ^{13}C-angereichertem oder hochreinem Methanol methylierten Zeolith-Katalysatoren bei identischen Reaktionstemperaturen und mit vergleichbaren Mengen erfolgt. Die ^{13}C-MAS-NMR-UV/Vis-Untersuchungen der mit Ethanol und Aceton beladenen H-SAPO-34-Katalysatoren zeigten, dass eine Beladung von mindestens 0.1 Molekülen pro Brücken-OH-Gruppe (SiOHAl) notwendig ist, um eine vergleichbare Menge an Aromaten und Carbeniumiumionen zu erhalten, wie bei den methylierten Proben bei gleicher Reaktionstemperatur. Diese Ethanol- und Aceton-Beladung ist jedoch mindestens zwei Größenordnungen höher als der Ethanol- und Acetonanteil in dem ^{13}C-angereicherten Methanol. Die geschilderten Experimente belegen daher, dass Verunreinigungen im Methanol

nicht für die mittels ^{13}C-MAS-NMR-UV/Vis-Spektroskopie beobachtete Bildung von primären Kohlenwasserstoffen durch Oberflächen-Methoxy-Spezies verantwortlich sind.

Reaktivität von Oberflächen-Methoxy-Spezies an sauren Zeolith-Katalysatoren

Mit Hilfe der Stopped-Flow-MAS-NMR-Technik erhält man die Möglichkeit, selektiv die Reaktivität von Oberflächen-Methoxy-Spezies zu untersuchen. Bei einer Reaktionstemperatur oberhalb von 473 K wurde beobachtet, dass Oberflächen-Methoxy-Spezies auf sauren Zeolith-Katalysatoren miteinander reagieren. Es kommt zu ersten C-C-Verknüpfungen und zur Bildung der primären Komponenten des für den MTO-Prozess wichtigen Kohlenwasserstoff-Pools.

Es wurde die ^{13}C-MAS-NMR-Spektroskopie zur Untersuchung der Reaktion von Oberflächen-Methoxy-Spezies mit Ammoniak, Alkylhaliden, Hydrochlorid, Kohlenmonoxyd, Acetonitril und Sauerstoff an sauren Zeolith-Katalysatoren eingesetzt. Nachfolgend sind die Resultate der o.g. Reaktionen zusammengefasst.

i) Oberflächen-Methoxy-Spezies reagieren mit Ammoniak bereits bei Raumtemperatur an sauren Zeolith-Katalysatoren zu Methylamin und Methylammoniumkationen. Methanol reagiert mit Ammoniak an sauren Zeolith-Katalysatoren unter gleichen Reaktionsbedingungen jedoch nicht. Die Experimente weisen darauf hin, dass die Oberflächen-Methoxy-Spezies reaktiver als Methanol bei der Amin-Methylierung wirken. Davon ausgehend ist die Amin-Methylierung mittels Methanol von der Bildung von Oberflächen-Methoxy-Spezies an sauren Katalysatoren abhängig.

ii) Die Transformation von Oberflächen-Methoxy-Spezies zu anderen Alkoxy-Spezies wird durch die Reaktion zwischen Oberflächen-Methoxy-Spezies und entsprechenden Alkylhaliden an sauren Zeolith-Katalysatoren realisiert. Damit werden neue Wege zur weiteren Untersuchung von reaktiven Zwischenprodukten, wie Oberflächen-Ethoxy-Spezies, eröffnet.

iii) Oberflächen-Methoxy-Spezies reagieren leicht mit Hydrochlorid zu Methylchlorid als ein einzigem Produkt. Diese Experimente zeigten, dass Oberflächen-Methoxy-Spezies an der Hydrochlorierung von Methanol an Festkörper-Katalysatoren beteiligt sein können.

iv) Die klassische Koch-Carboxylierung und die Ritter-Reaktion, die meistens in Lösung stattfinden, konnten auch durch die Reaktion zwischen Oberflächen-

Methoxy-Spezies und Kohlenmonoxid bzw. Acetonitril an sauren Zeolith-Katalysatoren durchgeführt werden.

v) Während der Oxidation der Oberflächen-Methoxy-Spezies mit Sauerstoff bildet sich Kohlenmonoxid und Kohlendioxid noch bevor die chemische Umsetzung der Oberflächen-Methoxy-Spezies zum Olefin einsetzt. Die geschilderten Experimente belegen daher, dass Kohlenmonoxid weder als reaktives Zwischenprodukt auftritt noch als Katalysator zum MTO-Prozess beiträgt.

Zusammensetzung und Charakterisierung des gebildeten Kokses während der stationären Phase des MTO-Prozesses

Der Rückstand (Koks), der auf dem sauren Feststoffkatalysator verbleibt, ist für die Katalysatordesaktivierung im industriellen MTO-Prozess verantwortlich. Die Untersuchung der Katalysatordesaktivierungen und -regenerationen ist ein wichtiger Schritt zur Verbesserung des Verständnisses der Reaktionsmechanismen. Im Hinblick auf die spätere industrielle Anwendung würde es vorteilhaft sein, die Untersuchungen des MTO-Prozesses an H-SAPO-34-Katalyatoren mit nicht ^{13}C-angereichertem Methanol im normalen Festbettreaktor mittels *In-situ*-UV/Vis-Spektroskpie und gleichzeitiger GC-Analyse unter realen Gleichgewichtsbedingungen durchführen zu können. Die optimale Reaktionstemperatur für die Methanol-zu-Olefin-Umsetzung betrug 673 K. Die Erhöhung der Standzeit führte zur Ausbildung von stärkeren UV/Vis-Banden zwischen 385 und 425 nm, die ein Hinweis für die Bildung von polycyclischen Aromaten sind. Andererseits hängt die Lage und Form der UV/Vis-Banden im Bereich von 385 bis 425 nm von den Mengen unterschiedlicher polycyclischer Aromaten mit kettenförmiger Topologie, wie z.B. Polymethylanthracen, ab. Mittels GC-Analyse konnte ein Anstieg der Ethen-Selektivität und eine Abnahme der Propen-Selektivität nachgewiesen werden. Dies kann als Auswirkung der Katalysatordesaktivierung gewertet werden.

Weiterhin wurde die quantitative Charakterisierung der Koksablagerungen auf dem im Festbettreaktor eingesetzten Katalysator bei Raumtemperatur mit Hilfe von verschiedenen Techniken, wie z.B. ^{13}C-MAS-NMR-Spektroskopie, CH-Elementaranalyse und TGA-Analyse, durchgeführt. Nach der erfolgten Desaktivierung wurde der Katalysator bei der TGA-Analyse reiner synthetischer Luft bis 873 K ausgesetzt. Dabei wurden die meisten katalytisch aktiven Koksablagerungen abgebaut (verbrannt), während der nur sehr geringe

Anteil von “hartem Koks” auf dem Katalysator verblieb. Die Experimente mit wechselnder Injektion von $^{13}CH_3OH$ und nicht ^{13}C-angereichertem aktiven Koksablagerungen mit Hilfe der ^{13}C-MAS-NMR-Spektroskopie stützten den Paring-Mechanismus für die Bildung von Alkylgruppen an den Polyalkylaromaten. Gleichzeitig wurden keine Unterschiede in den UV/Vis-Banden bei einem $^{13}C/^{12}C$-Wechsel gefunden.

Natur und Regeneration des Kohlenwasserstoff-Pools unter Strömungsbedingungen

Erste *In-situ*-MAS-NMR-UV/Vis-Experimente mit dem modifizierten 7 mm-Doty-MAS-NMR-Probenkopf wurden zur Untersuchung der Methanolumsetzung an H-SAPO-34 unter Strömungsbedingungen mit einer gleichzeitigen GC-Analyse der flüchtigen Reaktionsprodukte durchgeführt. Bei Reaktionstemperaturen von 573 bis 623 K traten bereits ^{13}C-MAS-NMR-Signale von polyalkylierten Aromaten bei *ca.* 18 und 125-135 ppm auf. Gleichzeitig erschienen UV/Vis-Banden bei 300 nm (Monoenylcarbeniumionen), 345 nm (Dienylcarbeniumionen) und 430 nm (Trienylcarbeniumionen). Unter diesen Bedingungen war die Ausbeute an Propen höher als die von Ethen. Eine starke UV/Vis-Bande von polycyclischen Aromaten, wie z.B. Polymethylanthracen, trat bei 673 K auf. Weiterhin wurde gezeigt, dass sich die Selektivität von Ethen erhöht, was ein Hinweis darauf ist, dass der Katalysator anfängt zu desaktivieren. Die quantitative Auswertung der *In-situ*-^{13}C-MAS-NMR-Spektren der bei 623 und 673 K eingesetzten H-SAPO-34-Katalysatoren ergab eine durchschnittliche Zahl von *ca.* 0,4 aromatischen Ringen pro Chabazite-Käfig mit 4,1 bzw. 1,1 Alkylgruppen pro aromatischen Ring. Übereinstimmend mit früheren Ergebnissen verursacht die Zunahme der durchschnittlichen Zahl von Methylgruppen pro aromatischem Ring eine höhere Ethen-Selektivität.

Nach dem Spülen der Katalysatoren mit reinem Stickstoff bei 673 K wurden 25-27 % der Polyalkylaromaten an den koksablagernden Katalysatoren abgebaut, aber die polycyclischen Aromaten verblieben auf dem Katalysator. Nach der Regeneration der gebrauchten Katalysatoren mit reiner synthetischer Luft bei 673 und 773 K wurden 90 % aller organischen Ablagerungen abgebaut. Die auf den regenerierten H-SAPO-34-Katalysatoren verbleibenden organischen Verbindungen bestanden aus einer geringen Menge von aktiven Kohlenwasserstoffen, wie z.B. Phenolderivate, Dienyl- und Trienylcarbeniumionen.

3 Abstract

Since Chang and Silvestri at Mobil Oil have discovered the conversion of methanol to hydrocarbons (MTHC) on acidic zeolite catalysts in 1977, this method, considered as one of the most promising routes for producing gasoline and chemicals, has attracted significant research attention. With increasing oil prices and consumption demands for light olefins, the methanol-to-olefin (MTO) process, one close relative of MTHC, become more significant. It has been well established that the first step of the MTO process is the dehydration of methanol to form the equilibrium mixture among methanol, dimethyl ether and water. Subsequently, this equilibrium mixture converts to light olefins, which can further react to form paraffins, aromatics, naphthenes and higher olefins by hydrogen transfer, alkylation and polycondensation.

A considerable research effort has been directed worldwide into elucidating the mechanism. There have been at least 20 distinct mechanisms proposed for the MTO process. There is a consensus that the formation of light olefins is dominated by a “hydrocarbon-pool” route in which methanol is directly added onto these reactive organic compounds, while light olefins are formed *via* an elimination from these compounds. However, the first C-C band formation and the detailed chemistry of the MTO process still remains a matter of debate. In this dissertation, with the application of different spectroscopic techniques, the following issues concerning the MTO process will be discussed: (1) Effect of organic impurities on the hydrocarbon formation via the decomposition of surface methoxy species; (2) Reactivity of surface methoxy species formed on acidic zeolites; (3) Formation and characterization of the coke compounds formed during the MTO process; (4) Nature of the hydrocarbon pool under continuous-flow conditions and the catalyst regeneration.

Effect of organic impurities on the hydrocarbon formation via the decomposition of surface methoxy species

Generally, surface methoxy species with carbenium-ion-like properties may act as the reactive intermediates formed in the induction period of the MTO process. On the other hand, it is suggested that the initiation of the MTO reaction is typically caused by organic impurities in the methanol feed. Therefore, the possible effects of traces of organic impurities in the methanol feed on the initiation of the methanol conversion by surface methoxy species on

acidic microporous catalysts were studied. For this purpose, surface methoxy species were prepared on zeolite H-Y and the silicoaluminophosphate H-SAPO-34 from ^{13}C-enriched methanol (^{13}C-enrichment of 99 %, chemical purity of 98 %+ with total organic impurities of *ca.* 1000 ppm) and highly purified non-enriched methanol (organic impurities < 30 ppm), respectively.

The conversion of these surface methoxy species upon thermal treatments at 473-673 K was investigated by the combined ^{13}C MAS NMR and UV/Vis spectroscopy. It was found that the formation of primary aromatics and carbenium ions on the methylated zeolite catalysts occurs at identical reaction temperatures from the conversion of both ^{13}C-enriched and non-enriched surface methoxy species. ^{13}C MAS NMR and UV/Vis studies of H-SAPO-34 catalyst loaded with ethanol and acetone show that the coverage of at least 0.1 molecules per bridging OH group is necessary to obtain aromatics and carbenium ions in a similar fashion to those formed by the conversion of surface methoxy species. This coverage is, however, at least two orders of magnitude higher than the ethanol and acetone content present as organic impurities in the above-mentioned methanol feed. These findings indicate that traces of organic impurities present in the methanol feed do not govern the formation of primary hydrocarbons from surface methoxy species.

Reactivity of surface methoxy species formed on acidic zeolites

Due to the complexity of the heterogeneous catalyst system under study, the experimental evidence for the existence and reactivity of surface methoxy species on acidic solid catalysts is still lacking. However, with the application of *in situ* preparation method it is possible to observe the formation of surface methoxy species in acidic zeolites, which offers a new approach to further investigations of the reactivity of surface methoxy species. For the first time, the following ^{13}C solid-state NMR evidence for the high reactivity of surface methoxy species has been obtained:

i) Surface methoxy species react readily with ammonia on acidic zeolites at room temperature, by which methylamines and methylammonium cations are formed. Methanol and ammonia do not react on acidic zeolites under the same conditions, which indicates that surface methoxy species are very reactive in methylating amines on acidic zeolites and, if involved, their formation is the rate-determining step during the methylation of amines by methanol on acidic zeolites.

ii) The transformation of surface methoxy species to other alkoxy species can be achieved by the reaction of surface methoxy species and corresponding alkyl halides on acidic zeolites, which presents the possibility for further studies of more reactive intermediates such as surface ethoxy species.

iii) Surface methoxy species react readily with hydrochloride, giving methyl chloride as the sole product, which indicates that surface methoxy species may also be involved in methanol hydrochlorination on solid catalysts.

iv) The classic Koch carbonylation reaction and Ritter reaction in solution can be performed with surface methoxy species on acidic zeolites.

v) During the oxidation of surface methoxy species in the presence of oxygen, the formation of carbon monoxide and carbon dioxide starts earlier than the onset of the decomposition of surface methoxy species. It is further proven that carbon monoxide is neither an intermediate nor a catalyst during the MTO process.

Formation and characterization of the coke compounds under steady-state conditions

Under steady-state conditions of the MTO process, the formation of large organic compounds acting as coke trapped in the cages of acidic zeolite catalysts is the most important reason of catalyst deactivation in industrial processes. Therefore, it is significant to get a better understanding of the deactivation and regeneration mechanism. From a view point of the industrial application in future, it is also instructive to study the MTO process on H-SAPO-34 using the non-enriched materials in the standard fixed-bed reactor by *in situ* UV/Vis and on-line GC under real working conditions. The reaction of methanol conversion ran at 673 K with the optimal conditions. With the increase of time-on-stream, strong UV/Vis bands occurred from 385 to 425 nm, indicating the formation of polycyclic aromatics. The different positions and shapes of UV/Vis bands observed at 385 to 425 nm may be due to different amounts of similar polycyclic aromatics with chain-like topology, such as polymethylanthracenes. The results obtained by GC analysis were showing that an increase of ethylene selectivity and a decrease of propylene selectivity took place, due to the catalyst deactivation.

In addition, the coke deposits formed on the catalyst in the fixed-bed reactor were quantitatively characterized at room temperature by various analytic methods including ^{13}C MAS NMR spectroscopy, CH element analysis and TGA analysis. After burning off the

coked catalysts by synthetic air at 873 K during the TGA analysis, there was still a small amount of hard coke, which can not be easily removed by the regeneration with synthetic air in the industrial processes. ^{13}C MAS NMR spectroscopic investigations of the $^{13}C/^{12}C$ scrambling between $^{13}CH_3OH$ and non-enriched organic deposits on used H-SAPO-34 support the paring mechanism for the growth of alkyl groups at polyalkylaromatics during the methanol conversion on this catalyst. By UV/Vis spectroscopy it could be evidenced that no change of the nature of organic deposits occurred during the $^{13}C/^{12}C$ scrambling experiments.

Nature of the hydrocarbon pool under continuous-flow conditions and the catalyst regeneration

For the first time, the novel *in situ* ^{13}C MAS NMR-UV/Vis spectroscopy was applied to study the nature of organic deposits formed during the MTO process on H-SAPO-34 under continuous-flow conditions. Simultaneously, the volatile reaction products were analyzed by on-line GC. At reaction temperatures of 573 and 623 K, the occurrence of ^{13}C MAS NMR signals of polyalkylaromatics (18, 125-135 ppm) was accompanied by increasing UV/Vis bands of monoenylic (300 nm), dienylic (345 nm), and trienylic carbenium ions (430 nm). Under these conditions, the yield of propylene was higher than that of ethylene. At 673 K, a strong UV/Vis band of polycyclic aromatics, such as polymethylanthracenes (400 nm), and a change of the product selectivity from propylene to ethylene occurred, which indicated the onset of the catalyst deactivation. Quantitative evaluation of the *in situ* ^{13}C MAS NMR spectra of the partially coked catalyst SAPO-34 at 623 and 673 K gave a mean number of *ca.* 0.4 aromatic rings per chabasite cage with 4.1 and 1.1 alkyl groups per aromatic ring, respectively. According to the former studies, the decrease of the mean number of methyl groups per aromatic ring may be the reason for the above-mentioned change of the product selectivity from propylene to ethylene.

Purging of the partially coked catalyst at 673 K with dry nitrogen led to a decrease of the number of polyalkylaromatics by 25-27 % only, but not to a decrease of the polycyclic aromatics acting as coke deposits. Regeneration of the used H-SAPO-34 catalyst by synthetic air (20 vol. % O_2) at 673 and 773 K led to a removal of up to 90 % of all organic deposits. The remaining organic compounds on the regenerated H-SAPO-34 catalysts were found to consist of a small amount of reactive compounds including phenolic species, dienylic carbenium ions and trienylic carbenium ions.

4 Objectives and Organization of this Dissertation

4.1 General Introduction and Main Objectives

Petroleum oil and natural gas together with coal continue to be important and dominant energy sources and raw materials for chemicals. Methanol is one of the convenient liquid products from these natural resources, which would also be expected to be obtained by converting hydrogen with carbon dioxide as an alternative way to the synthesis gas route in future [1]. It is generally believed that methanol is an excellent fuel on its own right and it can be also readily converted catalytically to either gasoline (methanol-to-gasoline, MTG) or light olefins mainly including ethylene and propylene (methanol-to-olefin, MTO), strongly depending on the catalysts and process operation conditions.

As is well known, microporous acidic zeolites are widely used as solid catalysts to investigate and commercially apply in the field of the methanol conversion. In particular, the silicoaluminophosphate H-SAPO-34, and zeolites H-ZSM-5 and H-Y have been attracting an enormous interest as the most promising candidates. Among these, the commercial plant of the ZSM-5 based MTG process and the SAPO-34 based MTO process were first demonstrated in New Zealand and Germany, respectively. In order to meet the increasing demand of light olefins, however, H-SAPO-34 presents its advantages that it is extremely selective towards the formation of ethylene and propylene with the flexibility of altering the ratio between these two light olefins by optimizing the reaction conditions. The acid strength of H-Y is in the middle among these three kinds of catalysts. Therefore, it also offers a suitable alternative to study the methanol conversion, which gives the possibility to control the reaction steps and capture reaction intermediates.

The intensive investigation of the methanol conversion catalysis focusing on the mechanistic aspect began immediately after its discovery. Methanol is firstly dehydrated to dimethyl ether (DME). Then the equilibrium mixture formed, consisting of methanol, DME and water, is converted to light olefins. Nowadays, there is a general consensus that the steady state of the MTO process is dominated by the “hydrocarbon-pool” route. According to this route, methanol is added onto reactive organic species, such as large olefins, methylbenzenes, and cyclic carbenium ions, while light olefins are formed via elimination from these hydrocarbon-pool compounds. However, the first C-C bond formation during the induction

period and the overall chemistry concerning the reactive organic species over acidic catalysts remain a matter of debate, which are of fundamental interest and may also be of value for the optimization of existing industrial processes and their commercialization. On the basis of gas chromatographic results, it was suggested that the initiation of the MTO reaction was typically caused by organic impurities from the methanol feed. On the other hand, with the application of *in situ* stopped-flow MAS NMR spectroscopy, the intermediate surface methoxy species were able to be observed during the induction period of methanol conversion over acidic zeolites. However, the reactivity and intermediate role of surface methoxy species are still uncertain. Furthermore, getting insight into the chemistry of coke and finding methods to retard the catalyst deactivation by coking are important economical objectives as well.

It is generally accepted that MAS NMR spectroscopy provides a great possibility for the detailed separation and assignment of signals of adsorbates on the surface of solid catalysts, while diffuse reflectance UV/Vis spectroscopy possesses the high sensitivity for the detection of all compounds absorbing radiation in the UV/Vis region, such as olefins with conjugated double bonds, aromatics, unsaturated carbenium cations and unsaturated radical cations, which are characteristic species of the reactive hydrocarbon compounds in the MTO process and are not easy to be detected by MAS NMR spectroscopy. Therefore, the recently developed *in situ* MAS NMR-UV/Vis technique under continuous-flow conditions offers a new approach for studying the detailed mechanism of the MTO process. Further, this new technique is combined with online gas chromatography for determining the volatile products escaping from the solid catalysts. Therefore, it is possible to investigate heterogeneous catalytic processes under the optimal reaction conditions by analyzing the outlet products as well as the reactive surface species by several complementary spectroscopic methods.

With the application of different techniques in this dissertation, it would be expected to clarify whether traces of organic impurities present in the methanol feed will govern the initiation of the MTO process *via* the decomposition of surface methoxy species. It is quite interesting to acquire new insight into the nature and reactivity of surface methoxy species formed during the induction period of the MTO process on acidic zeolite catalysts. Concerning the industrial application, a standard fixed-bed reactor equipped with *in situ* UV/Vis spectroscopy was employed to study the formation of hydrocarbon compounds and the role of carbenium ions under steady-state conditions of the MTO process on acidic zeolite

catalysts. In comparison with the fixed-bed reactor, the novel *in situ* MAS NMR-UV/Vis technique under continuous-flow conditions was used. The issues concerning the regeneration of coked catalysts and the behaviors of the coke deposits are also of great importance for getting fundamental knowledge for optimizing the existing industrial processes.

4.2 Organization of this Dissertation

This dissertation consists of three main parts. The first part starts with a short foreword of the main objectives and the organization of this work. It is followed by the Introduction in Chapter 5 where there are two sections: Firstly, several topics concerning the methanol-to-olefin process on acidic zeolite catalysts are reviewed; the next section in this chapter focuses on the theoretical as well as practical aspects of the employed MAS NMR technique, diffuse reflectance UV-Vis spectroscopy, and *in situ* MAS NMR-UV/Vis spectroscopy in the field of heterogeneous catalysis.

Chapter 6 in the second part describes the preparation of two acidic catalysts widely used in the MTO process in this work: Silicoaluminophosphate H-SAPO-34 and zeolite H-Y. The structure and composition were characterized by XRD, ICP-AES as well as multinuclear solid-state MAS NMR spectroscopy.

The third part is devoted to the main investigations performed within the frame of this dissertation. The sequence from Chapter 7 to Chapter 10 is ordered by the complexity of the employed techniques as well as the reaction steps of the MTO process. In Chapter 7, the formation and identification of surface methoxy species was studied by *ex situ* MAS NMR combined with *ex situ* UV/Vis spectroscopy. The effect of organic impurities in the initiation of the MTO process was clarified. After *in situ* preparation of surface methoxy species, their reactivity was investigated by *ex situ* ^{13}C MAS NMR spectroscopy as described in Chapter 8. Following the initiation of the MTO process, the issue about the formation and characterization of hydrocarbon-pool compounds formed under steady-state conditions is present in Chapter 9. These studies were performed by using *in situ* UV/Vis and *ex situ* MAS NMR spectroscopy. Finally, the novel *in situ* MAS NMR-UV/Vis technique under continuous-flow conditions was employed to determine the nature of organic deposits of the methanol conversion on working catalyst and the regeneration of the partially coked catalyst, as presented in Chapter 10.

5 Introduction

5.1 Methanol-to-olefin Process

5.1.1 Background

The petrochemical industry produces many essential products that civilization has come to use and depend on. As time progresses, however, traditional resources such as crude oil used to make these kinds of products begin to decrease in availability [2], which drives the researchers to pursue new raw materials and techniques that have the potential to replace traditional petrochemical processes and components. For instance, the most important petrochemical initial products such as light olefins ($C_2^=$-$C_4^=$) are mainly produced by steam cracking and fluid catalytic cracking (FCC) of heavy feed stocks [3, 4]. Nowadays, with the great increase of petroleum consumption, an alternative technology of producing these light olefins would prove invaluable. One newly developed process of producing light olefins is the direct conversion of methanol, which can be processed catalytically to hydrocarbons (MTHC) including gasoline (methanol-to-gasoline, MTG) or olefins (methanol-to-olefin, MTO), strongly depending on the catalysts and/or the process operation conditions [4].

One century ago, the formation of hydrocarbons from methyl alcohol has been reported over zinc halides [5, 6], supported aluminum sulfate [7], and phosphorus pentoxide [8]. In the late 1970s, Chang and Silvestri [9] described that one group at Mobil Chemical in New Jersey and another group at Mobile Oil's Central Research Laboratory in Princeton, who were working on unrelated projects, discovered by accident the formation of hydrocarbons from methanol over the synthetic zeolite ZSM-5 [10, 11]. Light olefins were formed as intermediates before polymerization occurred on the strong acid sites.

The main reaction steps of the conversion of methanol to hydrocarbon can be summarized as shown in the following equation [4]:

$$2\ CH_3OH \underset{+H_2O}{\overset{-H_2O}{\rightleftharpoons}} CH_3OCH_3 \xrightarrow{-H_2O} \text{light olefins} \longrightarrow \begin{matrix}\text{n/iso-paraffins}\\ \text{higher olefins}\\ \text{aromatics}\\ \text{naphthenes}\end{matrix} \qquad (1)$$

Methanol is made from synthesis gas (a mixture of CO and H_2), which is formed by steam reforming of natural gas or gasification of coal. Methanol is made from methane in two steps: First it is converted to CO and H_2, and this is then reacted on $Cu/ZnO/Al_2O_3$ or similar catalysts. Natural gas is first converted *via* synthesis gas into methanol [4]. The first step in Equation (1) is the dehydration of methanol to dimethyl ether (DME) and water. Subsequently, the resulting equilibrium mixture of methanol, DME, and water on an acidic solid catalyst is converted to primary light olefins, such as ethylene and propylene. In the last step of this equation, the light olefins react to paraffins, higher olefins, aromatics, and naphthenes by hydrogen transfer, alkylation and polycondensation.

5.1.2 Acidic Zeolite Catalysts

In the past decades, most of the work concerning the conversion of methanol to hydrocarbons has been done on acidic zeolite catalysts, which have become an efficient means to selectively produce desired components while minimizing the production of undesired by-products. In general, the structure of zeolites can be considered as a three dimensional network of tetrahedra connecting four valence or three valence metal ions such as Si or Al, each having four oxygen atoms as neighbors. And *vice versa*, each oxygen atom has two metal ions as nearest neighbors, as depicted in Scheme 5.1. When all the metal ions in the TO_4 tetrahedra are Si, the primary building units of the zeolite lattice are denoted as Si(4Si) or Si(0Al). Broensted acid sites (SiOHAl), so-called bridging OH groups are generated when silicon, with a formal valence of four, is substituted by aluminum with a lower valence of three (see Scheme 5.1). The excess negative lattice charge has to be compensated by positively charged ions, and the most common way is a proton, resulting in a chemically stable situation [12]. On the other hand, silanol groups (SiOH) are located on the terminal lattice of zeolite particles or at framework defects.

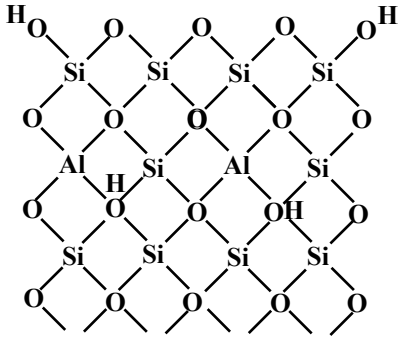

Scheme 5.1 Schematic representaion of bridging OH groups and terminal SiOH groups in an acidic zeolite.

Acidic zeolites contain Broensted acid sites, which are ideal for the conversion of methanol to hydrocarbons and have pore sizes that are on the molecular scale allowing only molecules of a specific size range to enter and exit in the catalyst cages. To some extent, the nature and extent of hydrocarbon reactions are governed by the catalyst acidity, topology, crystallite size, temperature, space velocity, and other process conditions [13].

The representative zeolite catalysts applied in the methanol conversion are summarized in Table 5.1. A brief introduction of the selected catalysts is given in the following.

Tab. 5.1 Representative zeolite catalysts applied in the MTO process.

Zeolite	Structure type	Ring size	Pore size	References
SAPO-34	CHA	8-ring	narrow pores	[13, 14]
SAPO-18	AEI	8-ring	narrow pores	[15, 16]
Erionite	ERI	10-ring	narrow pores	[17]
ZSM-5	MFI	10-ring	medium pores	[17, 18]
ZSM-11	MEL	10-ring	medium pores	[19, 20]
H-Ferrierite	FER	10-ring	medium pores	[12, 21]
Zeolite Y	FAU	12-ring	large pores	[22]

5.1.2.1 Properties of ZSM-5

In 1970s, the Mobil Oil Corporation originally disclosed the MTHC reactions over the molecular sieve called ZSM-5 (MFI topology). During the past decades, most of research groups have discussed the use of standard or modified ZSM-5 zeolites, or different isomorphous ZSM-5 by substituting Si by other metal ions rather than aluminum ions [4]. ZSM-5 has a high stability due to its high silica content, and its catalytic effectiveness is related to its unique pore structure. A stereoscopic view of the MFI framework structure is given in Fig. 5.1 [19, 23]. The following empirical formula can be used to represent the composition of ZSM-5 [23]:

$$[Na^{+}_{n}(H_2O)_{16}]\,[Al_n Si_{96-n} O_{192}], \text{ with } n < 27 \quad (2)$$

MFI type zeolites are medium pore zeolites with pore sizes in the range of 0.5 to 0.6

nm. It has a two-dimensional channel structure based on 10-membered oxygen rings. The channel intersections of H-ZSM-5 provide enough volume for cyclization reactions and intermolecular hydride transfer reactions by which a mixture of olefins can be converted into alkanes and aromatics [12, 23].

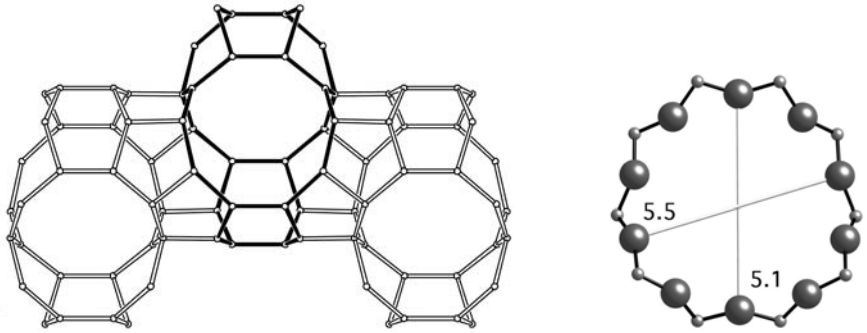

(a) (b)

Fig. 5.1 Framework of MFI-type zeolites (a) and 10-ring viewed along [010] (b) after Ref. [23].

An extensive review of the literature concerning the conversion of methanol to hydrocarbons using ZSM-5 has been published by Chang [10] and Froment *et al*. [21]. It was described that in all cases of using ZSM-5 as MTO or MTG catalysts, the formation of aromatics could not be avoided leading to a lower selectivity of light olefins, even at 100 % methanol conversion, and a rapid deactivation of the catalysts was obtained. In addition, Froment *et al*. [21] has also reviewed the effects of catalytic conditions, such as temperature, space time, partial pressure, as well as the catalyst preparation, including ion exchange method, isomorphous substitution, and n_{Si}/n_{Al} ratio of the materials have been investigated.

5.1.2.2 Properties of SAPO-34

In order to extend the catalyst life time and to improve the selectivity to light olefins, catalysts with a small pore size and lower acid strength were studied. Silicoaluminophosphates SAPO-*n* (*n* stands for different structure types) are potential catalysts for the MTO process. In a patent of Union Carbide, microporous silicoaluminophosphates were prepared as molecular sieve catalysts for the selective transformation of methanol to light-end olefins ($C_2^=$-$C_4^=$) [14, 25]. SAPO zeolites are extremely selective towards ethylene and propylene with the flexibility of altering the ratio between them by varying the reaction conditions. Consequently, SAPO zeolites are the encouraging alternatives to the use of ZSM-5 in the

MTO process.

SAPO-34 has the chabazite (CHA) structure as shown in Fig. 5.2 [23], with cages of *ca.* 1 nm in the diameter which are connected *via* 8-ring windows with a diameter of *ca.*0.38 nm. These cages form a three-dimensional network structure. Some fairly large molecules can fit in the cages of SAPO-34, but they cannot migrate from cage to cage; not even benzene can diffuse through the 8-ring windows connecting cages [26]. The acidity of this catalyst is obtained by substituting Si atoms by P atoms in the framework. The synthesis of SAPO-34 is performed using tetraethylammonium hydroxide (TEAOH) as a template, and this produces a material with *ca.* one acid site (SiOHAl) per cage. As an alternative to the conventional synthesis, it is possible to make the material with two acid sites per cage when morpholine is employed as a template [15]. In combination with a unique pore structure, this acidic solid catalyst allows selective conversion of methanol to olefins and excludes heavier products.

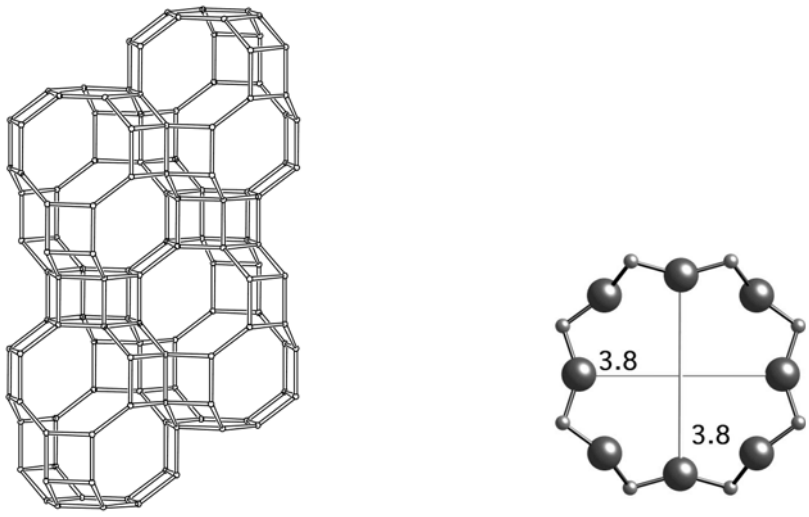

(a) **(b)**

Fig. 5.2 Framework of CHA-type zeolites (a) and 8-ring viewed along [001] (b) after Ref. [23].

5.1.2.3 Properties of Zeolite Y

Starting in the 1960s, zeolite H-Y was applied as a catalyst in the Fluid Catalytic Cracking (FCC) process because of its high intrinsic acidity, good selectivity towards gasoline compounds combined with low coke and gas formation, and good activity retention [3]. As large-pore zeolites, differently modified Y zeolites have also been used in the MTO process by Salvador *et al.* [27]. Zeolite Y belongs to the faujasite-type zeolites, as shown in Fig. 5.3

[23, 28].

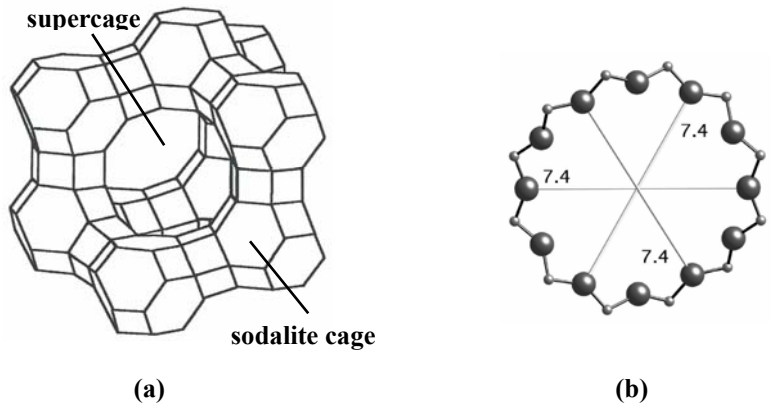

Fig. 5.3 Framework of FAU type zeolites (a) and 12-ring viewed along [111] (b) after Ref. [23].

The framework is composed of cubooctahedral sodalite cages linked together in a tetrahedral arrangement by double-6-membered rings of oxygen atoms to form large cavities, called supercages. The supercages are interconnected by 12-ring windows with a diameter of 0.74 nm consisting of 12 Si or A1 and 12 O atoms. One unit cell contains eight sodalite cages and eight supercages. The following empirical formula can be expressed to represent the composition of Na-Y zeolite with a n_{Si}/n_{Al} ratio of 2.7 [29]:

$$Na_{51.9}Al_{51.9}\,Si_{140.1}O_{384} \cdot xH_2O \qquad \text{with } x = 240 \tag{3}$$

5.1.3 Mechanisms of the MTO Process

Although the MTO or MTG process has been developed during the past three decades and it is realized on a demonstration and/or commercial scale, the extensive interest in the reaction mechanism has still been rising from both industrial and academic researchers. It is convenient to treat the overall chemistry as involving four stages as shown in Fig. 5.4, for which variable consensus have been reached in the literature [29]. First and quite clearly, there is equilibration among methanol, DME, and water. Second, there is quite often a kinetic induction period. The third and truly main step is the steady state of the reaction, leading to the formation of light olefins and subsequent secondary reactions. The fourth and final stage of the MTO process is the catalyst deactivation.

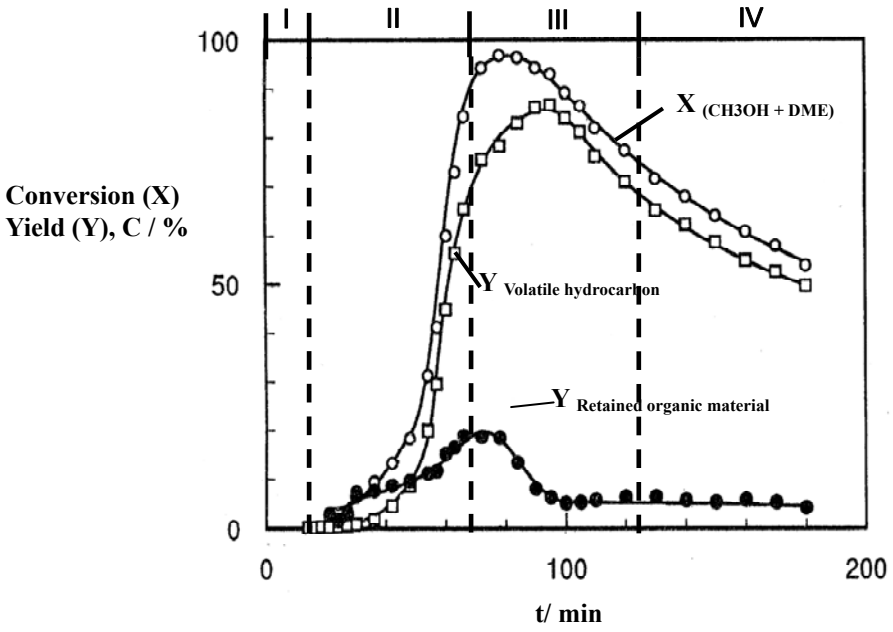

Fig. 5.4 Four reaction stages of the MTO process after Ref. [29].

5.1.3.1 Kinetic Induction Period of the MTO Process

During the past decades, there was a large debate on the initial C-C bond formation from the equilibrium mixture of methanol, DME, and water. More than 20 mechanistic proposals were suggested for this central mechanistic problem, some of which are named after the distinctive intermediates such as surface-bound alkoxy species as shown in equation (4) [30-32], oxonium ylides in equation (5) [33-35], carbenes in equation (6) [36], carbocations in equation (7) [37], or free radicals (not shown) [38]. The detailed mechanistic proposals concerning this topic were summarized in the review papers of Stoecker [4], Haw *et al*. [13] and Hutchings and Hunter [39].

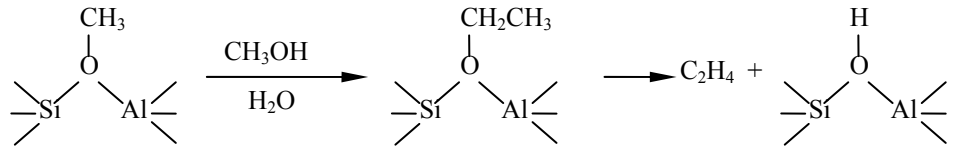

(4)

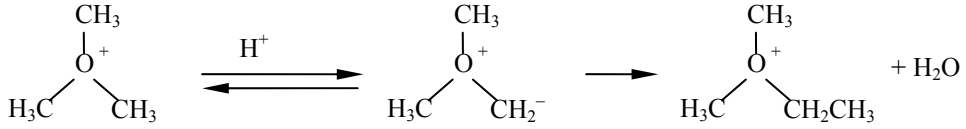

(5)

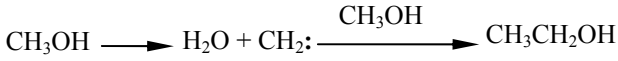

(6)

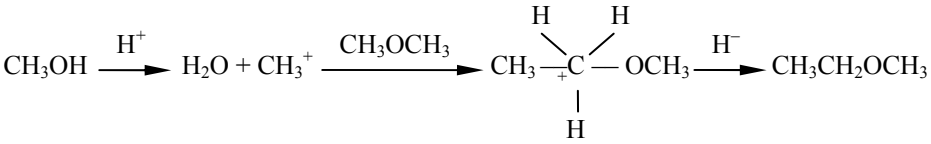

(7)

Recently, Haw and coworkers [40-41] claimed that the initiation of the MTO process is typically caused by organic impurities instead of any direct route from pure methanol and DME. A few ppms of organic impurities are sufficient for the creation of the primary hydrocarbon-pool compounds [40]. Moreover, the formation rate of the initial reaction centers and, therefore, the duration of the kinetic induction period are governed by impurities.

By Hunger and coworkers [31], with the application of MAS NMR spectroscopy, methoxy species were found to act as reactive surface species. In particular, they can form DME in the low temperature range of $T \leq 523$ K and may contribute to the formation of the initial hydrocarbons in the high temperature range of $T \geq 523$ K. The high reactivity of surface methoxy species has been demonstrated by their reactions with different reactant molecules, such as water, methanol, aniline, aromatics, and saturated hydrocarbons. During the induction period of the MTO process, the high reactivity of surface methoxy species may be responsible for the first C-C bond formations. Hence, these methoxy species may contribute to the formation of hydrocarbon-pool compounds, which play an active role under steady-state conditions of the MTO process.

A number of sophisticated techniques for experimentation have been utilized in improving the understanding of the mechanism of the initial C-C bond formation [4]. However, none of the above-mentioned direct mechanisms could have the sufficient experimental evidence to rule out each of others. Therefore, the key question of the first C-C bond formation is still a matter of debate.

5.1.3.2 The Steady-state Conditions of the MTO Process

With respect to the steady-state conditions of the MTO process, Hoelderich *et al.* [42], Dessau [43], and Kolboe and co-workers [44-46] suggested a hydrocarbon-pool mechanism to

explain the formation of light olefins as shown in Fig. 5.5 [4]. According to this proposal, reactive large carbonaceous species, such as polymethylbenzenes, large olefins, cyclic carbenium ions, and probably methylbenzenium cations, are initially formed during the induction period of the reaction. Methanol is further added onto these reactive organic species, while light olefins are formed *via* the elimination of alkyl chains from these organic centers under steady-state conditions of the reaction. The hydrocarbon-pool species were proposed to possess many characteristics of ordinary coke, which may be described by $(CH_x)_n$ with $0 < x < 2$. Recent studies [13, 47-50] have verified that the MTO process under steady-state conditions is dominated by this hydrocarbon-pool route. *In situ* MAS NMR spectroscopy under continuous-flow conditions has been also applied to shed more light on this hydrocarbon-pool route involved in the MTO process under steady-state conditions using zeolites H-ZSM-5, H-SAPO-34, and H-SAPO-18 as catalysts [31, 50].

Moreover, the formation of large organic compounds acting as coke trapped in the cages of acidic zeolite catalysts is the most important reason of catalyst deactivation in industrial processes. Therefore, finding ways to limit deactivation by coking and to regenerate coked catalysts is an important economic objective [51]. Due to the specific effects of the micropore system and catalytically active Broensted acid sites in zeolites, the investigation of hydrocarbon-pool compounds and coke deposits is obviously a severe and complex task in the field of heterogeneous catalysis [52].

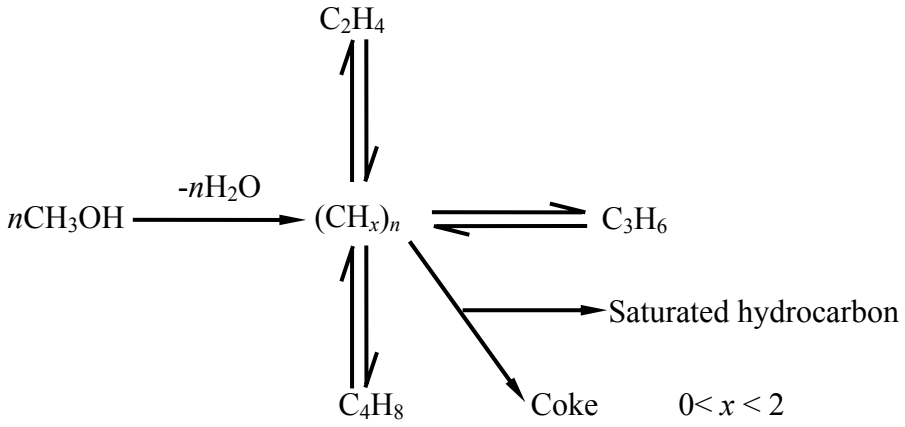

Fig. 5.5 Schematic representation of the hydrocarbon-pool mechanism after Ref. [4].

5.1.4 Industrial Processes

Upon the development of the MTG and MTO process, the next stage was the demonstration of these techniques in a commercial scale. In 1986, in response to a request from the New

Zealand government, Mobil Oil Research and Development Corporation built the first fixed-bed pilot plant with a capacity of 640 L per day (four barrels per day) (Fig. 5.6 [55]) to demonstrate the feasibility of the gas-to-gasoline (GTG) process [4, 54]. The plant mainly consisted of three process units. Methanol was formed by steam reforming of natural gas with the application of boiler feed water (BFW) treatment. The MTG reaction ran at temperatures of around 673 K and at an inlet pressure of 19-23 bar, and the fixed-bed reactor contained the ZSM-5 catalyst. Subsequently, in the heavy gasoline treatment (HGT), the following reactions took place: Disproportionation, isomerization, transalkylation, ring saturation, dealkylation, and cracking [55].

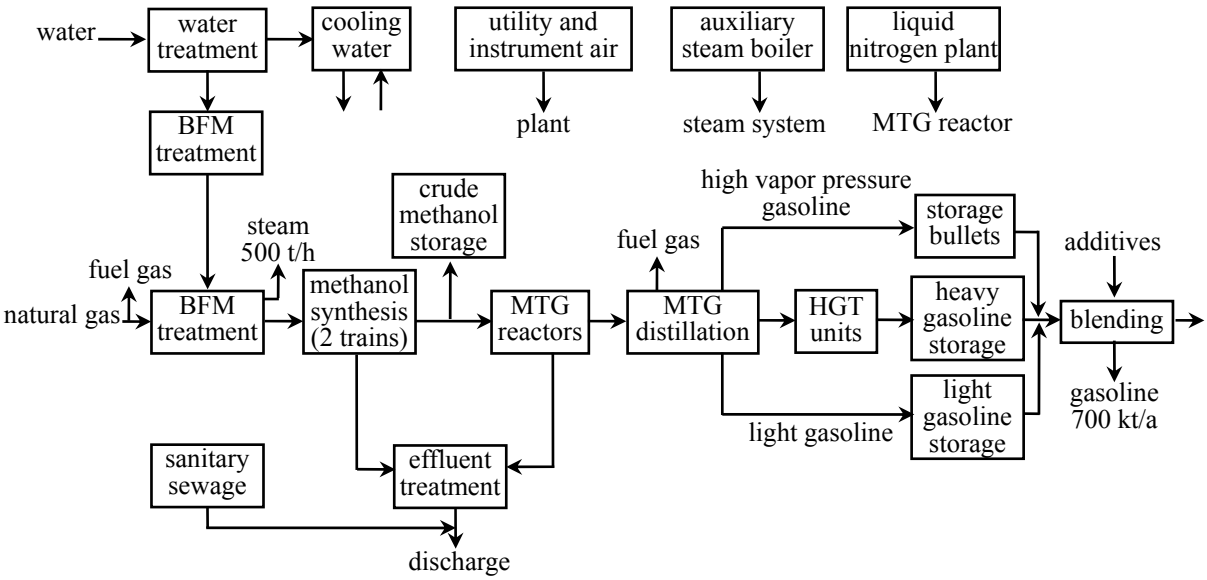

Fig. 5.6 Simplified block flow diagram of the New Zealand GTG plant after Ref. [55].

From 1982 to 1985, Mobil Oil Research and Development Corporation, Union Rheinische Braunkohlen Kraftstoff AG, and Uhde GmbH (Dortmund, Germany) jointly designed and operated a fluidized-bed MTG demonstration plant with a capacity of 15.9 m^3 gasoline per day applying ZSM-5 as catalyst. This plant was located in Wesseling (Germany) [9]. In cooperation with Norsk Hydro (Oslo, Norway), UOP (Des Plaines, Illinois) announced in 1996 that their SAPO-34 based MTO process was realized in the construction of the plant with a capacity of 250 000 t/a for production of ethylene using natural gas as a feedstock. The UOP/HYDRO MTO unit employed a fluidized-bed reactor coupled with a fluidized-bed regenerator. The heat of reaction was controlled by the steam generation. The catalyst was sent continuously to the regenerator, where the coke was burned off and steam was also generated in the regenerator to remove the exothermic heat from coke combustion [55]. The

MTO process by UOP/HYDRO has the advantage of high selectivity to ethylene because of the catalyst structure.

5.2 Solid-state NMR and UV/Vis Spectroscopy in Heterogeneous Catalysis

5.2.1 Introduction

Heterogeneous catalysis starts to play a key role for successive industrial innovations and academic insight since its discovery in 1823 [56]. Typical fields for the application of solid catalysts are petrochemical, pharmaceutical, and environmental industries [57]. Monitoring catalytic processes and elucidation of reaction mechanisms in heterogeneous catalysis are crucial for understanding the reactions of many important chemical processes and allow the optimized design of catalysts and operation conditions. The goal of this monitoring involves the observation of reaction intermediates, the discrimination between spectator species and active sites, the determination of unusual oxidation states and coordination environments of metal ions in catalyst materials as well as the migration and mobility of species on the catalyst surface [58-60].

In addition to kinetic investigations, modern *in situ* spectroscopic methods have attracted considerable interest in this field, where the Latin word *in situ* refers to the study of catalytic materials at their working place under real reaction conditions. The opposite Latin word *ex situ* corresponds to conventional spectroscopic characterization, which is done before and after reaction and does not provide sufficient insight into a working catalyst. Therefore, it is perspective to adapt *in situ* spectroscopic methods.

The most important spectroscopic methods already used *in situ* techniques to study solid catalysts, under reaction conditions, which includes Fourier transform infrared spectroscopy (FT-IR) [61-63], Raman spectroscopy (RS) [64-65], X-ray absorption spectroscopy (XAS) [66-68], solid-state nuclear magnetic resonance (SS NMR) [69-72], electronic spectroscopy in the UV/Vis region (UV/Vis) [73-75], Moessbauer spectroscopy (MS) [76], and electron paramagnetic resonance (EPR) [77-78]. Nowadays, the further development toward the combination of several complementary spectroscopic techniques in one experiment has been demonstrated its potential and attraction. In this dissertation, special attention has been devoted to the application of SS NMR and UV/Vis spectroscopy, and their combination for

in situ characterizations in the field of heterogeneous catalysis.

5.2.2 Solid-state NMR Spectroscopy

5.2.2.1 Principles of Solid-state NMR Spectroscopy

The fundamentals of nuclear magnetic resonance (NMR) spectroscopy can be referred to the literature [79-80]. This dissertation mainly focuses on the application of solid-state (SS) NMR spectroscopy. SS NMR is applicable to any nucleus that possesses a nuclear spin such as ^{1}H, ^{13}C and ^{15}N nuclei, which are suitable isotopes allowing the study of a wide variety of reactants and adsorbate complexes interesting in the field of heterogeneous catalysis. In comparison with liquids and gases, NMR signals in solid catalysts are strongly broadened by anisotropic magnetic interactions. Therefore, the high resolution of SS NMR spectra requires sophisticated experimental techniques to average all existing solid-state interactions.

The dominating interactions of a nuclear spin I that are responsible for the broadening line of SS NMR signals are described by the total Hamiltonian $\widehat{\mathbf{H}}$:

$$\widehat{\mathbf{H}} = \widehat{\mathbf{H}}_{\mathrm{II}} + \widehat{\mathbf{H}}_{\mathrm{IS}} + \widehat{\mathbf{H}}_{\mathrm{CSA}} + \widehat{\mathbf{H}}_{\mathrm{Q}} \qquad (8)$$

where $\widehat{\mathbf{H}}_{\mathrm{II}}$, $\widehat{\mathbf{H}}_{\mathrm{IS}}$, $\widehat{\mathbf{H}}_{\mathrm{CSA}}$, and $\widehat{\mathbf{H}}_{\mathrm{Q}}$ are the Hamiltonians of the homonulcear and heteronuclear magnetic dipole-dipole interaction, anisotropic chemical shift interaction, and quadrupolar interaction, respectively. The detailed expressions for these Hamiltonians are given in Ref. [81]. For nuclear spins I = ½, such as ^{13}C nuclei, which are not characterized by an electric quadrupolar moment, however, only the first three terms are needed.

5.2.2.2 Dipolar Interaction

The Hamiltonian $\widehat{\mathbf{H}}_{\mathrm{II}}$ of homonulcear interaction describes the dipolar coupling between the nuclei i and j having the same nuclear spins I [82]:

$$\widehat{\mathbf{H}}_{\mathrm{II\,homo}} = ½\,\gamma^2\hbar^2 r_{ij}^{-3}(\hat{I}_i\hat{I}_j - 3\hat{I}_{iz}\hat{I}_{jz})\,(3\cos^2\theta_{\mathrm{ij}} - 1) \qquad (9)$$

where γ is nuclear magnetogyric ratio of the interacting nuclei i and j, r_{ij} is the internuclear distance, and θ_{ij} is the angle between r_{ij} and the external magnetic field B_0 (Fig. 5.8).

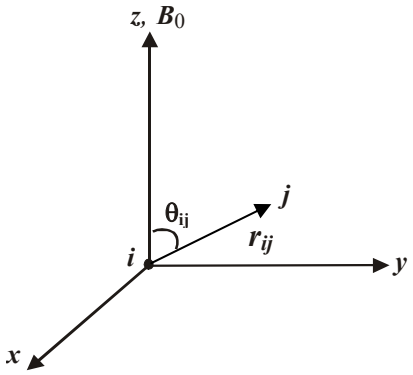

Fig. 5.8 Internuclear vector r_{ij} in the laboratory frame (x, y, z).

In the case of a dipolar interaction between nuclei with different nuclear spins I and S (heteronuclear dipolar interaction), the Hamiltonian $\hat{\mathbf{H}}_{\text{IS hetero}}$ is given by:

$$\hat{\mathbf{H}}_{\text{IS hetero}} = \tfrac{1}{2}\,\gamma_I\gamma_S\hbar^2 r_{IS}^{-3}\hat{I}_{Iz}\hat{I}_{Sz}\,(1 - 3\cos^2\theta_{\text{IS}}) \qquad (10)$$

where γ_I, γ_S are nuclear magnetogyric ratios of the nuclei I and S, r_{IS} is the internuclear distance, and θ_{IS} the angle between r_{IS} and the external magnetic field B_0.

The strong dependence of the dipolar interaction on the internuclear distance r_{ij} makes this type of interaction interesting for the investigation of the local structure in the vicinity of the resonating nuclei.

5.2.2.3 Chemical Shift Anisotropy

Another factor of NMR line broadening for solid samples is chemical shift anisotropy (CSA). In the principal axis system (PAS), the Hamiltonian of the chemical shielding interaction is given by [81]:

$$\hat{\mathbf{H}}_{\text{CSA}} = \gamma\cdot\hbar\cdot I\cdot\sigma_{\alpha\beta}\cdot B_0 \qquad (11)$$

where the shielding tensor σ can be reduced to its diagonal elements σ_{xx}, σ_{yy}, and σ_{zz} with [81]:

$$|\sigma_{zz}| \geq |\sigma_{yy}| \geq |\sigma_{xx}| \tag{12}$$

The shift of the resonance frequency in the magnetic field B_0 is due to the σ'_{zz} component in the laboratory frame (LAB). A rotational transformation with the Euler angels α and β leads to:

$$\sigma'_{zz} = \sigma_{xx} \sin^2 \beta \cos^2 \alpha + \sigma_{yy} \sin^2 \beta \sin^2 \alpha + \sigma_{zz} \cos^2 \beta \tag{13}$$

It is convenient to introduce the isotropic part σ_{iso}, the shielding anisotropy $\Delta\sigma$ and the asymmetry parameter η:

$$\sigma_{iso} = \frac{1}{3}\left(\sigma_{xx} + \sigma_{yy} + \sigma_{zz}\right) \tag{14}$$

$$\Delta\sigma = (\sigma_{zz} - \sigma_{iso}) \tag{15}$$

$$\eta = \frac{\left(\sigma_{yy} - \sigma_{xx}\right)}{\Delta\sigma} \tag{16}$$

Transformation of the Hamiltonian into the LAB leads to:

$$\hat{\mathbf{H}}_{\mathrm{CSA}} = \gamma \cdot \hbar \cdot \mathrm{I}_Z \cdot B_0 \left[\sigma_{iso} + \Delta\sigma \left(\frac{3\cos^2 \beta - 1}{2} + \frac{\eta}{2} \sin^2 \beta \cos 2\alpha \right) \right] \tag{17}$$

Corresponding to a resonance frequency ω of:

$$\omega = \omega_0 \left[\left(1 - \sigma_{iso}\right) - \Delta\sigma \left(\frac{3\cos^2 \beta - 1}{2} + \frac{\eta}{2} \sin^2 \beta \cos 2\alpha \right) \right] \tag{18}$$

5.2.2.4 Magic-Angle Spinning

Magic-angle spinning (MAS) is a procedure, which enables to average the dipolar interaction and the much weaker anisotropic chemical shift interaction. The procedure consists of a rotation (ω_{rot}) of the solid powder sample around a fixed axis in the angle of 54°44′ to the

direction of the external magnetic field B_0 (Fig. 5.9). It can be shown that rapid rotation around this macroscopic axis leads to highly resolved SS NMR spectra similar to those of liquids [86].

In the case of a fast macroscopic rotation, the term $(3\cos^2\theta_{ij}-1)$ occurring in the Hamiltonians of most of the solid-state interactions, such as the dipolar interaction (Equations (9) and (10)) and the chemical shift anisotropy (Equations (17)), can be replaced by their time average [82, 86]:

$$(3\cos^2\theta_{ij} - 1)_{\text{average}} = \tfrac{1}{2}\,(3\cos^2\theta - 1)(3\cos^2\theta'_{ij} - 1) \qquad (19)$$

where θ_{ij} is the angle between the internuclear vector r_{ij} and the direction of the external magnetic field B_0. θ is the angle between the rotation axis and B_0, and θ'_{ij} is the angle between r_{ij} and the rotation axis (Fig. 5.10). When $\theta = \theta_m = 54°44'$, the geometric terms on the right side of equations (10) and (19) become zero.

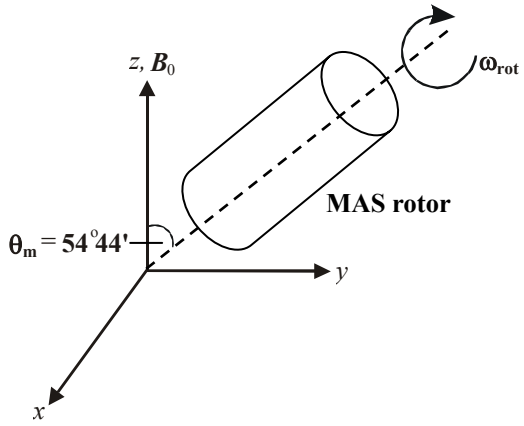

Fig. 5.9 Principle of magic-angle spinning.

In the case of the quadrupolar interaction, the term $(3\cos^2\theta-1)$ is only present in the first-order frequency distribution function [80]. Since the time average of $(3\cos^2\theta-1)$ is zero under fast magic-angle spinning, the first-order quadrupolar interaction can be removed under these conditions. In contrast, the geometric term of the second-order quadrupolar interaction causes only a scaling by a factor of *ca.* 0.3 under magic-angle spinning conditions [80].

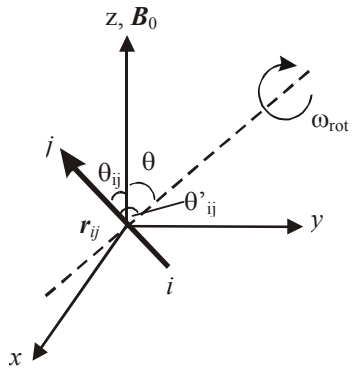

Fig. 5.10 Graphical explanation of the angles θ, θ_{ij}, and θ_{ij}'.

5.2.2.5 Cross-polarization Experiments

Cross-polarization (CP) is a typical double resonance technique, which can be applied not only in static but also magic-angle spinning NMR experiments [82] for enhancing the sensitivity of rare isotopes like ^{13}C nuclei. The principle of this technique is demonstrated in Fig. 5.11.

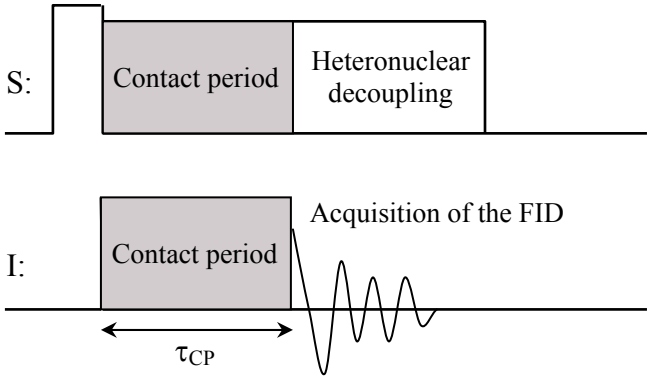

Fig. 5.11 Schematic representation of a cross-polarization experiment.

The experiment starts with a $\pi/2$-pulse applied to the *S*-spins (for example, ^{1}H). Spin polarization is transferred from the *S*-spins to the *I*-spins (*e.g.* ^{13}C nuclei) during the contact period with duration of τ_{CP} if the Equation (20) is fulfilled [87]:

$$\alpha_S \cdot \gamma_S \cdot B_{1S} = \alpha_I \cdot \gamma_I \cdot B_{1I} \tag{20}$$

The parameter α_S is equal to $[S(S+1) - m(m-1)]^{1/2}$ provided that the radio frequency (rf) pulse applied to the *S*-spins selectively induces transitions between the levels with the magnetic spin quantum numbers *m* and *m*–1. An analogous expression holds for α_I. The parameters α_S and α_I are equal to 1 for $I = S = 1/2$, and Equation (20) is then termed Hartmann-Hahn condition [88]. B_{1I} and B_{1S} denote the magnetic field amplitudes of the rf pulses applied to the *I*-spins and *S*-spins, respectively. The free induction decay (FID) can be observed for the *I*-spins after the contact period. The intensity $I_{CP}(\tau_{CP})$ of the corresponding signal is given by [89]:

$$I_{CP}(\tau_{CP}) \propto \left(1 - \frac{T_{CP}}{T_{1\rho}}\right)^{-1} \left(\exp\{-\tau_{CP}/T_{1\rho}\} - \exp\{-\tau_{CP}/T_{CP}\}\right) \tag{21}$$

$T_{1\rho}$ is the time constant for the decay of the *S*-spin magnetization under spin locking conditions. The so-called CP time constant, T_{CP}, is inversely proportional to M_2^{IS}, *i.e.*, the efficiency of the cross-polarization depends on the strength of the heteronuclear dipole interaction between the *S*-spins and *I*-spins. It has to be mentioned, furthermore, that the maximum values of $I_{CP}(\tau_{CP})$ are obtained for rigid lattices, and that $I_{CP}(\tau_{CP})$ vanishes if the nuclei exhibit rapid thermal motions [90]. High-power decoupling (HPDEC) of the *S*-spins during the acquisition of the *I*-spin FID leads to the suppression of the influence of residual heteronuclear dipolar interactions.

CP experiments lead to an enhancement of the signal intensity for the *I*-spins if the *S*-spins exhibit a higher magnetogyric ratio and/or a higher concentration than the *I*-spins. The maximum signal enhancement achievable by CP experiments amounts to:

$$\frac{I_{CP}}{I_{SP}} = \frac{\gamma_S}{\gamma_I} \cdot \frac{1}{1+\varepsilon} \tag{22}$$

with

$$\varepsilon = \frac{N_I}{N_S}\left(\frac{\alpha_I}{\alpha_S}\right)^2 \tag{23}$$

where I_{SP} denotes the intensity of the signal of the *I*-spins measured with single pulse excitation, and N_I and N_S are the numbers of *I*- and *S*-spins, respectively, in the sample.

5.2.3 Diffuse Reflectance UV/Vis Spectroscopy

5.2.3.1 Diffuse Reflectance Mode

Ultraviolet and visible spectroscopy (UV/Vis) allows the study of electronic transitions between orbitals or bands in the case of atoms, ions, and molecules in the gaseous, liquid or solid state [91]. Although spectroscopic studies in the gaseous and liquid phase and in individual crystals usually take place in transmission mode, it is very difficult to make transmission experiments for opaque solid samples. An alternative mode is the diffuse reflectance spectroscopy (DRS), which is widely used in the field of heterogeneous catalysis.

DRS is based on the reflection of light by a powdered sample, and the dimensions of the individual particles in such powdered sample are comparable to the wavelength. When the light is scattered, there are two extreme situations of reflection: Specular and diffuse reflection (Fig. 5.12) [59, 73]. In the case of specular reflection from a smooth and non-absorbing medium (see the left figure), the light beam is reflected under the same angle by the surface as that of the incoming light beam, while diffuse reflected light from a non-absorbing medium involves photons, which are scattered in all directions.

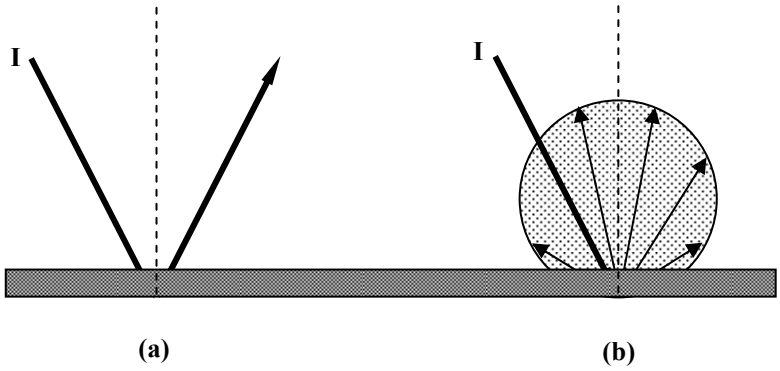

Fig. 5.12 Light scattering at smooth and non-absorbing surfaces after irradiating the particle surface with light I: Specular reflected light (a) and diffuse reflected light (b).

5.2.3.2 Schuster-Kubelka-Munk Theory

For quantitative assessment, the Schuster-Kubelka-Munk (S-K-M) theory is widely accepted and allows quantitative measurement of the absorption spectrum of a solid catalyst from DRS measurement [73]. According to the S-K-M theory, the diffuse reflectance F of a layer of infinite thickness R_∞ is related to the absorption coefficient K and the scattering coefficient S:

$$F(R_\infty) = \frac{(1 - R_\infty)^2}{2R_\infty} = \frac{K}{S} = k \cdot C \tag{24}$$

where C is the absorption center concentration. At a given wavelength, k is constant. Hence, Equation (24) gives a linear relation between F(R_∞) and the concentration C. This Equation is valid only under the following conditions:

a) diffuse monochromatic irradiation of the powdered sample,
b) isotropic light scattering,
c) infinite layer thickness,
d) low concentration of absorbing centers,
e) uniform distribution of absorbing centers,
f) absence of fluorescence.

5.2.3.3 Electronic Transitions in Organic Compounds

In general, electron transfer may take place in transition metal ions (*d-d* transitions and ligand-to-metal or metal-to-ligand charge transfer transitions), inorganic molecules and organic molecules [73]. This dissertation will only focus on the application of UV/Vis in heterogeneous catalysis, particularly for the observation of chemically excited states of hydrocarbons, such as unsaturated carbenium ions, aromatic compounds, and hydrocarbons with conjugated double bonds.

When sample molecules are exposed to light having an energy that matches a possible electronic transition within the molecules, some of the light energy will be absorbed as the electron is promoted to a higher energy orbital, and the resulting species is called an excited state species. There are various kinds of electronic excitations that may occur in organic molecules as shown in Fig. 5.13 [91]. Among these six transitions outlined, only the two lowest ones (left-most $n \rightarrow \pi^*$ and $\pi \rightarrow \pi^*$) are reached by the energies available in the spectral range of 200-800 nm spectrum. Others appear in the mid-UV (below 200 nm) region and are not detected with a standard spectrometer working in air [91].

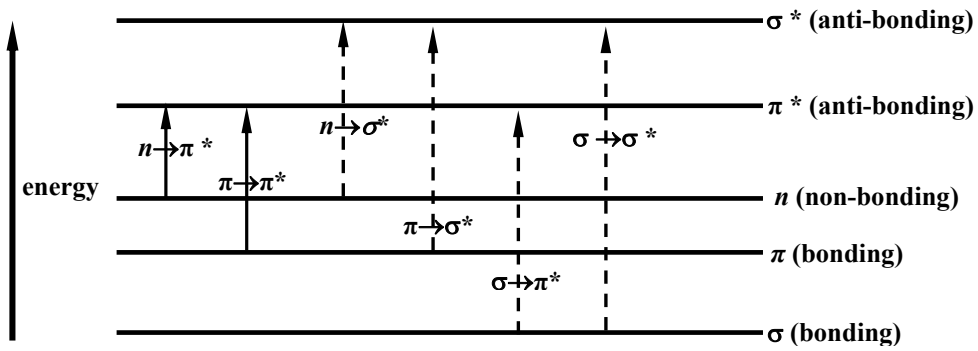

Fig. 5.13 Various types of electronic excitation occurring in organic molecules [91].

5.2.4 *In situ* MAS NMR-UV/Vis Spectroscopy

In heterogeneous catalysis, most of spectroscopic methods focus on the study of catalysts before or after the reactions. In industrial applications, however, processes are mainly performed under continuous-flow conditions, *i.e.*, with a continuous reactant feed and removal of products. A recent development is the solid-state *in situ* MAS NMR-UV/Vis spectroscopy under continuous-flow conditions, shown in Fig. 5.14 [71-72].

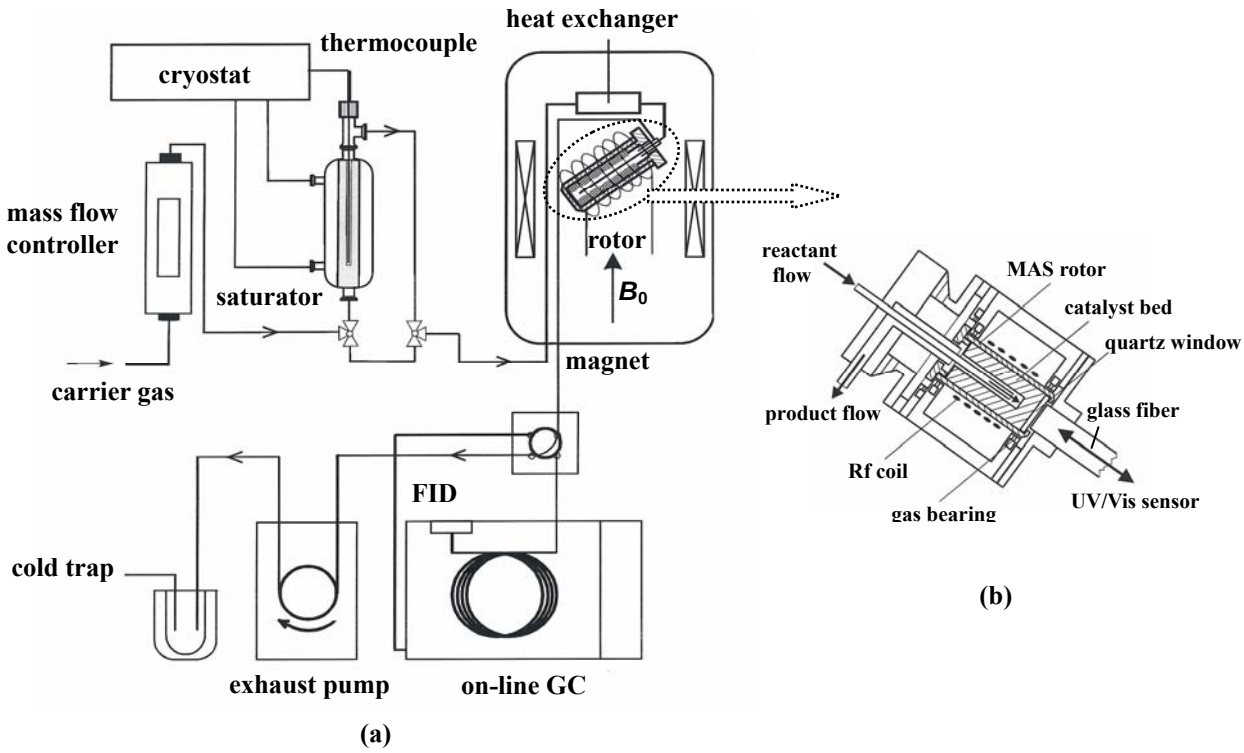

Fig. 5.14 Scheme of an *in situ* MAS NMR-UV/Vis flow probe coupled with a sampling loop and on-line GC (a) and design of a modified MAS NMR-UV/Vis rotor reactor with axially placed tubes for the injection of reactants and the exhaust of products (b).

The key part inside the magnet is the spinning MAS rotor which works as a micro-flow reactor as well, as depicted in Fig. 5.14 (b). The carrier gas, loaded with reactants in a saturator at a given temperature, is injected into the catalyst bed inside the rotor reactor *via* a glass injection tube. The catalyst bed has the shape of a hollow cylinder and rotates around the fixed injection tube with an outer diameter of 1.8 mm. The volatile reaction products escaping from the exhaust tube with an diameter of 3.0 mm can be detected *via* an on-line GC HP 5890 (Hewlett Packard) equipped with a Coating Poraplot Q capillary column (Chrompack Plot fused silica, length 50 m, inner diameter 0.32 mm). The exhaust flow containing the volatile reaction products was sampled and analyzed by on-line GC. A constant flow of methane, added to the methanol feed, was used as an internal GC standard and allowed a quantitative assessment of the reaction products. A commercial flow inducer (ISMATEC MCP 6.05) works as an exhaust pump and ensures a constant flow of the product molecules from the MAS NMR rotor reactor *via* the sampling loop to a cold trap.

6 Preparation and Characterization of Acidic Catalysts

6.1 Preparation of Acidic Catalysts

6.1.1 Preparation of H-SAPO-34

The microporous silicoaluminophosphate SAPO-34 was prepared according to the method for the synthesis of [Ni]SAPO-34, but omitting the nickel salt [92]. The preparation procedure of the hydrogel is described as follows: 55.22 g of tetraethyl ammonium hydroxide (TEAOH) solution (20 wt. %) was reduced to 31.55 g (35 wt. %) in a rotary evaporator. Under stirring and ice cooling, 15.32 g aluminiumtriisopropylate (ATI) was slowly added into the above solution, and further stirring for 1 h. Afterwards, 2.25 g of silica sol (30 wt. % VP AC 4083), 8.65 g of phosphoric acid (85 wt. %), and 7.5 g of demineralized water were successively dropped into the mixture while stirring and ice cooling. Under stirring, the system was warmed up to room temperature. Thereafter, the formed gel was transferred into a Teflon vessel of 3.0 cm inner diameter and put into an autoclave to provide the hydrothermal crystallization. It was statically placed in an oven at 473 K for 16 h. The crystals formed were washed 3-4 times with demineralized water and separated by using a centrifuge, followed by drying at 353 K for 12 h.

The residual template in the as-synthesized SAPO-34 was removed by calcination. The detailed procedure is as following: The material was heated with a heating rate of 1 K/min to 393 K in a muffle oven under flowing dry nitrogen (58 l/h). After keeping the temperature at 393 K for 4 h, the temperature was raised with 1 K/min to 873 K. Subsequently, the material was calcined in a flow of synthetic air (58 l/h, 20 vol. % O_2) for 6 h until complete removal of the template [93].

After the calcination, the SAPO-34 samples were subsequently subjected to an activation procedure. The samples were packed into the glass tubes with a diameter of *ca.* 0.5 cm, which could be connected to a vacuum line. Then the samples were heated at 393 K for 6 h. Subsequently, the temperature was increased up to the final temperature of 673 K with a rate of 1 K/min. At this temperature, the material was further dehydrated at a pressure below 10^{-2} Pa for 12 h leading to H-SAPO-34. The dehydrated H-form catalysts were sealed and kept in glass tubes until their further use.

6.1.2 Preparation of H-Y

Zeolite Na-Y with a molecular composition of $Na_{51.9}\ Al_{51.9}\ Si_{140.1}\ O_{384} \cdot xH_2O$ ($n_{Si}/n_{Al} = 2.7$) was purchased from Degussa AG, Hanau, Germany. The NH_4^+-form material of this zeolite was prepared by a fourfold ion exchange of 100 g Na-Y in a surplus of 1 M aqueous solution of NH_4NO_3, and stirred at the temperature of 353 K overnight. Subsequently, the zeolite was washed with demineralized water until no nitrate ions could be detected by nitrate ion test sticks, and then dried at room temperature. The hydrogen form of this zeolite was obtained by heating the NH_4^+-form material with a rate of 20 K/h up to 723 K in vacuum and calcination at a pressure of $p < 10^{-2}$ mbar for 12 h.

6.2 Characterization of Acidic Catalysts

6.2.1 X-Ray Powder Diffraction Analysis

X-ray powder diffraction patterns (XRD) were recorded on a Siemens D5000 diffractometer using Cu K_a radiation with a nickel filter and steps of 0.04° per 3.0 s from 5° to 50°. Before the measurement, the samples were placed on the sample holder and pressed to a flat surface. The XRD patterns of the calcined H-SAPO-34 and H-Y were collected in Fig. 6.1.

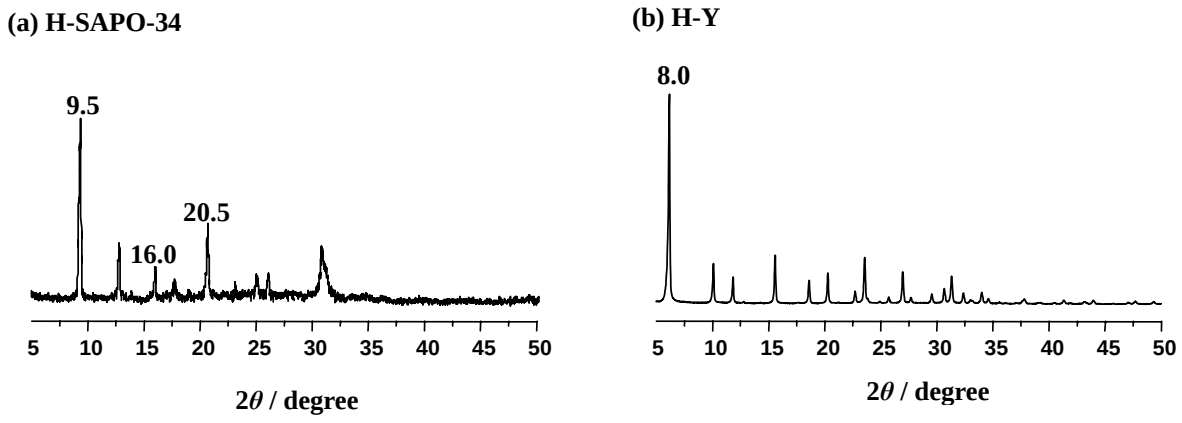

Fig. 6.1 XRD patterns of the catalysts H-SAPO-34 (a) and H-Y (b) recorded after calcination.

The left XRD pattern shows a pure crystalline phase with the CHA structure, which is identical to that of SAPO-34 reported in the literature [94], indicating that the material obtained after calcination was not collapsed. The right XRD pattern of zeolite Y indicates

highly crystallized material without impurities. The characteristic peaks show a typical FAU structure [23].

6.2.2 Elemental and Thermogravimetric Analysis

The main elements involving Na, Si, Al, and P were determined by Inductively Coupled Plasma-Atomic Emission Spectroscopy (ICP-AES). Thermogravimetric analyses (TGA) were performed in the temperature range of 298-873 K using SETARAM Setsys 16/18 equipment. The chemical compositions of zeolites H-SAPO-34 and H-Y are given in Tab. 6.1.

Tab. 6.1 Chemical compositions of zeolites H-SAPO-34 and H-Y as determined by ICP-AES.

	n_{Na} mmol/g	n_{Al} mmol/g	n_{Si} mmol/g	n_P mmol/g	$n_{Si}/n_{Al}+ n_p+ n_{Si}$	n_{Si}/n_{Al}	Ion exchange degree (%)
SAPO-34	-	8.13	1.60	6.34	0.10	-	-
Zeolite Y	0.31	3.14	8.62	-	-	2.75	90.0

6.2.3 Multinuclear Solid-state MAS NMR Spectroscopy

6.2.3.1 ^{1}H MAS NMR Experiments

The samples used for ^{1}H MAS NMR studies were dehydrated according to the procedure described in Chapter 6.1. The dehydrated samples sealed in a glass tube were opened in a glove box without contact to air. ^{1}H MAS NMR spectra were measured at room temperature using a Bruker MSL 400 spectrometer at a resonance frequency of 400.1 MHz with a single $\pi/2$ pulse excitation. The ^{1}H spin-counting was carried out with a repetition time of 10 s and a spinning frequency for the 4 mm MAS rotor of 8.0-8.5 kHz. Quantitative ^{1}H MAS NMR measurements were performed by a comparison of the signal intensities with that of an external intensity standard. The external standard consisted of dehydrated zeolite HNa-Y (ion exchange degree of 35 %) with 1.776 mmol protons per gram and a weight of 58.5 mg. All ^{1}H MAS NMR spectra were referenced to tetramethylsilane (TMS). The decomposition and simulation of NMR spectra were performed using the Bruker software WINNMR and

WINFIT.

6.2.3.1.1 ^{1}H MAS NMR Spectroscopy of H-SAPO-34

The ^{1}H MAS NMR spectrum of the activated H-SAPO-34 in Fig. 6.2 consists of a signal of bridging OH groups (SiOHAl) at 3.8 ppm and a weak high-field shoulder caused by a small number of SiOH groups at 1.8 ppm [95]. The contents of SiOHAl groups and SiOH groups are 97.4 % and 2.6 %, respectively. The concentration of SiOHAl groups of 1.44 mmol/g determined by their ^{1}H MAS NMR intensity agrees well with the number of silicon atoms of 1.6 mmol/g (Table 6.1). This indicates that nearly each silicon atom incorporated into the framework of H-SAPO-34 causes one bridging OH group.

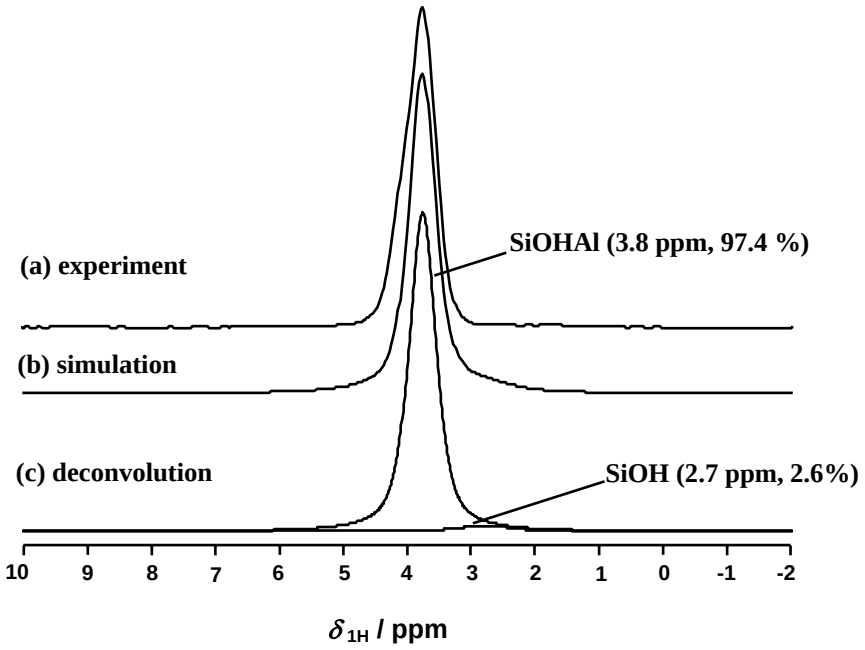

Fig. 6.2 ^{1}H MAS NMR spectrum of zeolite H-SAPO-34 activated at 673 K: (a) experiment, (b) simulation, and (c) deconvolution.

6.2.3.1.2 ^{1}H MAS NMR Spectroscopy of Zeolite H-Y

Fig. 6.3 shows the ^{1}H MAS NMR spectrum of zeolite H-Y, which was recorded after the dehydration and deammoniation of the NH_4^+-form zeolite Y at 723 K. This spectrum consists of silanol groups at 1.8 ppm, bridging OH groups in supercages at 3.8 ppm, and SiOHAl groups in sodalite cages at 4.8 ppm [86]. A quantitative evaluation using an external intensity standard indicates that *ca.* 51.4 % of protons of H-Y present as SiOHAl groups in supercages,

and 48.2 % are assigned to SiOHAl groups in sodalite cages. There is a quite low content of SiOH groups, which are located on the outer surface of zeolite particles or at framework defects. The concentration of SiOHAl groups of 1.72 mmol/g, as determined by the quantitative evaluation of ^{1}H MAS NMR spectrum in comparison with an external intensity standard, is slightly higher than that of H-SAPO-34.

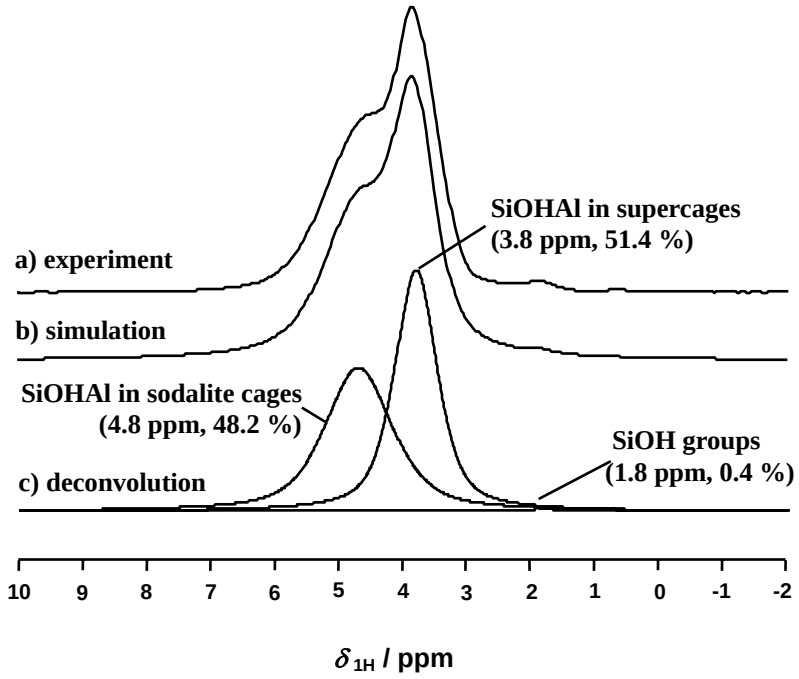

Fig. 6.3 Deconvolution of the ^{1}H MAS NMR spectrum of zeolite H-Y activated at 723 K: (a) experiment, (b) simulation and (c) deconvolution.

6.2.3.2 ^{27}Al MAS NMR Investigations

^{27}Al MAS NMR measurements were performed on a Bruker MSL 400 spectrometer at a resonance frequency of 104.2 MHz. Before the measurements, the samples were hydrated in a desiccator containing a saturated aqueous solution of sodium chloride. As argued by Klinowski *et al.* [96], three conditions must be satisfied for quantitatively reliable ^{27}Al MAS NMR measurements: (i) Complete hydration of the samples, (ii) a short excitation pulse, and (iii) a sample spinning frequency which is larger than the static line broadening. In the present studies, a $\pi/18$ pulse excitation, a repetition time of 0.5 s, and a spinning frequency of 8.0-8.5 kHz were used. The ^{27}Al MAS NMR shifts were referenced to a 0.5 M aqueous solution of aluminum nitrate.

The ^{27}Al MAS NMR spectra of H-SAPO-34 recorded in the as-synthesized state and

after calcination are shown in Fig. 6.4. The spectra consist of up to three signals at 31 to 41 ppm due to tetrahedrally coordinated framework aluminum atoms, at 6 to 13 ppm caused by a small number of pentacoordinated aluminum atoms, and at –13 to –11 ppm explained by octahedrally coordinated aluminum atoms partially coordinated to water molecules [97]. Fig. 6.5 shows ^{27}Al MAS NMR spectra of hydrated NH_4^+-form zeolites Y. The chemical shift of the tetrahedrally coordinated framework aluminum atoms is *ca.* 60 ppm. There is no signal of extra-framework aluminum appearing at about 0 ppm. These results indicate that the prepared materials were not dealuminated.

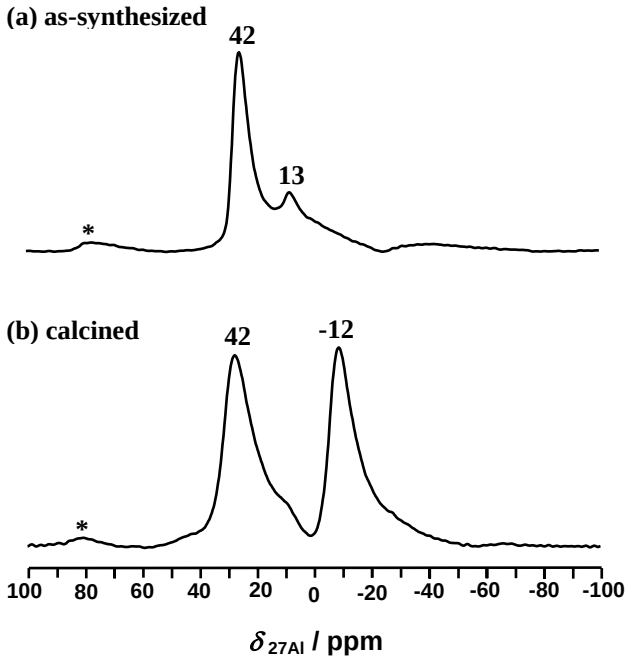

Fig. 6.4 ^{27}Al MAS NMR spectra of SAPO-34 recorded in the as-synthesized state (a) and after calcination (b).

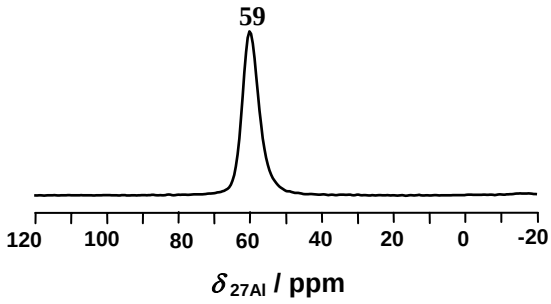

Fig. 6.5 ^{27}Al MAS NMR spectra of the hydrated NH_4^+-form zeolite Y.

6.2.3.3 ^{29}Si MAS NMR Investigations

^{29}Si MAS NMR measurements were performed on a Bruker MSL 400 spectrometer at a

resonance frequency of 79.5 MHz using a 7 mm rotor with a rotation frequency of 3.5 kHz. Before the measurements, the samples were hydrated in a desiccator containing saturated aqueous solution of sodium chloride. A single π/2 pulse excitation and a repetition time of 30 s were used. All ^{29}Si MAS NMR shifts were referenced to TMS. The deconvolution of NMR spectra was performed using the Bruker software WINNMR.

The ^{29}Si MAS NMR spectra of SAPO-34 and NH_4^+-form zeolite Y after calcination are shown in Fig. 6.6. For SAPO-34, the spectrum consists of a single signal at –92 to –89 ppm due to tetrahedrally coordinated framework silicon atoms with four aluminum atoms in the next nearest coordination sphere of T-atoms ($Si(OAl)_4$) [86, 93]. The signals in the spectrum of NH_4^+-form zeolite Y occurred at -105, -101, -95, and -91 ppm, which are ascribed to Si(0Al), Si(1Al), Si(2Al), and Si(3Al) silicon species, respectively. Here, the numbers of 0, 1, 2, 3 correspond to the numbers of aluminum atoms in the second coordination sphere [86].

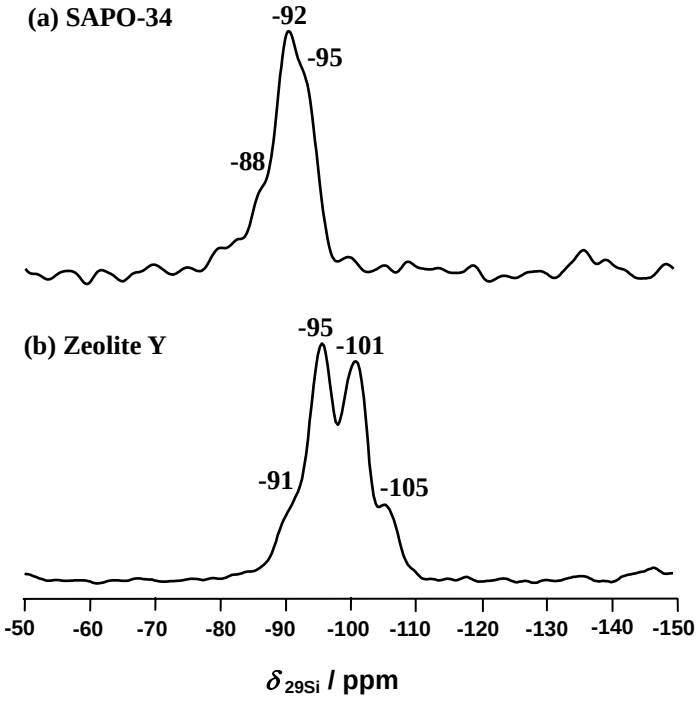

Fig. 6.6 ^{29}Si MAS NMR spectra of SAPO-34 (a) and NH_4^+-form zeolites Y (b) recorded before calcination.

6.2.3.4 ^{31}P MAS NMR Investigations

^{31}P MAS NMR measurements were performed on a Bruker MSL 400 spectrometer at a resonance frequency of 161.98 MHz with a single π/2 pulse excitation. The ^{31}P spin-counting

was carried out with a repetition time of 30 s and a spinning frequency for the 4 mm MAS rotor of 8.0 kHz. All ^{31}P MAS NMR shifts were referenced to H_3PO_4, 85%.

The ^{31}P MAS NMR spectra of SAPO-34 in Fig. 6.7 are dominated by signals at –28 to –26 ppm due to tetrahedrally coordinated phosphorus atoms in the aluminophosphate regions of the framework [93]. Phosphorus atoms coordinated to water molecules were not detected. This indicates that the silicoaluminophosphate framework of SAPO-34 was not damaged after calcination.

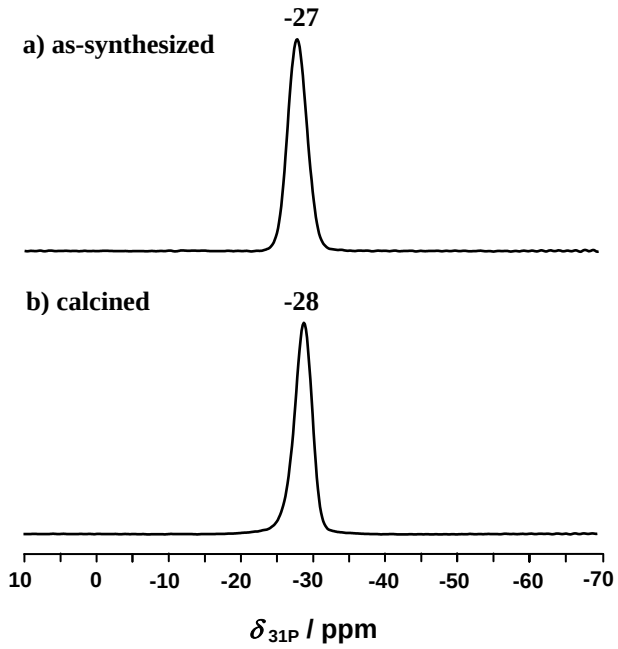

Fig. 6.7 ^{31}P MAS NMR spectra of SAPO-34 recorded in the as-synthesized state (a) and after calcination (b).

7 Effect of Organic Impurities on the Hydrocarbon Formation *via* the Decomposition of Surface Methoxy Species on Acidic Zeolite Catalysts

7.1 Introduction

The preparation and identification of alkoxy species on the surface of solid catalysts is of substantial significance in the context of heterogeneously catalyzed reactions, particularly such as the conversion of methanol to olefins. With the application of ^{13}C MAS NMR spectroscopy, there are several groups having confirmed the formation of surface methoxy species on zeolite catalysts under batch conditions with externally prepared samples [98-100]. Bosacek *et al.* [101-103] suggested that the behavior of surface methoxy species on zeolites can be explained by the equalized electronegativity of the oxygen. According to the explanation, the polarity of surface methoxy species increases with increasing electronegativity of the lattice oxygen, and with decreasing absolute value of the oxygen negative charge [101]. The stopped-flow ^{13}C MAS NMR results [30] demonstrated the role of surface methoxy species in the first stage of methanol conversion on the surface of acidic zeolites H-Y and H-ZSM-5. In agreement with earlier catalytic and spectroscopic studies [4, 39, 104], recent ^{13}C MAS NMR investigations indicated that the decomposition of surface methoxy species results in the formation of primary hydrocarbons on acidic zeolite catalysts [31]. Furthermore, it was demonstrated that surface methoxy species can contribute to the methylation of aromatics, acting as compounds of the reactive hydrocarbon-pool in the MTO process [31]. Theoretical calculations have recently been performed in an attempt to improve the understanding of the reaction mechanisms in the MTO process [104-107].

On the other hand, it has been suggested that an initiation of the methanol conversion towards hydrocarbons on acidic zeolite catalysts might be affected by co-feeding impurities in the methanol feed [108]. On the basis of GC experiments, Haw and coworkers [40] lent further support to this suggestion by claiming that the initiation of the MTO process is typically caused by organic impurities instead of any direct route from pure methanol and DME.

Traces of organic impurities are, in general, present in the commercial methanol [109]. To clarify, whether they exclusively govern the conversion of surface methoxy species, the present work compares the formation of primary hydrocarbons on the methylated zeolite

catalysts prepared from the ^{13}C-enriched methanol (^{13}C-enrichment of 99%, chemical purity of 98%+ with total organic impurities of *ca.* 1000 ppm) and from the highly purified non-enriched methanol (organic impurities < 30 ppm) on zeolite H-Y and H-SAPO-34.

In recent years, a number of combined spectroscopic methods were developed to investigate heterogeneously catalyzed reaction systems simultaneously with different techniques [72, 110-112]. In the present work, the recently introduced MAS NMR-UV/Vis spectroscopy [72] was used to study the initiation stage of the methanol conversion on acidic zeolite catalysts *via* the surface methoxy species route. ^{13}C MAS NMR spectroscopy is a suitable tool to observe the formation of surface methoxy species and their conversion in a general manner although with limited sensitivity for some of the reaction products, while UV/Vis spectroscopy detects the formation of primary aromatics and unsaturated carbenium ions with high sensitivity. This advantage of the combined MAS NMR-UV/Vis spectroscopy was utilized to clarify, whether traces of organic impurities present in the ^{13}C-enriched methanol govern the formation of primary hydrocarbons by conversion of surface methoxy species on zeolite catalysts.

7.2 Experimental Part

7.2.1 Sample Preparation

The preparation of calcined and dehydrated zeolite H-Y and silicoaluminophosphate H-SAPO-34 was described in Chapter 6. The zeolite catalysts were characterized by ICP- AES, XRD, and ^{1}H, ^{27}Al, and ^{29}Si MAS NMR spectroscopy, indicating that the materials obtained after ion exchange and calcination was neither damaged nor dealuminated.

The preparation of ^{13}C-enriched surface methoxy species was performed by adsorption of the ^{13}C-enriched methanol (^{13}C-enrichment of 99 %, chemical purity of 98+ %, purchased from Cambridge Isotope Laboratories, Inc.). In addition, methanol with a natural abundance of ^{13}C-isotopes (chemical purity ≥ 99.9 %, purchased from Sigma-Aldrich), further purified by fractional distillation, was used (denoted as $^{12}CH_3OH$). GC/MS analysis showed that ^{13}C-enriched methanol contains *ca.* 1000 ppm of organic impurities (mainly ^{13}C-enriched ethanol). The highly purified $^{12}CH_3OH$ contained less than 30 ppm of organic impurities (mainly acetone and ethanol). ^{13}C-1-ethanol (^{13}C-1-enrichment of 99 %, purchased from

ISOTEC) and ^{13}C-2-acetone (^{13}C-2-enrichment of 99 %, purchased from Cambridge Isotope Laboratories, Inc.) were used as model compounds of typical impurities.

7.2.2 ^{13}C MAS NMR and UV/Vis Investigations

To ensure the identical preparation procedures for ^{13}C-enriched and highly purified non-enriched surface methoxy species, the preparation of surface methoxy species on the acidic catalysts H-Y and H-SAPO-34 was performed *via* a vacuum line. The calcined and dehydrated catalysts (300 mg) filled in a glass tube (outer diameter of *ca.* 6 mm and length of *ca.* 180 mm) were subjected to methanol at a pressure of 7.5 mbar and at a temperature of 393 K for 30 min. Thereafter, an evacuation for 6 h at 393 K and additional evacuation for 6 h at 473 K were performed. Subsequently, the methylated catalysts were sealed for further thermal treatment at a given temperature between 473 and 673 K for 20 min.

In some experiments, 300 mg of dehydrated H-SAPO-34 were loaded with ^{13}C-1-ethanol or ^{13}C-2-acetone and fused in a glass tube. After heating at a given temperature between 473 and 673 K for 20 min, the glass tube was opened in a glove box and the catalysts were transferred into a 7 mm MAS NMR-UV/Vis rotor.

The ^{13}C MAS NMR investigations were performed with a modified 7 mm Bruker MAS NMR probe on a Bruker MSL 400 spectrometer at a resonance frequency of 100.6 MHz. The HPDEC MAS NMR spectra were recorded after an excitation with a $\pi/2$ pulse and with a repetition time of 5 s. CP MAS NMR spectra were obtained with a contact time of 5 ms and with a repetition time of 2 s. The sample spinning rate of *ca.* 3.5 kHz was applied. Using an external intensity standard (dehydrated zeolite H–Y loaded with $^{13}CH_3OH$), a ^{13}C spin-counting with a repetition time of 30 s was performed. The ^{1}H MAS NMR investigations were performed with a 4 mm Bruker MAS NMR probe on a Bruker MSL 400 spectrometer at a resonance frequency of 400.1 MHz. The sample spinning rate of *ca.* 8.0 kHz was applied. The ^{1}H spin-counting was carried out with a repetition time of 10 s applying dehydrated zeolite HNa-Y with an exchange degree of 35 % as an external intensity standard. All the ^{1}H and ^{13}C MAS NMR spectra were referenced to TMS. The decomposition and simulation of NMR spectra were performed using the Bruker software WINNMR and WINFIT.

UV/Vis spectra were recorded with an AvaSpec-2048 Fiber Optic spectrometer, an

AvaLight-DH-S deuterium light source, and a glass fiber reflection probe FCR-7UV20-3-SR-S1 by Avantes. The dehydrated and unloaded zeolites H-Y and H-SAPO-34 were used as reference standards for the UV/Vis measurements.

7.3 Results and Discussion

7.3.1 ^{1}H MAS NMR Investigation of the Identical Formation of Surface Methoxy Species by ^{13}C -enriched and Non-enriched Methanol

The identical formation of surface methoxy species from ^{13}C-enriched and highly purified non-enriched methanol was clarified by ^{1}H MAS NMR measurements. Fig. 7.1a shows the ^{1}H MAS NMR spectrum of zeolite H-Y, which was used as the parent sample for the preparation of surface methoxy species. The signals at 4.8 and 3.8 ppm are due to bridging OH groups in sodalite cages and super cages, respectively [95]. After methylation of zeolite H-Y by ^{13}C-enriched methanol (denoted as $^{13}CH_3$-Y) and by highly purified non-enriched methanol (denoted as $^{12}CH_3$-Y), the ^{1}H MAS NMR spectra shown in Figs. 7.1b and 7.1c, respectively, were recorded. The chemical shift of the dominating signals at 3.8 to 4.0 ppm is consistent with the resonance position reported for the methyl protons of surface methoxy species formed on zeolite catalysts [113].

In Figs. 7.1d to 7.1f, the ^{1}H MAS NMR spectra of the silicoaluminophosphates H-SAPO-34, $^{13}CH_3$-SAPO-34, and $^{12}CH_3$-SAPO-34 are shown. The signal at 3.8 ppm in Fig. 7.1d is due to bridging OH groups of the parent H-SAPO-34. Upon methylation of this catalyst by ^{13}C-enriched methanol and highly purified non-enriched methanol, signals of methoxy species occurred at 3.8 to 4.1 ppm (Figs. 7.1e and 7.1f).

For the quantitative evaluation, the total intensities of the ^{1}H MAS NMR spectra of parent H-Y and H-SAPO-34 were set to I = 100. The total intensities obtained for $^{13}CH_3$-Y in Fig. 7.1b (I = 180) and $^{12}CH_3$-Y in Fig. 7.1c (I = 184) are very close. The close intensities were also found for $^{13}CH_3$-SAPO-34 in Fig. 7.1e (I = 222) and $^{12}CH_3$-SAPO-34 in Fig. 7.1f (I = 216). Hence, the formation of surface methoxy species from ^{13}C-enriched methanol and highly purified non-enriched methanol on the above-mentioned materials occurred in an identical manner. The coverage of surface methoxy species calculated from the increase of the total intensities are 0.40 (Fig. 7.1b) and 0.42 (Fig. 7.1c) for $^{13}CH_3$-Y and $^{12}CH_3$-Y,

respectively, and 0.61 (Fig. 7.1e) and 0.58 (Fig. 7.1f) for $^{13}CH_3$-SAPO-34 and $^{12}CH_3$-SAPO-34, respectively.

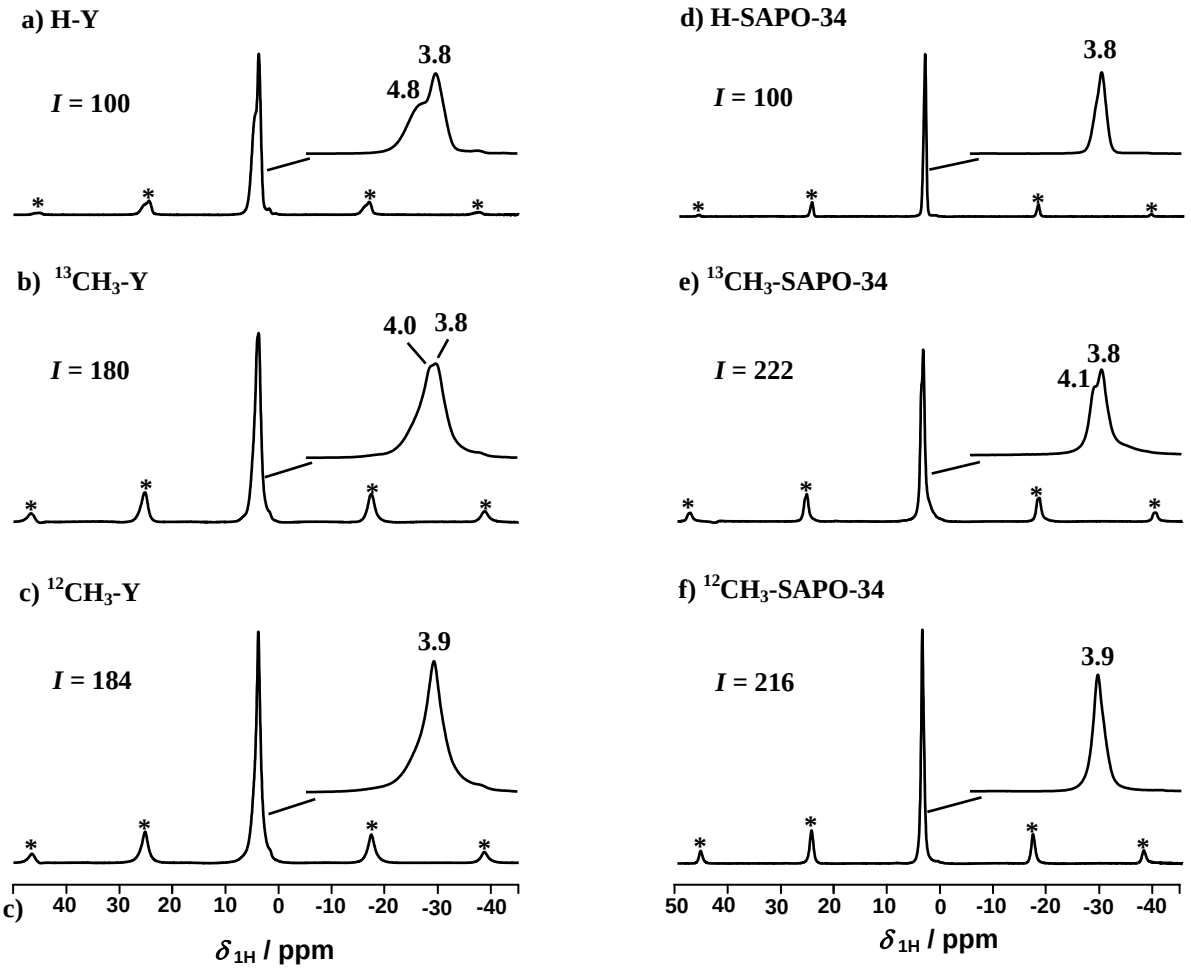

Fig. 7.1 ^{1}H MAS NMR spectra of acidic zeolite H-Y (a), ^{13}C-enriched methylated zeolite Y ($^{13}CH_3$-Y) (b), non-enriched methylated zeolite Y ($^{12}CH_3$-Y) (c), H-SAPO-34 (d), ^{13}C-enriched methylated SAPO-34 ($^{13}CH_3$-SAPO-34) (e), and non-enriched methylated SAPO-34 ($^{12}CH_3$-SAPO-34) (f). The asterisks denote the spinning sidebands.

The splitting of the ^{1}H MAS NMR signals of zeolites $^{13}CH_3$-Y (Fig. 7.1b) and $^{13}CH_3$-SAPO-34 (Fig. 7.1e) is due to $J_{1H\text{-}13C}$ couplings. As shown in Fig. 7.2, this splitting is diminished when the ^{1}H MAS NMR spectra of zeolites $^{13}CH_3$-Y and $^{13}CH_3$-SAPO-34 were recorded with ^{13}C-decoupling. This is additional evidence for the assignment of the ^{1}H MAS NMR signals at 3.9 ppm. The deconvolution of the ^{1}H MAS NMR spectra in Fig. 7.3 gives $J_{1H\text{-}13C}$ coupling constants of 220 (Fig. 7.3b) and 180 Hz (Fig. 7.3e) for zeolites $^{13}CH_3$-Y and $^{13}CH_3$-SAPO-34, respectively. In contrast to $^{13}CH_3$-SAPO-34 (Fig. 7.3e), obviously, the high concentration of methoxy groups and residual bridging OH groups in methylated zeolite $^{13}CH_3$-Y results in strong dipolar interactions that cannot be totally averaged out by the MAS

technique, thus leading to a significant broadening of the ^{1}H MAS NMR signals. In addition, the surface methoxy species on zeolites are bound to oxygen atoms at different framework positions and in different cages, both causing shift distributions. These values are in good agreement with those for methyl protons in the surface methoxy species [114]. The quantitative evaluation of the relative intensities given in Fig. 7.3 leads to coverages of the zeolites by surface methoxy species very close to those obtained from the evaluation of the total intensities in Fig. 7.1.

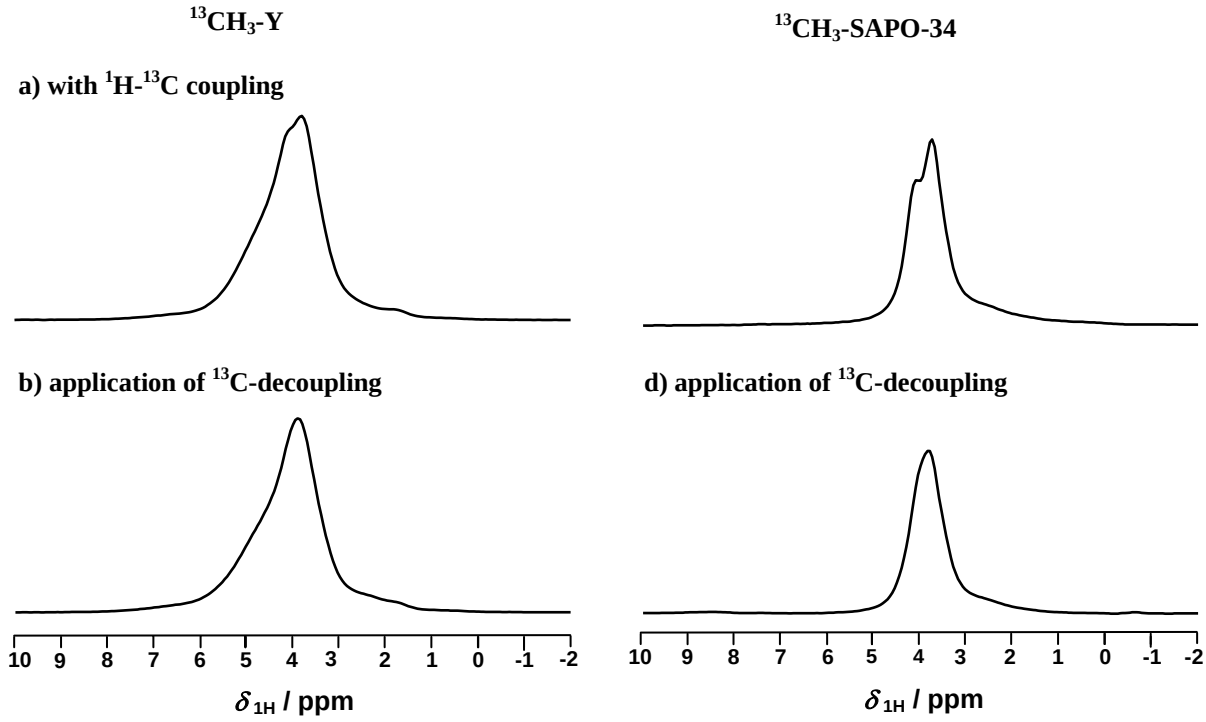

Fig. 7.2 ^{1}H MAS NMR spectra of $^{13}CH_3$-Y (a, b) and $^{13}CH_3$-SAPO-34 (c, d). The spectra (a) and (c) were recorded with ^{1}H single pulse excitation, while the spectra (b) and (d) were recorded with application of ^{13}C-decoupling.

In summary, the application of ^{1}H MAS NMR spectroscopy has proven the identical formation of surface methoxy species both from ^{13}C-enriched and highly purified non-enriched methanol on acidic zeolites. Therefore, it is further evident that the preparation method of surface methoxy species on acidic zeolites used in this dissertation is reliable and reproducible.

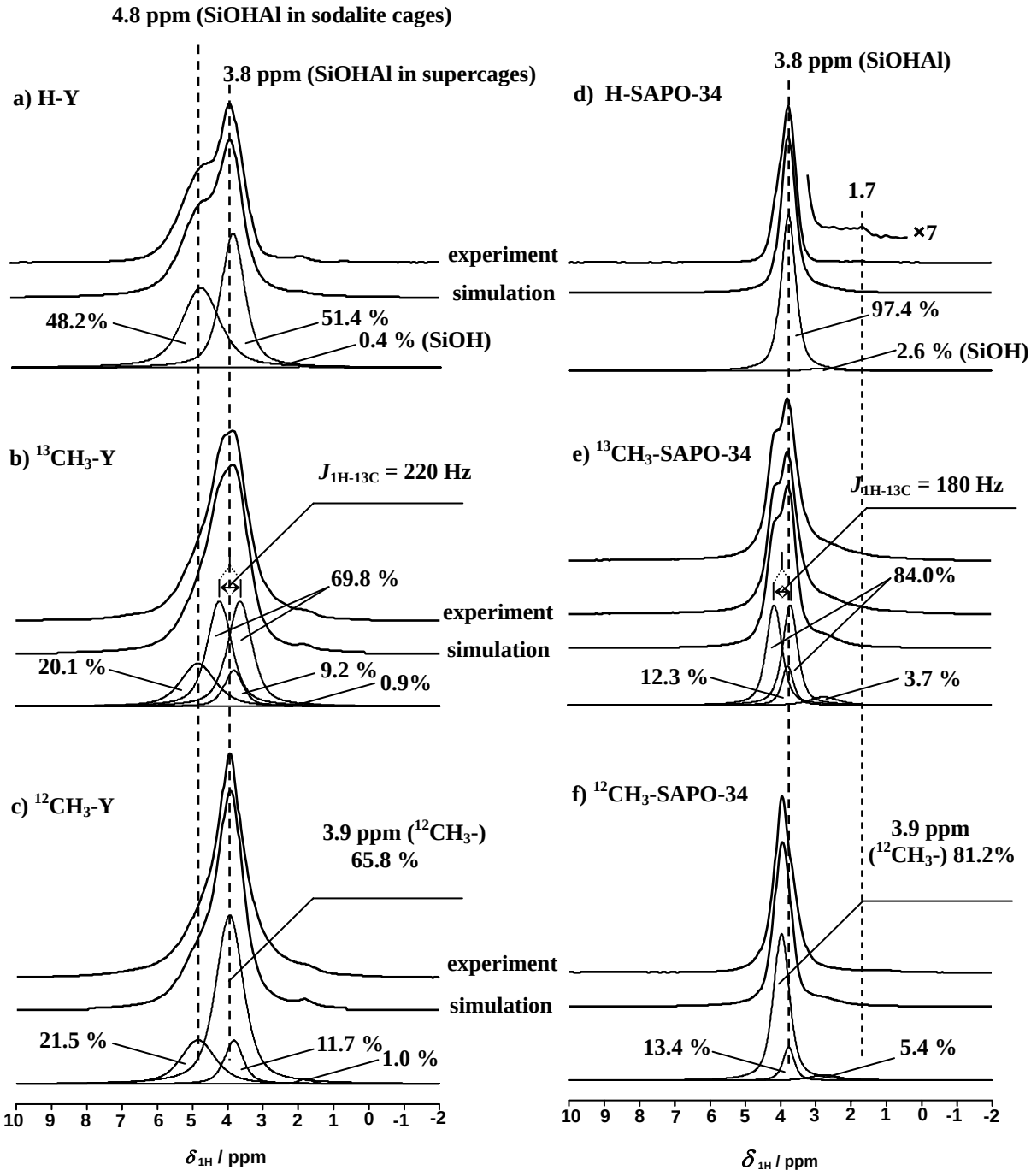

Fig. 7.3 Deconvolution of the ^{1}H MAS NMR spectra of acidic zeolite H-Y (a), ^{13}C-enriched methylated zeolite Y ($^{13}CH_3$-Y) (b), non-enriched methylated zeolite Y ($^{12}CH_3$-Y) (c), H-SAPO-34 (d), ^{13}C-enriched methylated SAPO-34 ($^{13}CH_3$-SAPO-34) (e), and non-enriched methylated SAPO-34 ($^{12}CH_3$-SAPO-34) (f). The results of the quantitative evaluation of the relative intensities are given for each spectrum.

7.3.2 MAS NMR-UV/Vis Investigation of the Conversion of Surface Methoxy Species on Methylated Zeolite Y (CH_3-Y)

Fig. 7.4a, left, shows the ^{13}C CP MAS NMR spectrum of methylated zeolite Y prepared from

^{13}C-enriched methanol. The spectrum is dominated by the signal of ^{13}C-enriched surface methoxy species at 56 ppm with spinning sidebands, which is characteristic of a methylated zeolite Y ($^{13}CH_3$-Y) [30]. The weak signal at 63 ppm is caused by a small amount (relative intensity of *ca.* 2 %) of side-on adsorbed DME [30]. The UV/Vis spectrum of zeolite $^{13}CH_3$-Y (Fig. 7.4a, middle) shows no UV/Vis bands. This finding indicates that the formation of surface methoxy species on zeolite H-Y at temperatures of up to 473 K is not accompanied by the formation of primary aromatics and unsaturated carbenium ions.

Upon heating of zeolite $^{13}CH_3$-Y at 513 K, the conversion of surface methoxy species to hydrocarbons occurred evidently, as indicated by the disappearance of the ^{13}C CP MAS NMR signal at 56.2 ppm and the appearance of new signals in the aliphatic range of *ca.* 10 to 45 ppm (Fig. 7.4b, left). Only weak signals of a small amount of aromatic compounds can be observed at *ca.* 120 to 150 ppm (see inset). The UV/Vis spectrum of this sample contains broad bands at *ca.* 320 to 380 nm (Fig. 7.4b, middle) indicating the formation of monoenylic and dienylic carbenium cations [113-115]. Upon thermal treatment at 593 and 673 K (Figs. 7.4c and 7.4d, middle), new UV/Vis bands occur at 380 and 430 nm due to the formation of dienylic and trienylic carbenium ions or hexamethyl benzenium cations [115-117]. The ^{13}C CP MAS NMR spectra of these two samples (Figs. 7.4c and 7.4d, left) show an increase of the signals of aromatic compounds at *ca.* 120 to 150 ppm.

The preparation of non-enriched surface methoxy species on zeolite H-Y from highly purified non-enriched methanol ($^{12}CH_3OH$, total organic impurities < 30 ppm) was performed under identical conditions as the preparation of ^{13}C-enriched methoxy species. Due to the low natural abundance of ^{13}C-isotopes in the non-enriched material, no ^{13}C CP MAS NMR investigations of zeolite $^{12}CH_3$-Y could be performed. The UV/Vis spectra obtained from non-enriched surface methoxy species on zeolite H-Y after thermal treatments at temperatures between 473 and 673 K are shown in Fig. 7.4, right. The comparison of the UV/Vis spectra recorded for the methylated zeolites $^{13}CH_3$-Y and $^{12}CH_3$-Y indicates the formation of the same organic compounds (aromatics and unsaturated carbenium ions) upon identical thermal treatments for both methylated catalysts. This finding indicates that traces of organic impurities present in the ^{13}C-enriched methanol (*ca.* 1000 ppm) have no influence on the formation of primary hydrocarbons on zeolite Y.

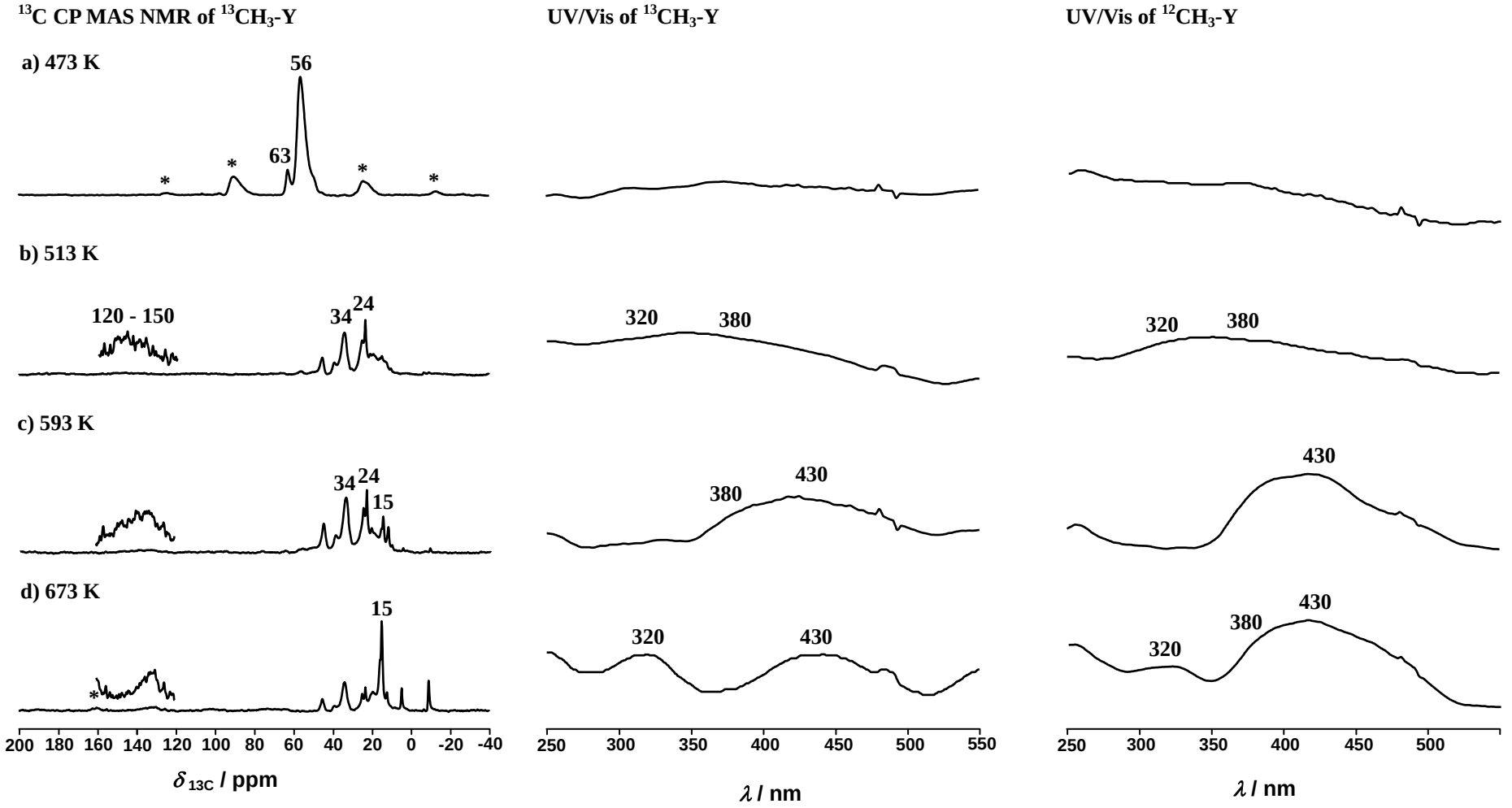

Fig. 7.4 ^{13}C CP MAS NMR (left) and UV/Vis spectra (middle and right) of zeolite H-Y methylated by $^{13}CH_3OH$ ($^{13}CH_3$-Y, middle) and highly purified $^{12}CH_3OH$ ($^{12}CH_3$-Y, right) after thermal treatments at 473 (a) to 673 K (d) for 20 min. Asterisks in the NMR spectra denote spinning sidebands. The narrow UV/Vis peaks at *ca.* 460 to 500 nm are caused by the equipment.

7.3.3 MAS NMR-UV/Vis Investigation of the Conversion of Surface Methoxy Species on Methylated SAPO-34 (CH_3-SAPO-34)

The silicoaluminophosphate H-SAPO-34 is characterized by a lower number of bridging OH groups with lower acid strength in comparison with zeolite H-Y, but it gives high selectivity of light olefins in the MTO process [1]. Therefore, it is also interesting to study the decomposition of surface methoxy species on this catalyst. The procedure of the investigation is the same as that for the study of the conversion of surface methoxy species on zeolite Y.

The ^{13}C CP MAS NMR-UV/Vis spectra of the methylated $^{13}CH_3$-SAPO-34 recorded upon thermal treatments at 473 to 673 K are shown in Fig. 7.5, left and middle. The ^{13}C CP MAS NMR spectrum of $^{13}CH_3$-SAPO-34 recorded upon thermal treatment at 473 K is dominated by the signal of surface methoxy species at 56 ppm (Fig. 7.5a, left). The comparison of the intensity of the signal at 56 ppm with the external intensity standard gives a concentration of *ca.* 0.6 methoxy species per SiOHAl group. Again, no UV/Vis bands occur for this sample, which indicates that the formation of surface methoxy species on H-SAPO-34 at 473 K is not accompanied by the formation of aromatics and unsaturated carbenium ions.

First, upon the thermal treatment at 513 K, the UV/Vis spectrum of $^{13}CH_3$-SAPO-34 shows a band at *ca.* 280 nm due to neutral aromatics (Fig. 7.5b, middle). Simultaneously, the ^{13}C CP MAS NMR signal of the surface methoxy species disappears and the formation of aliphatic and aromatic compounds can be observed at *ca.* 14 to 45 ppm and 120 to 150 ppm, respectively (Fig. 7.5b, left). Further thermal treatments up to a temperature of 673 K led to the formation of monoenylic, dienylic, and trienylic carbenium ions, which are responsible for the broad UV/Vis bands at *ca.* 320, 380, and 430 nm (Figs. 7.5c and 7.5d, middle). In contrast to zeolite $^{13}CH_3$-Y, however, the UV/Vis spectra of the $^{13}CH_3$-SAPO-34 recorded upon thermal treatments at 593 and 673 K show significantly larger bands in the region of neutral aromatics. This finding indicates the formation of methylbenzenes occluded in the chabazite cages of SAPO-34. These methylbenzenes are assumed to be the most reactive hydrocarbon-pool compounds in the MTO process [13].

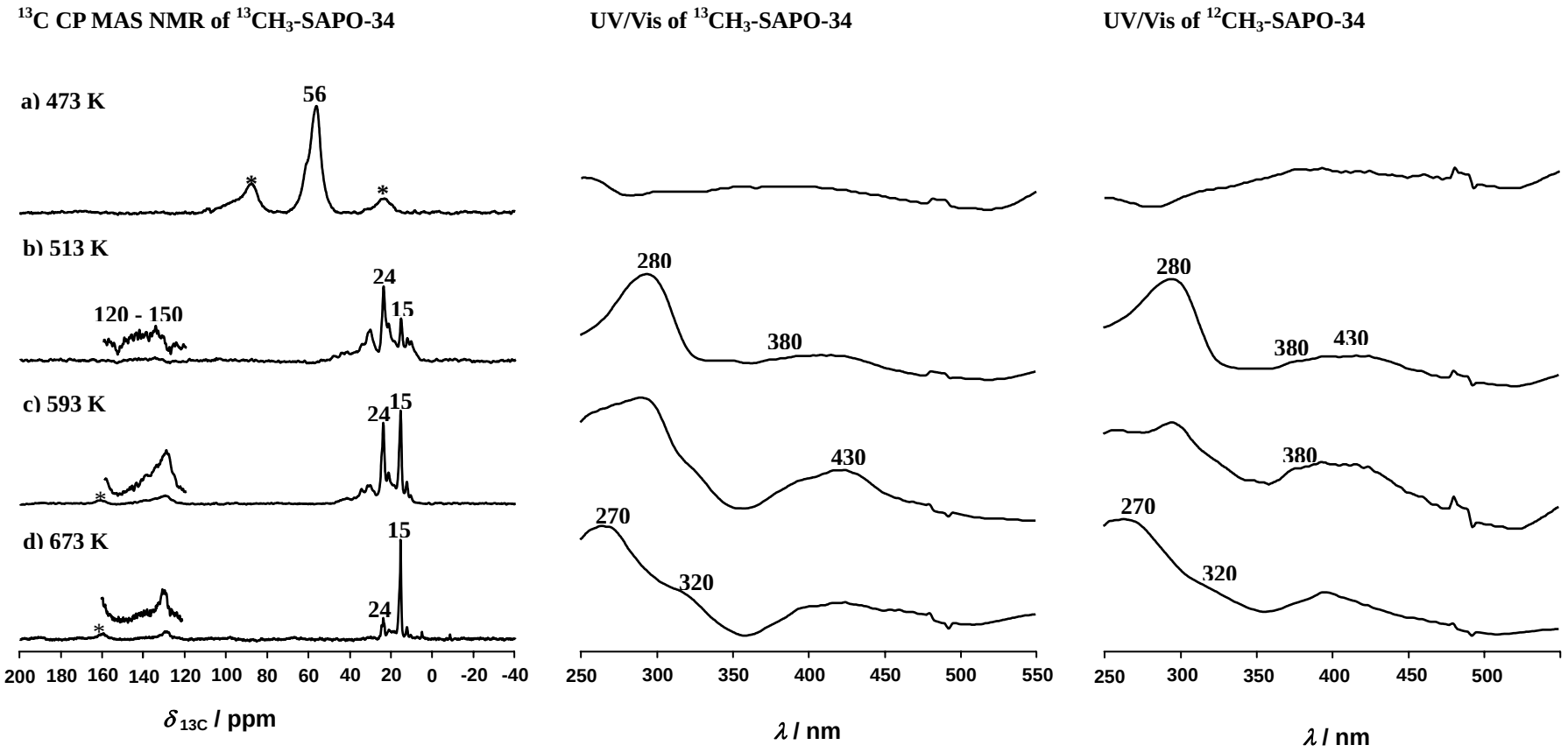

Fig. 7.5 ^{13}C CP MAS NMR (left) and UV/Vis spectra (middle and right) of the H-SAPO-34 methylated by $^{13}CH_3OH$ ($^{13}CH_3$-SAPO-34, middle) and highly purified $^{12}CH_3OH$ ($^{12}CH_3$-SAPO-34, right) after thermal treatments at 473 (a) to 673 K (d) for 20 min. Asterisks in the NMR spectra denote spinning sidebands. The narrow UV/Vis peaks at *ca.* 460 to 500 nm are caused by the equipment.

The preparation of non-enriched surface methoxy species on the silicoaluminophosphate H-SAPO-34 by the conversion of highly purified non-enriched methanol ($^{12}CH_3OH$, total organic impurities < 30 ppm) and the subsequent thermal treatments led to samples giving the UV/Vis spectra in Fig. 7.5, right. The UV/Vis spectra recorded for $^{13}CH_3$-SAPO-34 and $^{12}CH_3$-SAPO-34 indicate the formation of same neutral aromatics and carbenium ions upon identical thermal treatments. Hence, like in the case of zeolite Y, the traces of organic impurities occurring in the ^{13}C-enriched methanol (*ca.* 1000 ppm) have no influence on the formation of primary hydrocarbons on H-SAPO-34 as detected by UV/Vis spectroscopy.

7.3.4 Effect of Ethanol and Acetone on the Formation of Primary Hydrocarbons on H-SAPO-34

In addition to water, typical impurities in commercial methanol are ethanol and acetone [109]. The GC/MS analyses indicate that the most important impurity in ^{13}C-enriched methanol (^{13}C-enrichment of 99 %, chemical purity of 98+ %, derived from Cambridge Isotope Laboratories, Inc.) is ethanol. To study the influence of ethanol in the methanol feed on the decomposition of surface methoxy species, the conversion of ethanol on the H-SAPO-34 was investigated by ^{13}C MAS NMR-UV/Vis spectroscopy. For this purpose, the ^{13}C-1-enriched ethanol was loaded with different coverage from 0.02 to 0.25 molecules per SiOHAl group on the dehydrated H-SAPO-34. After thermal treatments of the ethanol-loaded H-SAPO-34 samples at 673 K for 20 min, the ^{13}C MAS NMR and UV/Vis spectra were recorded (Fig. 7.6). Starting with a loading of 0.05 ethanol molecules per SiOHAl group, weak signals and bands due to the formation of hydrocarbons from ethanol on H-SAPO-34 catalyst are evident (Fig. 7.6b). The UV/Vis bands comparable with those observed upon thermal conversion of the surface methoxy species on H-SAPO-34 (*cf.* Fig. 7.5d) occurred for the sample loaded with at least 0.10 ethanol molecules per SiOHAl group (Fig. 7.6c). Also in the case of the conversion of ethanol on H-SAPO-34, a strong UV/Vis band of neutral aromatics occurred at 270 nm, accompanied by a broad ^{13}C MAS NMR signal at *ca.* 120 to 150 ppm. A similar result was obtained after thermal treatment of the ethanol-loaded H-SAPO-34 catalysts at 593 K (not shown).

It is important to note that there are no UV/Vis bands of aromatics and carbenium ions up to a loading of H-SAPO-34 with 0.05 ethanol molecules per SiOHAl group. First

significant NMR signals and UV/Vis bands were observed upon a loading of H-SAPO-34 with 0.10 ethanol molecules per SiOHAl group (Fig. 7.6c), and their intensities are comparable with those obtained for the conversion of ^{13}C-enriched methanol on H-SAPO-34 (Fig. 7.5d). In the case of preparing 0.6 surface methoxy species per SiOHAl group on H-SAPO-34 from ^{13}C-enriched methanol (*cf.* Fig. 7.5), the maximum ethanol coverage is 0.6 × 1000 ppm, *i.e.*, 6×10^{-4} per SiOHAl group (assuming that the organic impurities are all due to ethanol).

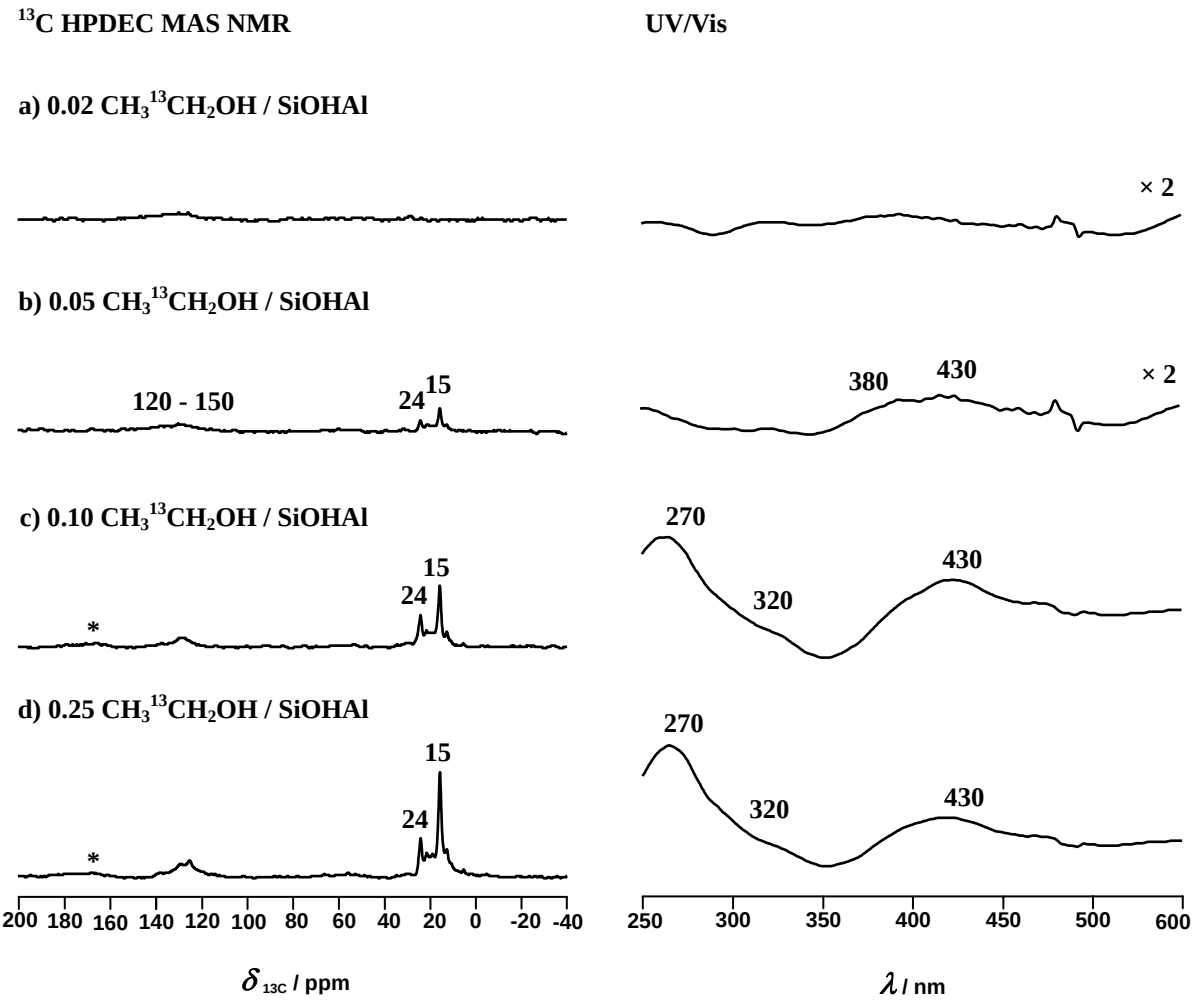

Fig. 7.6 ^{13}C HPDEC MAS NMR (left) and UV/Vis spectra (right) recorded after thermal treatment (673 K) of H-SAPO-34 loaded with 0.02 (a) to 0.25 molecules (d) ^{13}C-1-ethanol per SiOHAl group. Asterisks in the NMR spectra denote spinning sidebands. The narrow peaks at *ca.* 460 to 500 nm in the UV/Vis spectra are caused by the equipment.

The ethanol coverage, however, is *ca.* two orders of magnitude lower ($6 \times 10^{-4}/0.1 = 6 \times 10^{-3}$) than the loading of 0.10 ethanol molecules per SiOHAl group, which is required to give UV/Vis bands with similar intensities as shown in Fig. 7.5c. Therefore, traces of ethanol in

the ^{13}C-enriched methanol cannot be responsible for the NMR signals and UV bands shown in Fig. 7.5. In the case of preparation of 0.6 surface methoxy species per SiOHAl group on H-SAPO-34 *via* highly purified non-enriched methanol ($^{12}CH_3OH$, total organic impurities < 30 ppm), the ethanol coverage (0.6×30 ppm $= 1.8 \times 10^{-5}$) is, even, *ca.* four orders of magnitude lower ($1.8 \times 10^{-5}/0.1 = 1.8 \times 10^{-4}$) than that required to give the UV/Vis bands of significant and observable intensities.

A similar result was obtained after thermal treatment of acetone-loaded H-SAPO-34 upon thermal treatment at 673 K (Fig. 7.7). To reach comparable intensities of bands in the UV/Vis spectra as in Figs. 7.5d and 7.6c, the acetone coverage has to be at least 0.25 molecules per bridging OH group (see e.g. Fig. 7.7b). This acetone coverage is much higher than the coverage, which can be reached by traces of acetone in ^{13}C-enriched methanol.

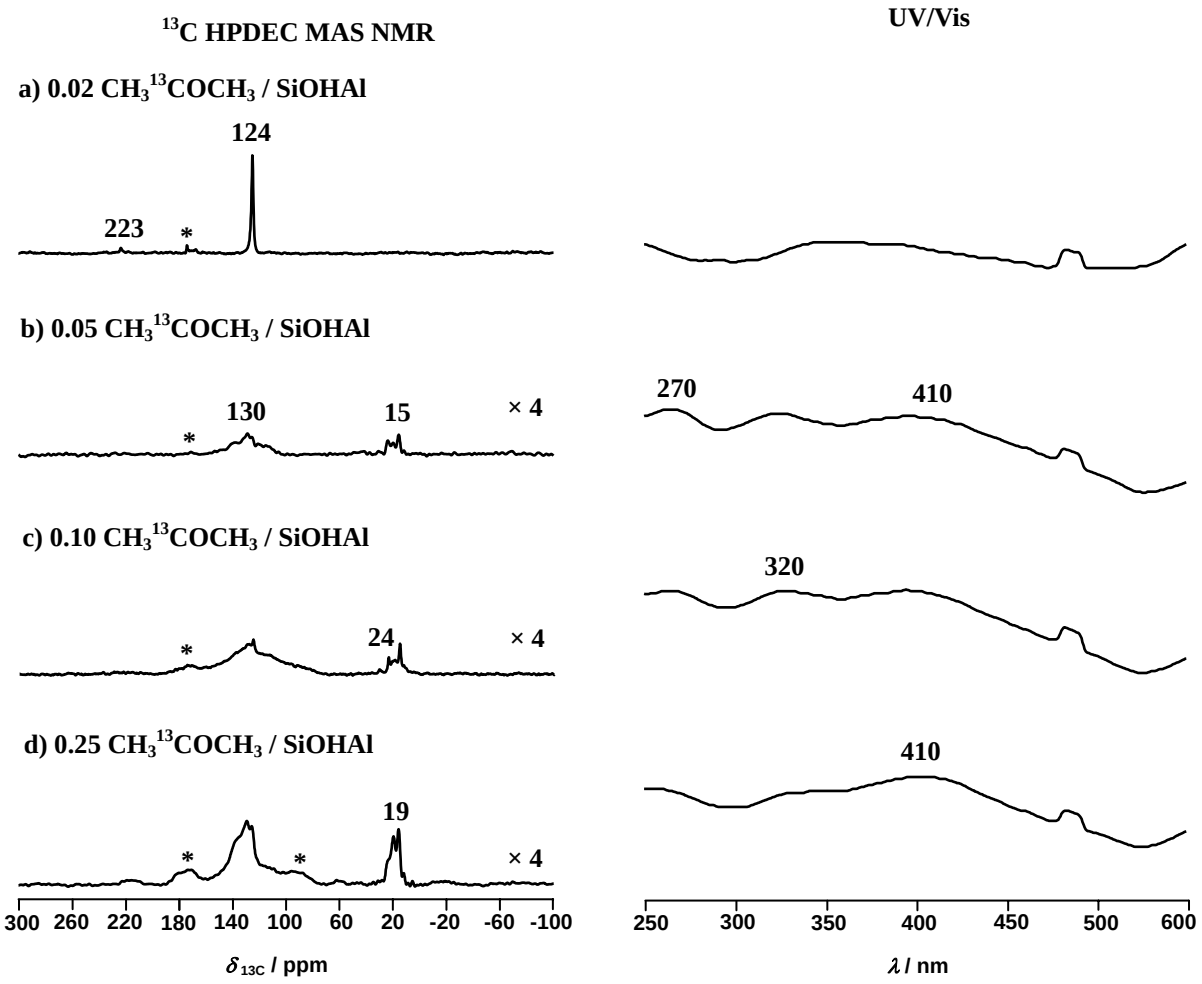

Fig. 7.7 ^{13}C HPDEC MAS NMR (left) and UV/Vis spectra (right) recorded after thermal treatment (673 K) of H-SAPO-34 loaded with 0.02 (a) to 0.25 molecules (d) ^{13}C-2-acetone per bridging OH group (SiOHAl). Asterisks in NMR spectra denote spinning sidebands. The narrow peaks at *ca.* 460 to 500 nm in UV/Vis spectra are caused by the equipment.

Commercial methanol consists of, in general, several hundred ppm of different organic impurities [109], the concentrations of which are between those of impurities in the highly purified non-enriched methanol (< 30 ppm) and the ^{13}C-enriched methanol (*ca.* 1000 ppm) used in the present study. For the above-mentioned concentrations of impurities, no effect on the formation of primary hydrocarbons during the conversion of the surface methoxy species on zeolite catalysts could be observed by MAS NMR-UV/Vis spectroscopy. Therefore, traces of organic impurities in the methanol should not govern the initiation of the methanol conversion on these catalysts *via* the surface methoxy species route.

7.4 Conclusions

The objective of this work is to clarify whether traces of organic impurities govern the formation of first hydrocarbons on acidic zeolite-type catalysts from the conversion of the surface methoxy species. For this purpose, samples of zeolite H-Y and silicoaluminophosphate H-SAPO-34 were methylated by adsorption of ^{13}C-enriched methanol (^{13}C-enrichment of 99 %, chemical purity of 98+ % with total organic impurities of *ca.* 1000 ppm) and highly purified non-enriched methanol (organic impurities < 30 ppm). The conversion of surface methoxy species on the two above-mentioned catalysts upon thermal treatments at 473-673 K was investigated by ^{13}C MAS NMR and UV/Vis spectroscopy. Since the formation of first aromatics and carbenium ions was observed at same reaction temperatures for both ^{13}C-enriched and non-enriched surface methoxy species, the influence of traces of organic impurities, present in the ^{13}C-enriched methanol, on the formation of primary hydrocarbons on the methylated zeolite catalysts could be excluded.

Ethanol and acetone are the most important organic impurities in commercial methanol. Therefore, the formation of primary hydrocarbons by the conversion of ethanol and acetone on H-SAPO-34 was investigated by the combined ^{13}C MAS NMR-UV/Vis spectroscopy. These experimental results show that the coverage of at least 0.1 ethanol and acetone molecules per bridging OH group is necessary to obtain neutral aromatics and carbenium ions, similar to those formed by the conversion of the methylated catalyst at the same reaction temperature. Considering the number of 0.6 surface methoxy species per bridging OH group prepared on H-SAPO-34, the ethanol and acetone coverage mentioned above is more than two orders of magnitude higher in comparison with the ethanol and acetone coverage, attainable

by impurities in the methanol feed. Therefore, studies of the ethanol-loaded and acetone-loaded H-SAPO-34 samples give additional evidence that the ^{13}C MAS NMR-UV/Vis spectra of the methylated SAPO-34 upon thermal treatment are not governed by ethanol and acetone occurring as traces of organic impurities.

8 Reactivity of Surface Methoxy Species Formed on Acidic Zeolites

8.1 Introduction

Mechanistic investigations of the formation of the primary products in the methanol conversion reaction is of fundamental interest and may also be of value for the optimization of existing industrial processes and their commercialization. Carbenium ions were considered as likely intermediates involved in a variety of reactions catalyzed by acidic zeolites [117]. However, the efforts to experimentally verify the long-lived existence of simple alkyl cations, *e.g.*, isopropyl or tertbutyl cations, in acidic zeolites are still lacking [118-121]. It was suggested in the literature [122] that free carbenium cations mostly exist as transition states rather than as persistent intermediates in acid-catalyzed reactions performed on acidic zeolites. Instead, surface alkoxy (alkoxide) species with carbenium-ion-like properties [119] may act as catalytic intermediates in zeolite chemistry [122]. This topic has been stimulating extensive research interest, and important progress has recently been made by using theoretical calculations [123-126]. Due to the complexity of heterogeneous reaction systems, however, experimental evidence for the existence and reactivity of surface alkoxy species is still lacking or ambiguous [32, 118-121, 127-128].

By the *in situ* stopped-flow (SF) MAS NMR technique, the observation of the formation of surface methoxy species from methanol [30] and surface ethoxy species from ethanol [127] on acidic zeolites could be realized. Furthermore, the intermediary role of surface methoxy species in the MTO process was demonstrated [31, 129]. On acidic zeolites at reaction temperatures lower than 473 K, surface methoxy species act as reactive methylating agents, which can react with methanol to form DME [30] and with toluene to form xylenes [31]. At reaction temperatures higher than 523 K, the decomposition of surface methoxy species takes place as a result of breakage of C-H bonds of the methyl group, which is further responsible for the first C-C coupling and, therefore, for the formation of primary hydrocarbons in the MTO process [31, 129].

The approach developed in our group [30] for the *in situ* preparation of surface methoxy species offers the possibility to further investigate the reactivity of surface methoxy species in heterogeneously catalyzed reactions. ^{13}C MAS NMR spectroscopy is utilized to study the reactions of surface methoxy species with ammonia, alkyl halides, hydrochloride, carbon monoxide, acetonitrile, and oxygen on solid acidic catalysts. On the basis of these

experimental findings, the reactivity of surface methoxy species is discussed in terms of C-O bond and C-H bond activation. In benefit of recent theoretical investigations, the relative stability and reactivity of surface alkoxy species on acidic zeolites are further compared.

8.2 Experimental Part

8.2.1 Sample Preparation

The detailed preparation procedure of dehydrated catalysts H-Y and H-SAPO-34 was described in Chapter 6. All catalysts were characterized by ICP-AES, XRD and solid-state ^{1}H, ^{27}Al, and ^{29}Si MAS NMR spectroscopy. The results indicated that the material obtained after cation exchange and calcination was neither damaged nor dealuminated. ^{13}C-enriched methanol (^{13}C-enrichment of 99 %), ^{13}C-enriched methyl iodide (^{13}C-enrichment of 99 %), and ^{13}C-1-enriched ethyl iodide (^{13}C-1-enrichment of 99 %) were purchased from Cambridge Isotopes. ^{13}C-enriched carbon monoxide (^{13}C-enrichment of 99 %) was purchased from Aldrich.

The preparation of surface methoxy species on acidic catalysts H-Y and H-SAPO-34 was performed *via* a vacuum line. The calcined and dehydrated catalysts (*ca.* 300 mg) filled in a glass tube (outer diameter of *ca.* 6 mm and length of *ca.* 180 mm) were subjected to ^{13}C-enriched methanol at the pressure of 7.5 mbar and at the temperature of 393 K. Thereafter, an evacuation for 6 h at 393 K and additional evacuation for 6 h at 473 K were performed. Subsequently, the methylated catalysts were sealed in the glass tubes until their further use. By ^{13}C spin-counting experiments, the coverage of zeolite H-Y by surface methoxy species was determined to 0.44 per acid site. In the case of zeolite H-SAPO-34, 0.6 surface methoxy species per acid site were formed. The methylated catalyst (*ca.* 300 mg) in the glass tube was then loaded with volatile reactants on a vacuum line and sealed for further thermal treatment. After heating, the glass tube was opened in a glove box and the catalyst was transferred into a 7 mm MAS NMR rotor for solid-state MAS NMR measurements. In the case of oxidation reactions, the methylated catalyst was loaded with *ca.* 5 mbar of oxygen and transferred into an MAS NMR insert (outer diameter of 5.6 mm with constrictions, Wilmad) inside a glove box and, subsequently, sealed. The sealed glass inserts were heated to the reaction temperature for 20 min.

8.2.2 ^{13}C MAS NMR Investigations

All ^{13}C MAS NMR investigations were performed with a 7 mm Bruker MAS NMR probe on a Bruker MSL 400 spectrometer at the ^{13}C resonance frequency of 100.6 MHz. HPDEC MAS NMR spectra were recorded after an excitation with a $\pi/2$ pulse and with a repetition time of 5 s. For ^{13}C spin-counting experiments, a repetition time of 30 s and an external intensity standard (dehydrated zeolite H-Y loaded with $^{13}CH_3OH$) was applied. ^{13}C CP MAS NMR spectra were performed with a contact time of 5 ms and with a repetition time of 2 s. Sample spinning frequencies of *ca.* 3.5 to 4.5 kHz were applied. All ^{13}C MAS NMR spectra were referenced to TMS.

8.3 Results

8.3.1 Reaction of Surface Methoxy Species and Ammonia at Room Temperature

Heterogeneously catalyzed alkylation of amines by alcohols, for example, the methylation of ammonia by methanol on zeolite catalysts has attracted significant interest in recent years [130-132]. Different mechanisms have been proposed for the reaction of methanol and ammonia on acidic zeolites. It has been suggested that ammonia and methyl amines are preferentially adsorbed on Broensted acid sites, due to their higher proton affinities in the gas phase than that of methanol [130]. According to most of the proposed mechanisms, the reaction does not involve surface methoxy species [130]. However, the existence of surface methoxy species has been experimentally observed by *in situ* IR spectroscopy during the reaction of methanol and ammonia on acidic zeolite H-ZSM-5 [132]. In addition, the formation of surface methoxy species during aniline methylation on acidic zeolite H-Y has been shown by *in situ* MAS NMR spectroscopy [133-134]. In this dissertation, the reaction of surface methoxy species and ammonia was, therefore, studied by this method. It was found that surface methoxy species react readily with ammonia on acidic zeolites H-Y and H-SAPO-34 at room temperature, by which methylamines and methylammonium cations are formed.

Fig. 8.1a shows the ^{13}C MAS NMR spectrum recorded after the preparation of surface methoxy species ($^{13}CH_3$-Y) on zeolite H-Y from ^{13}C-enriched methanol. The dominating signal at 56 ppm with spinning sidebands is due to surface methoxy species [30]. The signal

at 63 ppm is originated from side-on adsorbed DME, while the broad signal at 50 ppm is caused by terminal methoxy species ($SiOCH_3$) [30].

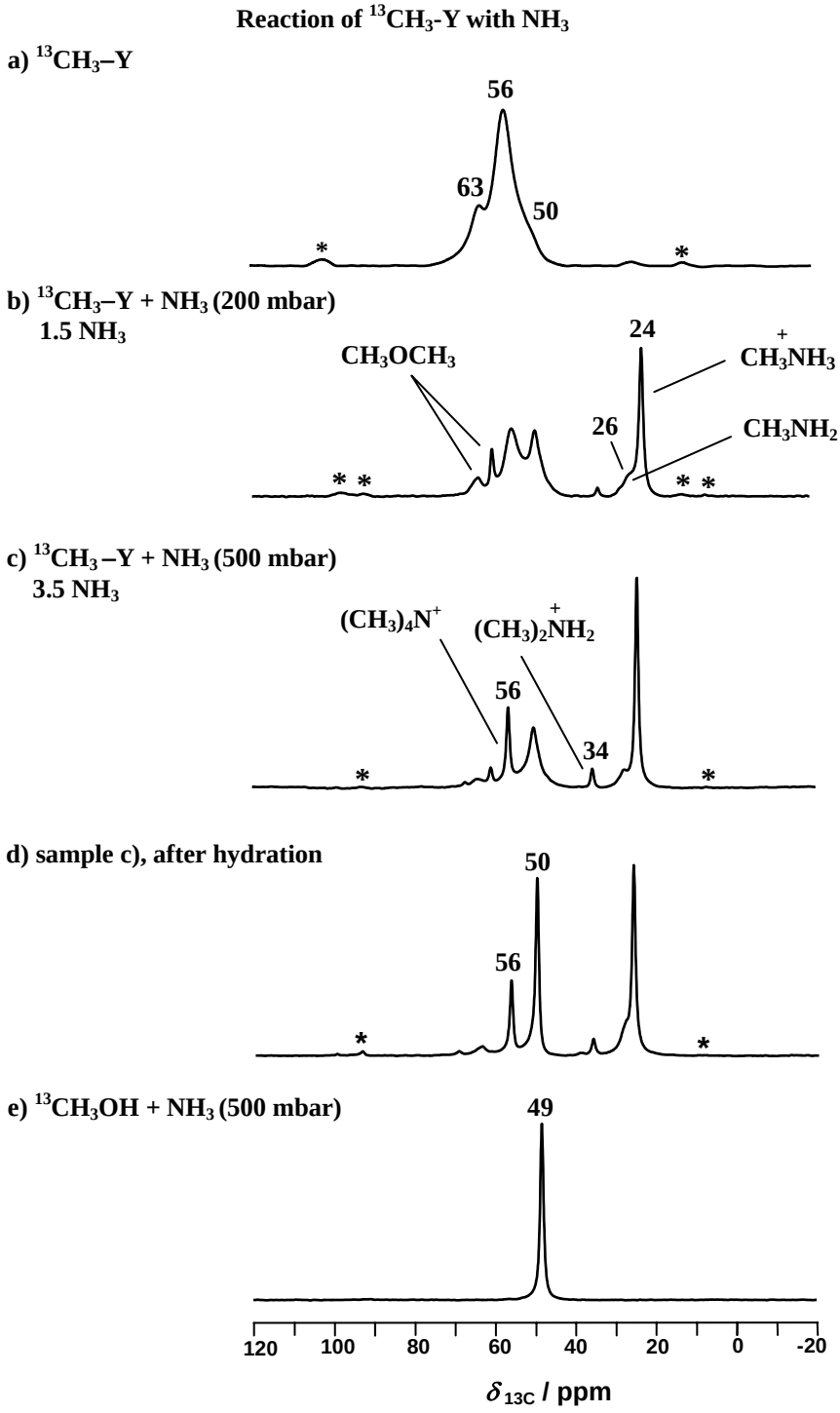

Fig. 8.1 ^{13}C HPDEC MAS NMR spectra of methylated zeolites Y ($^{13}CH_3$-Y), recorded before loading of ammonia (a), after loading of 200 mbar of ammonia at room temperature (b), after loading of 500 mbar of ammonia at room temperature (c). Fig. 8.1d was recorded after the catalyst sample (c) was fully hydrated at room temperature. As a control experiment, Fig. 8.1e shows the ^{13}C MAS NMR spectrum of acidic zeolite H-Y after loading of methanol and ammonia at room temperature, in which the ^{13}C signal of methanol (49 ppm) is 1 ppm high-field shifted due to the co-existence of ammonia on the acidic zeolite H-Y. Asterisks denote spinning sidebands.

Upon loading of 200 mbar of ammonia on the methylated zeolite Y (approximately 1.5 NH_3 per surface methoxy species) at room temperature, the ^{13}C MAS NMR spectrum shown in Fig. 8.1b was recorded. Accompanied by the decrease of the intensity of surface methoxy species at 56 ppm, new signals appear at 26 and 24 ppm, which are assigned to methylamine, CH_3NH_2, and protonated methylamine, $CH_3NH_3^+$, respectively [135]. Upon loading of 500 mbar of ammonia on the methylated zeolite Y (approximately 3.5 NH_3 per surface methoxy species) at room temperature, additional signals at 34 and 56 ppm become evident (Fig. 8.1c). The signal at 34 ppm is due to the protonated dimethylamine, $(CH_3)_2NH_2^+$ [134]. In comparison with the signal of surface methoxy species (Fig. 8.1a), the signal at 56 ppm in Fig. 8.1c is much narrower and, therefore, assigned to the tetramethylammonium cations, $(CH_3)_4N^+$ [134-136]. The assignments are further supported by the ^{13}C MAS NMR spectrum in Fig. 8.1d, which was recorded after the catalyst was fully hydrated at room temperature. As indicated in Fig. 8.1d, the signal of $(CH_3)_4N^+$ at 56 ppm survived from hydration, upon which surface methoxy species would not exist [31]. The broad signal at 50 ppm (Fig. 8.1c) is narrowed after hydration, which indicates the reaction of terminal surface methoxy species with water to methanol [31]. The reaction pathways of surface methoxy species and ammonia on acidic zeolite under study are depicted in Scheme 8.1. Similar to the case of N, N-dimethylanilinium cations, which have a ^{13}C chemical shift of *ca.* 48 ppm [134], the ^{13}C MAS NMR signal of trimethylammonium cations, $(CH_3)_3NH^+$, may be overlapped by the signal at 50 ppm and, therefore, cannot be unambiguously observed in Fig. 8.1.

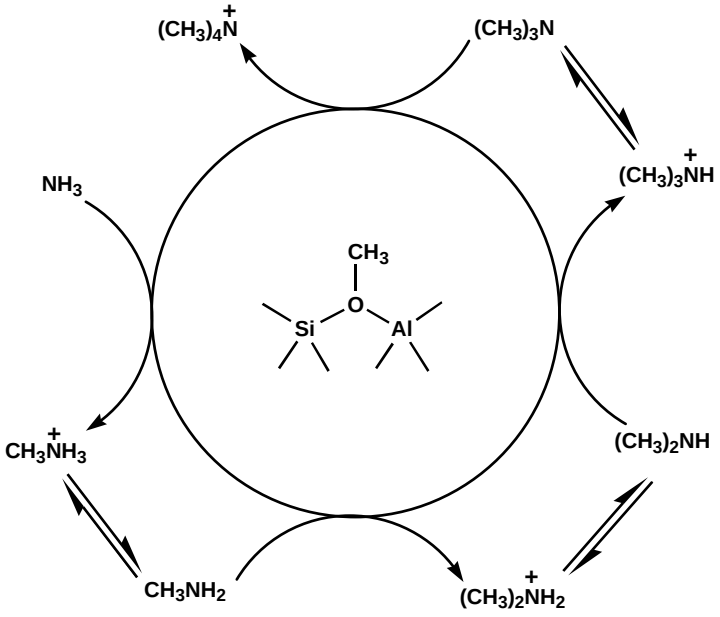

Scheme 8.1 Reaction pathways of surface methoxy species and ammonia on acidic zeolites.

It is important to note that methylamines and methylammonium cations have previously been observed only after the reaction of methanol and ammonia on acidic zeolites at temperatures higher than 513 K [135-136]. As shown in Figs. 8.1b and 8.1c, however, the same products are readily formed *via* the reaction of surface methoxy species and ammonia on acidic zeolite H-Y at room temperature. As a control experiment, acidic zeolite H-Y was loaded with methanol and ammonia under identical conditions as for preparing the sample used to obtain the spectrum in Fig. 8.1c. The ^{13}C MAS NMR spectrum recorded thereafter (Fig. 8.1e) shows only the signal of methanol at *ca.* 49 ppm, which indicates that methanol and ammonia do not react on acidic zeolite H-Y at room temperature. The significant difference in reactivity between surface methoxy species and methanol were also observed during the methylation of ammonia on silicoaluminophosphate H-SAPO-34 (not shown). In addition, Ivanova *et al.* [133] reported that the N-alkylation of aniline by surface methoxy species occurs at room temperature on zeolite H-Y. In contrast, the N-alkylation of aniline by methanol starts at 373 K on acidic zeolite H-Y [133-134]. The above-mentioned findings indicate that surface methoxy species are very reactive in methylating amines on acidic zeolites and, if involved, their formation is a rate-determining step during the methylation of amines by methanol on acidic zeolites. Of course, the overall reaction rate may be governed by further transfer of these methylammonium cations from the zeolite into the gas phase, which includes the methylation/demethylation (or disproportionation) and adsorption/desorption equilibria [130-131].

8.3.2 Reaction of Surface Methoxy Species and Alkyl Halides

Recently, the first ^{13}C MAS NMR evidence for the formation of surface ethoxy species upon the dehydration of ethanol on acidic zeolite H-Y has been reported [127]. By applying a stopped-flow protocol similar to that for the preparation of surface methoxy species [30], surface ethoxy species were observed, which gave a ^{13}C CP MAS NMR signal at 72.6 ppm accompanied by spinning sidebands characteristic for strongly bound surface species [127]. Formation of surface ethoxy species on acidic zeolite H-Y was further confirmed by an analysis of the chemical shielding tensor and by the reaction of these species with water [127]. In addition, the transformation of surface methoxy species to surface ethoxy species and other alkoxy species was shown for the first time, which is achieved by the reaction of surface methoxy species and alkyl halides on acidic zeolite H-Y.

^{13}C MAS NMR spectroscopy was applied to investigate the reaction of surface methoxy species ($^{13}CH_3$-Y) and ^{13}C-1-enriched ethyl iodide ($CH_3{}^{13}CH_2I$) as shown in Fig. 8.2.

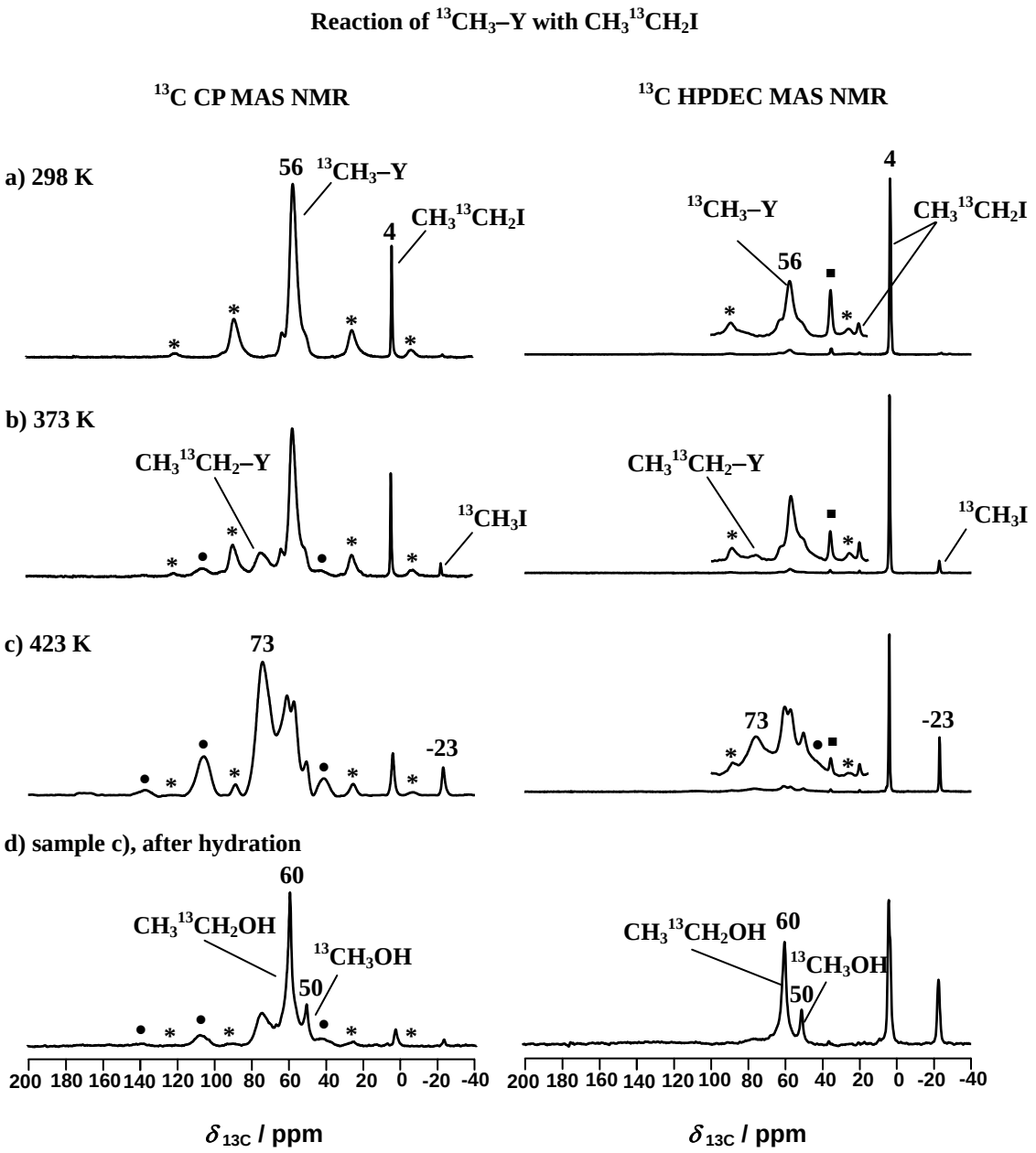

Fig. 8.2 ^{13}C CP MAS NMR (left) and ^{13}C HPDEC MAS NMR (right) spectra recorded after the reaction of ^{13}C-1-enriched ethyl iodide ($CH_3{}^{13}CH_2I$) and surface methoxy species ($^{13}CH_3$–Y) at 298 K (a), 373 K (b), 423 K (c). Figure (d) shows the ^{13}C MAS NMR spectrum recorded after the catalyst sample (c) was hydrated at room temperature. The spinning sidebands of $^{13}CH_3$–Y are denoted as *, those of $CH_3{}^{13}CH_2$–Y as •, and those of $CH_3{}^{13}CH_2I$ as ▪. The methylated zeolite $^{13}CH_3$–Y was *in situ* prepared from ^{13}C-enriched methanol.

Fig. 8.2a, left, shows the ^{13}C CP MAS NMR spectrum recorded after loading of

$CH_3{}^{13}CH_2I$ on the methylated zeolite Y, $^{13}CH_3$-Y, at room temperature. The signal at 4 ppm is due to the methylene carbon atoms of the reactant, $CH_3{}^{13}CH_2I$. A weak signal appears at –23 ppm, which is assigned to methyl iodide $^{13}CH_3I$ [102]. The reaction of surface methoxy species and ethyl iodide becomes more evident at 373 and 423 K, as indicated in Figs. 8.2b and 8.2c, respectively. A new signal at 73 ppm occurred with spinning sidebands in Fig. 8.2b, left, and dominates the spectrum in Fig. 8.2c, left. In agreement with the literature [127], the signal at 73 ppm is assigned to the methylene carbon atoms of surface ethoxy species, $CH_3{}^{13}CH_2$-Y. The above-mentioned assignments are further supported by the ^{13}C CP MAS NMR spectrum shown in Fig. 8.2d, left, which was recorded after the catalyst was hydrated at room temperature. The formation of $CH_3{}^{13}CH_2OH$ at 60 ppm and $^{13}CH_3OH$ at 50 ppm indicates the hydrolysis of surface ethoxy species [127] and surface methoxy species [31] by water. The ^{13}C HPDEC MAS NMR spectra simultaneously recorded for each sample are shown in Fig. 8.2, right. Similar signals occur in each ^{13}C HPDEC MAS NMR spectrum as those in the corresponding ^{13}C CP MAS NMR spectrum, although with different relative intensities. The reaction of surface methoxy species and ethyl iodide is depicted in Scheme 8.2, which shows the transformation of surface methoxy species to surface ethoxy species on the catalyst.

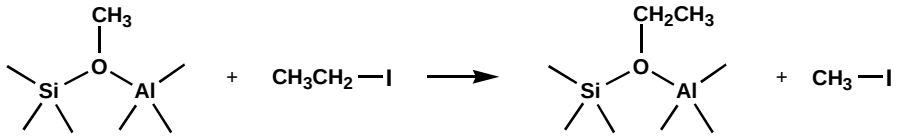

Scheme 8.2 Reaction of surface methoxy species and ethyl iodide.

A similar reaction was found for surface methoxy species reacting with other alkyl halides, by which the corresponding alkoxy species are expected to be formed. Fig. 8.3 shows some representative ^{13}C HPDEC MAS NMR spectra recorded after the reaction of ^{13}C-enriched surface methoxy species and non-enriched alkyl halides on zeolite H-Y and silicoaluminophosphate H-SAPO-34. The formation of ^{13}C-enriched methyl iodide $^{13}CH_3I$ (Figs. 8.3a to 8.3d) or methyl bromide $^{13}CH_3Br$ (Fig. 8.3e) indicates that the reaction of surface methoxy species and alkyl halides takes place in a similar manner as described in Scheme 8.2. For example, after the reaction of ^{13}C-enriched surface methoxy species ($^{13}CH_3$-Y) and non-enriched isopropyl iodide [$(CH_3)_2$CH-I] at room temperature, the signal of ^{13}C-enriched methyl iodide ($^{13}CH_3I$) occurs at –23 ppm in the ^{13}C HPDEC MAS NMR spectrum (Fig. 8.3c). This signal dominates the ^{13}C HPDEC MAS NMR spectrum after the

reaction at 373 K (Fig. 8.3d).

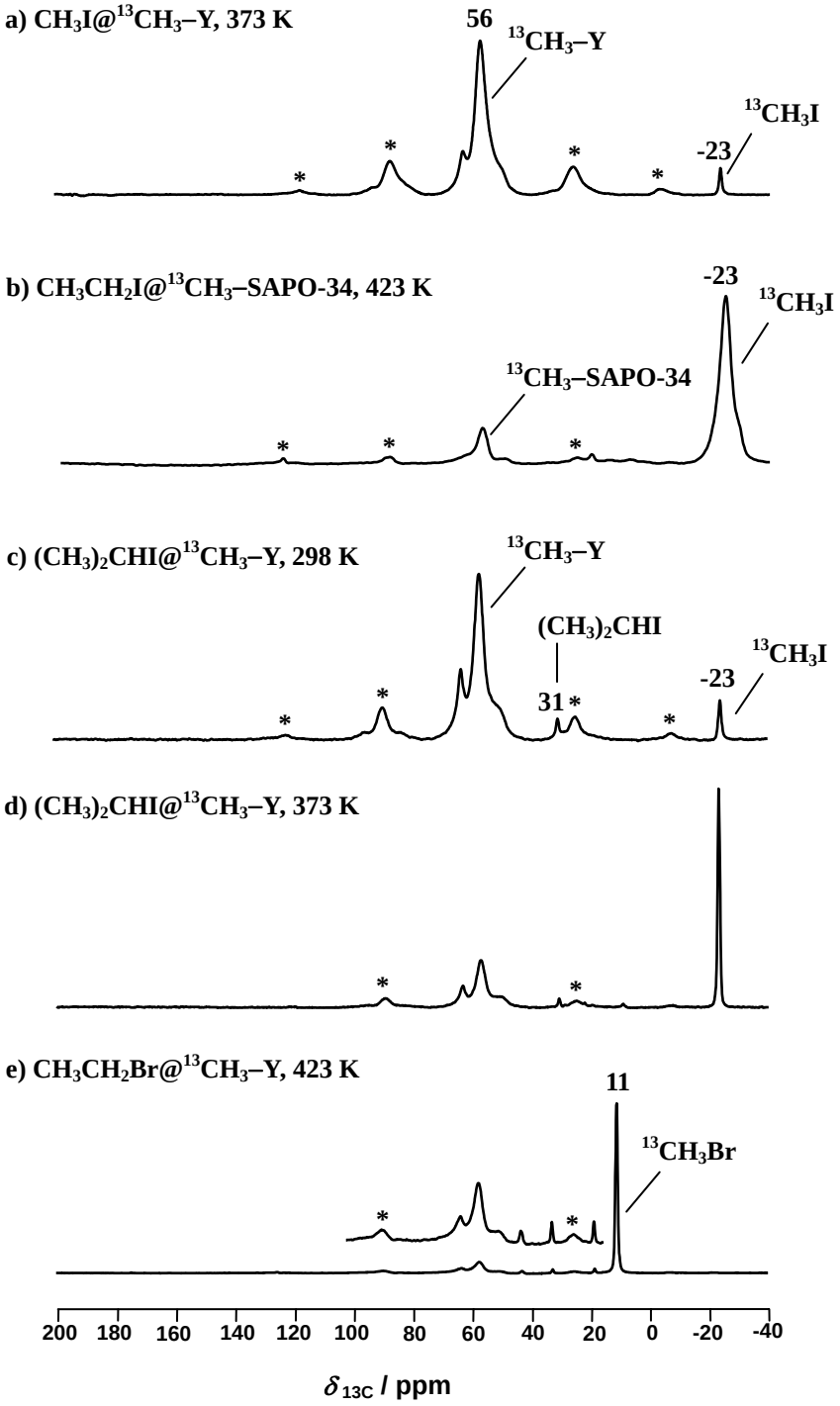

Fig. 8.3 ^{13}C HPDEC MAS NMR spectra recorded after the reaction of methyl iodide (CH_3I) on methylated zeolite Y ($^{13}CH_3$–Y) at 373 K (a), ethyl iodide CH_3CH_2I on methylated silicoaluminophosphate SAPO-34 ($^{13}CH_3$–SAPO-34) at 423 K (b), isopropyl iodide [$(CH_3)_2CHI$] on methylated zeolite Y ($^{13}CH_3$–Y) at 298 K (c) and 373 K (d), and ethyl bromide CH_3CH_2Br on methylated zeolite Y ($^{13}CH_3$–Y) at 423 K (e). Asterisks denote spinning sidebands. The methylated catalysts $^{13}CH_3$–Y and $^{13}CH_3$–SAPO-34 were *in situ* prepared from ^{13}C-enriched methanol.

Another example is the reaction of ^{13}C-enriched surface methoxy species and non-enriched ethyl bromide on zeolite H-Y. Fig. 8.3e shows the ^{13}C HPDEC MAS NMR spectrum recorded after the reaction at 423 K. The dominating signal at 11 ppm, which is due to the ^{13}C-enriched methyl bromide ($^{13}CH_3Br$), indicates the transformation of surface methoxy species to surface ethoxy species by the reaction of surface methoxy species and ethyl bromide on zeolite H-Y. However, it is not easy to figure out the detailed mechanism for the reaction of surface methoxy species and alkyl halides. For example, the reaction depicted in Scheme 8.2 can take place either in one step or in sequential steps, which start with the formation of surface ethoxy species and HI, followed by the subsequent reaction of HI with surface methoxy species.

8.3.3 Reaction of Surface Methoxy Species and Hydrochloride

Methyl chloride, which is used as a general methylating agent and as an intermediate in the manufacture of silicons, synthetic rubber and methyl cellulose, is commercially produced by two processes: Hydrochlorination of methanol and chlorination of methane [137]. In industry, the hydrochlorination reaction of methanol and hydrochloride, mainly on alumina-based solid catalysts, is usually preferred [137]. A recent investigation on the interaction of methanol and η-Al_2O_3 catalyst shows that chemisorbed methoxy is the only surface species present on the catalyst [139]. A further study indicates that surface methoxy species are involved as a reactive intermediate in hydrochlorination of methanol on η-Al_2O_3 catalyst [139]. Additionally, zeolites have also been suggested as active catalysts for the methanol hydrochlorination process [141].

In order to gain mechanistic information of hydrochlorination of methanol on solid catalysts, the reaction of surface methoxy species and hydrochloride was, therefore, investigated by ^{13}C MAS NMR spectroscopy. Fig. 8.4a, left, shows the ^{13}C HPDEC MAS NMR spectrum recorded after the reaction of the methylated catalyst ($^{13}CH_3$-Y) and hydrochloride (HCl) at room temperature. As can be seen, a new signal appears at 24 ppm, which is due to the formation of methyl chloride, $^{13}CH_3Cl$. Upon further reaction at 353 K, the signal of methyl chloride at 24 ppm increases, accompanied by the decrease of the signal of surface methoxy species at 56 ppm (Fig. 8.4b, left). Scheme 8.3 describes the reaction of surface methoxy species and hydrochloride on zeolite catalyst, by which the Broensted acidity

of the zeolite is recovered. As a comparison, the reaction of ^{13}C-enriched methanol and hydrochloride on acidic zeolite H-Y was investigated under same conditions and the ^{13}C HPDEC MAS NMR results are shown in Fig. 8.4, right. Similar to the cases of surface methoxy species, the reaction of methanol and hydrochloride on acidic zeolite H-Y gives methyl chloride as the product, which is evidenced by the appearance of the ^{13}C MAS NMR signal of methyl chloride at 24 ppm (Fig. 8.4, right). These results indicate that surface methoxy species may also be involved in methanol hydrochlorination on solid catalysts, which is in agreement with the recent work of Lennon and co-workers [140], who reported their investigation of methanol hydrochlorination on an η-Al_2O_3 catalyst by means of temperature programmed reaction spectroscopy (TPRS).

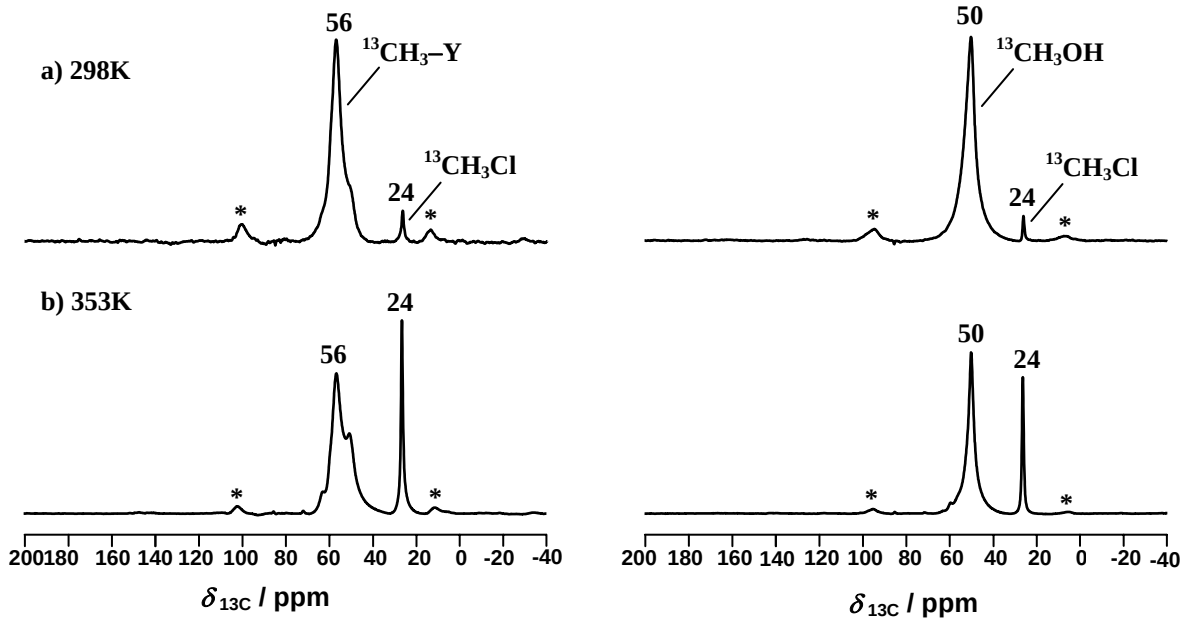

Fig. 8.4 ^{13}C HPDEC MAS NMR spectra recorded after the reaction of hydrochloride on methylated zeolite Y ($^{13}CH_3$-Y) (left), and after the reaction of methanol and hydrochloride on acidic zeolite H-Y (right) at 298 K (a) and 353 K (b), respectively. Asterisks denote spinning sidebands.

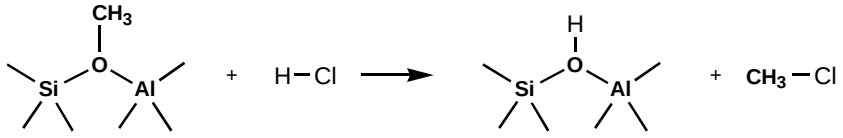

Scheme 8.3 Reaction of surface methoxy species and hydrochloride on zeolite catalysts.

8.3.4 Koch-type Carbonylation Reaction: The Reaction of Surface Methoxy Species and Carbon Monoxide

The classic Koch carbonylation reaction between olefins and carbon monoxide in the

presence of water provides evidence for the existence of carbenium ions in superacidic solutions [142]. The first solid-state NMR evidence of the Koch carbonylation reaction on solid acid catalysts was reported in 1995 by Stepanov *et al.* [143]. By ^{13}C MAS NMR spectroscopy, these authors observed the formation of trimethylacetic acid in high yields upon co-adsorption of isobutene, carbon monoxide, and water (or co-adsorption of *tert*-butyl alcohol and carbon monoxide) on acidic zeolite H-ZSM-5 under mild conditions [143]. Based on this finding, high and stable catalytic performance was recently found for the Koch carbonylation reaction on various solid acidic catalysts [144-145].

Similar to the case in superacidic solutions [142], the proposed mechanism (Scheme 8.4) of the Koch carbonylation reaction on acidic zeolites [143, 146] involves the trapping of an alkyl carbenium ion (R^+, transient species, generated from an olefin or alcohol on an acidic zeolite) by carbon monoxide to form an acylium cation, $R\text{-}^+C{=}O$. The latter cation is very unstable and is readily quenched by water to give a carboxylic acid, R-COOH.

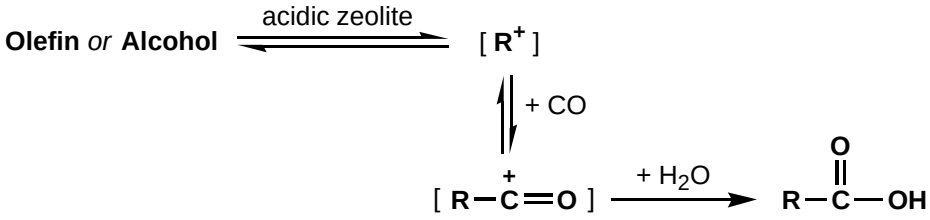

Scheme 8.4 Koch carbonylation reaction on acidic zeolites.

As further demonstrated by Stepanov *et al.* [147], alkoxy species, which possess carbenium-ion-like properties may also follow the Koch carbonylation reaction on acidic zeolites. Fujimoto *et al.* [148] were the first who reported the carbonylation of methanol by carbon monoxide at 473 K on acidic zeolites H-Y, H-ZSM-5, and H-Mordenite. The main carbonylated products of which are acetic acid (CH_3COOH) and methyl acetate (CH_3COOCH_3). The carbonylation reaction of methanol on acidic zeolites was proposed to follow the mechanism of the Koch reaction shown in Scheme 8.4, with the formation of surface methoxy species as the key intermediate. A similar pathway, which involves the reaction of surface methoxy species and carbon monoxide, was also suggested recently by Iglesia and co-workers for the carbonylation reaction of dimethyl ether on acidic zeolites [149].

The suggestion of Iglesia and co-workers [149] is verified by the ^{13}C MAS NMR

investigations presented in Fig. 8.5. Fig. 8.5a shows the ^{13}C CP MAS NMR spectrum recorded after the reaction of ^{13}C-enriched carbon monoxide (^{13}CO) and non-enriched DME (CH_3OCH_3) on acidic zeolite H-Y at 473 K. In agreement with previous findings [143, 149-150], the ^{13}C MAS NMR signal at 184 ppm with characteristic spinning sidebands is assigned to the carbonyl carbon of acetic acid, $CH_3{}^{13}COOH$. This assignment was further supported by the adsorption of $CH_3{}^{13}COOH$ on zeolite H-Y. The ^{13}C CP MAS NMR recorded thereafter shows the identical chemical shift and very similar spinning sidebands as observed for the signal at 184 ppm in Fig. 8.5a. On the other hand, ^{13}CO, which also has the ^{13}C chemical shift of *ca.* 184 ppm [143], is only weakly adsorbed on zeolite H-Y and does not show any appreciable signal with sideband pattern in the ^{13}C CP MAS NMR spectrum (not shown).

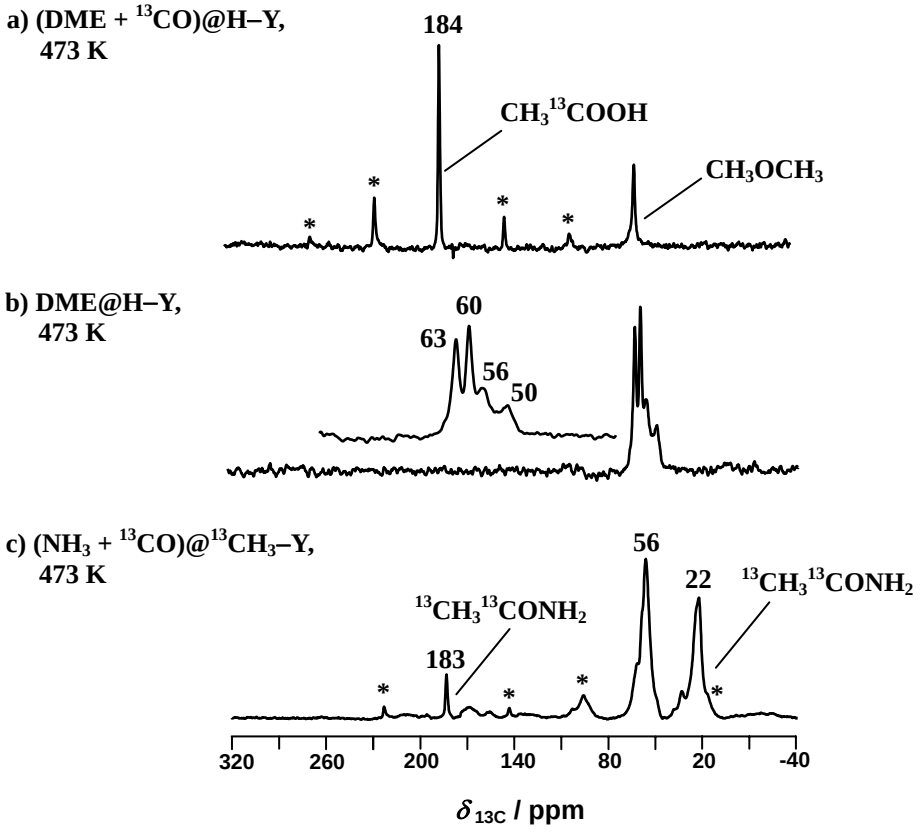

Fig. 8.5 ^{13}C CP MAS NMR spectra recorded after the reaction of dimethyl ether (DME) and ^{13}CO at 473 K on acidic zeolite H-Y (a), after the reaction of DME at 473 K on acidic zeolite H-Y (b), and after the reaction of ammonia and ^{13}CO on methylated zeolite Y ($^{13}CH_3$-Y) at 473 K (c). Asterisks denote spinning sidebands.

As a control experiment, Fig. 8.5b shows the ^{13}C CP MAS NMR spectrum recorded after the reaction of non-enriched DME on acidic zeolite H-Y at 473 K. The signals at 63 and 60 ppm are due to side-on and end-on adsorbed DME, respectively [30]. The signals appearing at 56 and 50 ppm indicate the reversible formation of surface methoxy species and

methanol by the decomposition of DME on acidic zeolites at high temperatures, which agrees well with the work of Iglesia and co-workers [149] and of Forester and Howe [32]. The formation of surface methoxy species, methanol, and water upon the decomposition of DME is, accordingly, depicted in Scheme 8.5. Therefore, the above-mentioned results provide the first ^{13}C MAS NMR evidence for the mechanism of the carbonylation reaction of dimethyl ether by carbon monoxide on acidic zeolites, which was originally proposed by Iglesia and co-workers [149].

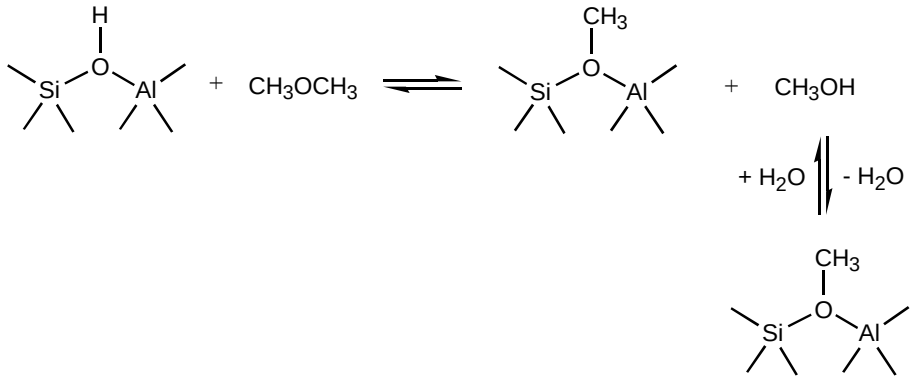

Scheme 8.5 Formation of surface methoxy species, CH_3OH, and H_2O upon the decomposition of DME.

In agreement with previous work [143], formation of the unstable acylium cation, $CH_3–C^+=O$, by the reaction of surface methoxy species and CO, was not directly observed by ^{13}C MAS NMR spectroscopy. However, the transient existence of this cation was further evidenced by the trapping experiment with ammonia, the idea of which was originally presented in the work of Gorte and his co-workers [150]. Fig. 8.5c shows the ^{13}C CP MAS NMR spectrum recorded after the reaction of ^{13}C-enriched carbon monoxide, ammonia, and the methylated catalyst, $^{13}CH_3$-Y, at 473 K. The formation of acetamide, $^{13}CH_3{}^{13}CONH_2$, is evidenced by ^{13}C MAS NMR signals at 22 ppm for the methyl carbon and 183 ppm for the carbonyl carbon. This finding indicates the trapping of unstable acylium cation, $CH_3–C^+=O$ with ammonia, by which the stable product acetamide is formed. The result agrees well with previous work of Gorte and his co-workers [150], who observed the formation of acetamide from the reaction of ammonia and acylium cation on zeolite H-ZSM-5 by TPD-TGA measurements.

8.3.5 Ritter-type Reaction: The Reaction of Surface Methoxy Species and Acetonitrile

Stepanov and Luzgin [151] investigated the reaction of acetonitrile with olefins (1-octene) or

alcohols (*tert*-butyl alcohol) on acidic zeolite H-ZSM-5. In the case of acetonitrile and alcohol coadsorbed on zeolite H-ZSM-5 at room temperature, the intermediate N-alkylnitrilium cation and the final product N-alkylamide were observed simultaneously by MAS NMR spectroscopy. The experimental results were rationalized in accordance with the classic Ritter reaction [151]. Surface alkoxy species react with acetonitrile to produce the intermediate of N-alkylnitrilium cation, which can be further hydrolyzed to form N-alkylamide as the final product [151].

In this dissertation, the reaction of surface methoxy species and acetonitrile on zeolite Y was investigated by ^{13}C MAS NMR spectroscopy. Fig. 8.6a shows the ^{13}C HPDEC MAS NMR spectrum recorded after non-enriched acetonitrile (CH_3CN) was loaded on the methylated zeolite Y ($^{13}CH_3$-Y) at room temperature. Besides the signal of surface methoxy species at 56 ppm, two weak signals of acetonitrile occur at 118 and 0 ppm. No reaction can be observed at this temperature. Upon thermal treatment of the catalyst sample at 473 K for 20 min and subsequent hydrolysis, the ^{13}C HPDEC MAS NMR spectrum shown in Fig. 8.6b was obtained. The broad signal at 27 ppm in Fig. 8.6b is due to the formation of N-methyl acetamide, $CH_3CONH^{13}CH_3$. The broadening of this signal is typically caused by the ^{13}C–^{14}N dipolar coupling, which is strongly affected by the quadrupolar ^{14}N nuclei [152].

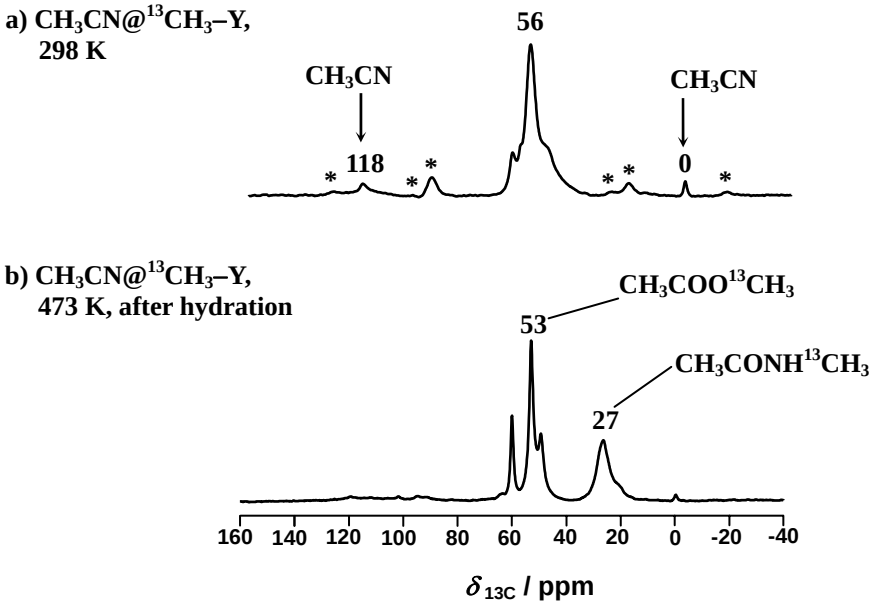

Fig. 8.6 ^{13}C HPDEC MAS NMR spectra recorded after the reaction of acetonitrile on methylated zeolite Y ($^{13}CH_3$-Y) at 298 K (a) and 473 K (b), respectively. Asterisks denote spinning sidebands.

In agreement with Stepanov and Luzgin [151], the formation of N-methyl acetamide observed in Fig. 8.6b is depicted in Scheme 8.6. The additional signal occurring at 53 ppm in Fig. 8.6b is assigned to methyl acetate, $CH_3COO^{13}CH_3$. The formation of methyl acetate is caused by the reaction of surface methoxy species with acetic acid. The latter species can be formed by the hydrolysis of acetonitrile on acidic zeolites [151].

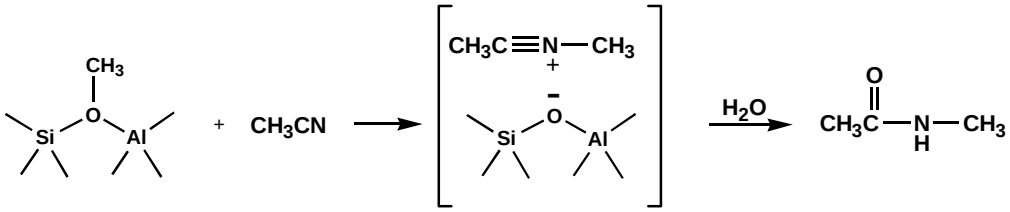

Scheme 8.6 Ritter-type reaction of surface methoxy species and acetonitrile.

8.3.6 Oxidation of Surface Methoxy Species

Recent ^{13}C MAS NMR investigations indicate that the decomposition of surface methoxy species at reaction temperatures of *ca.* 523 K and higher results in the formation of hydrocarbons on acidic zeolite catalysts [31, 128]. Hutchings and Hunter [39] were the first who investigated the conversion of methanol and DME on acidic zeolite H-ZSM-5 at 573 K in the presence of oxygen. It was found that zeolite catalysts were irreversibly deactivated, especially in a fixed-bed reactor at higher oxygen concentrations [39]. The effect of oxygen co-feeding was explained by the formation of formic acid and formaldehyde, the latter of which would undergo polymerization in strong acidic media [39]. Therefore, the influence of low concentration of oxygen on the decomposition of surface methoxy species was investigated by ^{13}C MAS NMR spectroscopy in this disseration. Fig. 8.7 shows the ^{13}C HPDEC MAS NMR spectra recorded after thermal treatments of the methylated catalyst, $^{13}CH_3$-Y, in the presence of oxygen (*ca.* 5 mbar). Carbon monoxide and carbon dioxide are formed at *ca.* 493 K, which give ^{13}C MAS NMR signals at 184 and 124 ppm, respectively (Figs. 8.7b to 8.7e). In agreement with the literature [31, 128], the decomposition of surface methoxy species to hydrocarbons starts at *ca.* 523 K, as indicated in Fig. 8.7c. The hydrocarbons formed in this case (Figs. 8.7c to 8.7e) are essentially identical to those in the absence of oxygen (Fig. 4 in Ref. 31).

It is important to note that the formation of carbon monoxide and carbon dioxide (Fig. 8.6b) starts earlier than the onset of the decomposition of surface methoxy species to hydrocarbons. In agreement with Hutchings and Hunter [39], these NMR results of the

oxidation of surface methoxy species by oxygen (Fig. 8.6) are interpreted as the formation of formaldehyde and formic acid, which further decompose to carbon monoxide and carbon dioxide. Carbon monoxide is neither an intermediate nor a catalyst during the MTO process, as clarified by Munson *et al.* [153]. Therefore, in the presence of oxygen, the oxidation of surface methoxy species competes with the thermal decomposition of surface methoxy species. However, oxygen may not play an active role to initiate the formation of primary hydrocarbons in the MTO process, as implied in previous work of Hutchings and Hunter [39] and in the present study.

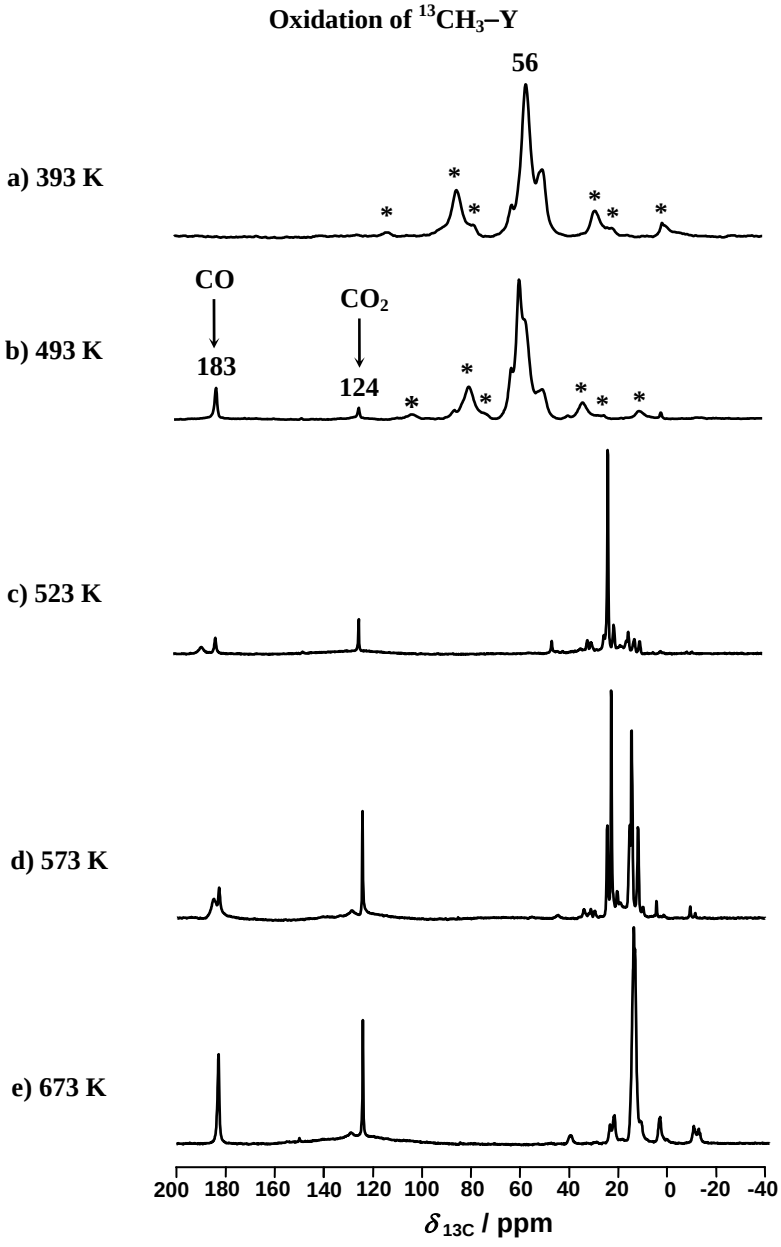

Fig. 8.7 ^{13}C HPDEC MAS NMR spectra recorded after thermal treatments of methylated zeolite Y ($^{13}CH_3$-Y) in the presence of oxygen (5 mbar) at elevated temperatures of 393 (a) to 673 K (e). Asterisks denote spinning sidebands. The methylated catalyst $^{13}CH_3$-Y was *in situ* prepared from ^{13}C-enriched methanol.

8.4 Discussion and Conclusions

Intermediates involved in heterogeneously catalyzed reactions can vary in nature from highly reactive species to relatively unreactive ones. In either case, the life-time of the intermediates must be long enough for successful detection by the spectroscopic method being applied. Similar to the strategy achieved in solution chemistry, it is also possible to further isolate the long-lived intermediates formed in some heterogeneously catalyzed systems and investigate independently their nature and chemical reactivity thereafter. This approach is exemplified in the dissertation where the isolation of surface methoxy species on acidic zeolites can be followed by further investigations of their reactivity with probe molecules. In this section, the stability and reactivity of surface methoxy species are further discussed in comparison with other surface alkoxy species (> C_1 species).

Carbenium ions are key intermediates involved in a variety of acid-catalyzed reactions performed in solution [117]. Due to the low dielectric constants of acidic zeolites and the absence of solvation effects in zeolites [154-155], however, simple carbenium ions may exist as highly-activated and short-lived transition states and, therefore, only represent saddle points on the potential energy surface [119, 122-123]. Indeed, persistent carbenium ions experimentally identified in zeolites are mainly bulky cyclic cations, which are charge-delocalized in nature and sterically hindered to the negatively-charged zeolite framework [156]. On the other hand, covalent alkoxy species [118, 121, 127] have been consistently observed as long-lived intermediates upon the adsorption of small olefins or dehydration of simple alcohols on acidic zeolites. In 1989, Gorte and co-workers [119] first identified by ^{13}C NMR spectroscopy the formation of surface *tert*-butoxy species upon the adsorption of *tert*-butyl alcohol on acidic zeolite H-ZSM-5. Later in the same year, Haw *et al.* [121] reported the ^{13}C CP MAS NMR evidence for surface isopropoxy species formed from the reaction of propene on acidic zeolite H-Y. Subsequently, Stepanov and co-workers detected by ^{13}C NMR spectroscopy the formation of surface isobutoxy species upon the conversion of isobutanol [120] and the formation of oligomeric alkoxy species upon adsorption of ethene [147], both on acidic zeolite H-ZSM-5. IR investigations on the formation of oligomeric alkoxy species upon adsorption of ethene and propene on acidic zeolites H-ZSM-5 and H-Mordenite were reported by Zecchina and co-workers [157]. Adding to the rare evidence for the existence of surface alkoxy species (> C_1 species), surface ethoxy species formed from ethanol was recently observed on acidic zeolites H-Mordenite [158] and

H-Y [127]. The reactivity and the carbenium-ion-like nature of surface alkoxy intermediates formed in acidic zeolites were addressed in the pioneering work of Gorte and co-workers [119, 154]. Nevertheless, knowledge on the reactivity of surface alkoxy species (> C_1 species) is still severely lacking so far, largely due to the occurrence of rapid secondary reactions on the solid catalysts, which hindered the isolation of primary intermediates and complicates the interpretation of experimental results.

In contrast, surface methoxy species, *i.e.,* the simplest form and probably the most stable form of surface alkoxy species, have been extensively investigated, mostly in connection with mechanistic studies of methanol-to-hydrocarbons conversion on solid acids [4]. Table 8.1 summarizes IR and NMR evidence for the formation of surface methoxy species upon the reactions of methanol on various solid acids. In spite of the unequivocal observation of surface methoxy species on solid acids, the role of these surface methoxy species in heterogeneous catalysis has been disputed in a controversial manner. The reactivity of surface methoxy species in acidic zeolites may be better discussed in terms of C–O bond and C–H bond activation. The C–O bond reactivity of surface methoxy species has been evidenced by reactions with various probe molecules, some of which are included in Tab. 8.1. For example, surface methoxy species on acidic zeolites can react with water [31] to produce methanol at room temperature, with methanol [30] to form DME, with aniline to N-methylanilinium cations [133-134], with benzene [32, 159] or toluene [31] to alkyl-substituted aromatics (such as, toluene, xylenes and ethylbenzenes). Furthermore, they react with ethylene or propylene to produce olefins, which may undergo further oligomerization reactions [32]. The results in the present work further indicate that surface methoxy species can react with ammonia, alkyl halides, hydrochloride, carbon monoxide (Koch-type carbonylation reaction), and acetonitrile (Ritter-type reaction). Therefore, surface methoxy species act as an effective methylating agent in a variety of reactions with reactant molecules on solid acids, in which the C–O bond activation of surface methoxy species is involved.

The relative reactivity of surface alkoxy species in terms of C–O bond activation can be evaluated in benefit of recent theoretical investigations [124-125, 161] of olefin adsorption on acidic zeolites. As depicted in Fig. 8.8, the adsorption of small olefins on acidic zeolites starts with the formation of a π–complex (**2A** for ethene, **3A** for propene and **4A** for isobutene in Fig. 8.8) and, through a transition state, which most probably involves carbenium cations

Tab. 8.1 Experimental observations of surface methoxy species formed from methanol on solid acid catalysts.

Solid Acid	Reactant	Assignments of Surface Methoxy species and Additional Observations	Ref.
H-ZSM-5, n_{Si}/n_{Al} = 15, 26	CH_3OH, CD_3OH [a]	IR bands: 2980, 2868 and 1460 cm^{-1} (CH_3-ZSM-5); responsible for the methylation of olefins and benzene at 523 K; the onset of significant hydrocarbon formation is accompanied by the cleavage of C–D bonds in CD_3-ZSM-5 above 523 K.	[32]
H-Y (n_{Si}/n_{Al} = 1.9, 86 % ion exchange degree)	CH_3OH [b]	IR bands: 2800-3100 cm^{-1} (CH_3-Y); secondary reactions take place above 513 K with the formation of hydrocarbons.	[21]
H-ZSM-5 (n_{Si}/n_{Al} =17.8)	CD_3OH [b]	IR bands: 2220 and 2070 cm^{-1} (CD_3-ZSM-5); stable up to 512 K; desorption of surface methoxy groups is accompanied by the cleavage of C-D bonds.	[37]
H-Y (n_{Si}/n_{Al} = 2.5, 70 % ion exchange degree) Dealuminated H-Y (n_{Si}/n_{Al} = 12) H-ZSM-5 (n_{Si}/n_{Al} = 14, 18, 19)	CH_3OH [b]	IR bands: 2855-3000 and 2855 cm^{-1}; highly reactive above 573 K and readily participate in the formation of C-C bonds at 523-623 K.	[160]
H-Y (n_{Si}/n_{Al} = 2.5, 72 % ion exchange degree)	CH_3OH, CD_3OD [b]	IR bands: 2980 and 2850 cm^{-1} (CH_3-Y), 2130 and 2070 cm^{-1} (CD_3-Y); reaction with benzene at 533 K and decomposition above 581 K.	[159]
H-ZSM-5 (n_{Si}/n_{Al} = 24, 42, 78, 154)	CH_3OH [b]	IR bands: 2980, 2959 and 2855 cm^{-1} (CH_3-ZSM-5); decomposition above 573 K.	[162]
H-ZSM-5 (n_{Si}/n_{Al} = 27)	CH_3OH [b]	IR bands: 2856–2978 cm^{-1} (CH_3-ZSM-5); involved in the dehydration of methanol to DME at 493 K.	[163]
H-X (n_{Si}/n_{Al} = 1.1, ion exchange degree 40 %) H-Y(n_{Si}/n_{Al} = 2.6, ion exchange degree 40 % and 77 %)	CH_3OH [b]	IR bands: 2968 cm^{-1} (CH_3-X) and 2977 cm^{-1} (CH_3-Y); responsible for benzene methylation; decomposition at 570 K with the formation of hydrocarbons.	[164]

H-ZSM-5 (n_{Si}/n_{Al} = 35)	CH_3OH + NH_3 [c]	IR bands: 2957 and 2855 cm^{-1} (CH_3-ZSM-5).	[132]
H-Y (n_{Si}/n_{Al} = 2.6) H-ZSM-5 (n_{Si}/n_{Al} = 22)	$^{13}CH_3OH$ [b]	^{13}C MAS NMR signals: 56 ppm ($^{13}CH_3$-Y), 59.4 ppm ($^{13}CH_3$-ZSM-5).	[128]
H-Y (2.7, 90 % ion exchange degree), H-ZSM-5 (n_{Si}/n_{Al} = 22) H-SAPO-34 ($n_{Si}/(n_{Al}+n_{Si}+n_P$= 0.11)	$^{13}CH_3OH$[b,c]	^{13}C MAS NMR signals: 56.2 ppm ($^{13}CH_3$-Y), 59.2 ppm to ($^{13}CH_3$-ZSM-5), 56.6 ppm ($^{13}CH_3$-SAPO-34); react with water to methanol, with methanol to DME, with toluene to xylenes; decomposition at 523 K, responsible for the formation of hydrocarbons and for the methylation of cyclohexane.	[30-31]
H-Y (n_{Si}/n_{Al} = 2.6)	$^{13}CH_3OH$ + aniline [b]	^{13}C MAS NMR signals: 56 ppm ($^{13}CH_3$-Y); responsible for aniline methylation at 373 to 523 K.	[133]
H-ZSM-5 (n_{Si}/n_{Al} = 19, 26) H-Mordenite (n_{Si}/n_{Al} = 9)	$^{13}CH_3OH$ [b]	^{13}C MAS NMR signals: 59.9 ppm ($^{13}CH_3$-ZSM-5), 60.7 ppm ($^{13}CH_3$-Mordenite).	[165]
H-SAPO-34 (n_{Si}/n_{Al} = 0.17) H-ZSM-5 (n_{Si}/n_{Al} = 28, 36, 40)	$^{13}CH_3OH$ [b]	^{13}C MAS NMR signals: 53–59 ppm ($^{13}CH_3$-ZSM-5), 57 ppm ($^{13}CH_3$-SAPO-34).	[166]
H-ZSM-23 (n_{Si}/n_{Al} = 35) H-SAPO-11 (n_{Si}/n_{Al} = 0.25) H-SAPO-5 (n_{Si}/n_{Al} = 0.25)	$^{13}CH_3OH$ [b]	^{13}C MAS NMR signals: 56–62 ppm; form at the onset of hydrocarbon formation.	[167]
H-SAPO-34 (1.1 mmol/g)	$^{13}CH_3OH$ [d]	^{13}C MAS NMR signals: 56 ppm ($^{13}CH_3$-SAPO-34); decreases dramatically in the first 30 s during which the initiation reaction of MTO catalysis takes place.	[49]
Sulfated Zirconia	$^{13}CH_3OH$ [d]	^{13}C MAS NMR signals: 59 ppm; formation of surface methoxy species and hydrocarbons is observed 2 s after methanol injection.	[168]

[a] *in situ* IR cell as a pulse microreactor; [b] batch-like conditions; adsorption and evacuation; [c] flow conditions; [d] pulse-quench experiment; [e] IR bands of surface methoxy species summarized therein.

(**2B**, **3B** and **4B** in Fig. 8.8), the corresponding surface alkoxy species (σ–complex, **2C**, **3C** and **4C** in Fig. 8.8) are formed. Although the energy difference of species in Fig. 8.8 can not be quantitatively compared, the basic trends for their relative stability are evident. For example, theoretical calculations [124, 161] predict that the relative stability of surface alkoxy species being formed upon adsorption of corresponding olefins on acidic zeolites follows the order ethoxy (**2C**) > isopropoxy (**3C**) > *tert*-butoxy (**4C**). On the other hand, it is well known that primary carbenium-ion-like transition states exhibit much higher activation energies than tertiary carbenium-ion-like transition states, which results in the relative stability of carbenium ions in the order **4B** > **3B** > **2B** in Fig. 8.8, assuming that the energies for the corresponding π–complex (**2A**, **3A** and **4A** in Fig. 8.8) do not have much difference. In contrast to the case of alkoxy species (> C_1 species) formed from olefin adsorption on acidic zeolites, theoretical calculations have been dealing with the formation of surface methoxy species from dehydration of methanol only, which makes the systematic comparison complicated. Nevertheless, it is still reasonable to add methoxy species (**1C**) as the most stable alkoxy species and, accordingly, methyl cations (**1B**) as the most unstable carbenium cations in Fig. 8.8. The reactivity of surface alkoxy species in terms of C–O bond activation can be, therefore, discussed by looking into the energy differences from **C** to **B** in Fig. 8.8, which are directly related to the activation energies being considered.

The following results may be derived: i) according to the Hammond Postulate [169], the surface *tert*-butoxy species would possess more carbenium-ion-like nature than other alkoxy species presented in Fig. 8.8. On the contrary, the covalent-bond nature is more profound in the case of surface methoxy species. Indeed, theoretical calculations [170] do indicate that the C–O bond distances decrease in the order tertiary > secondary > primary alkoxides from 163 to 150 pm. ii) The nucleophilic substitution reaction with surface methoxy species is more S_N2-mechanism oriented, which means that the reaction is achieved in a single step and both nucleophile (reactant molecules) and surface methoxy species take part in the transition state. The involvement of reactant molecules in the transition state will, more or less, decrease the activation energy in comparison with the energy difference between **1C** and **1B** in Fig. 8.8. This explains why the reactions of surface methoxy species with reactant molecules having high nucleophility (water, ammonia or methylamines) take place at room temperature, while with low nucleophility (hydrochloride, carbon monoxide or acetonitrile) higher reaction temperatures are required. On the contrary, S_N1-mechanism may dominate the nucleophilic substitution reaction of the bulky *tert*-butoxy species on acidic zeolites. In

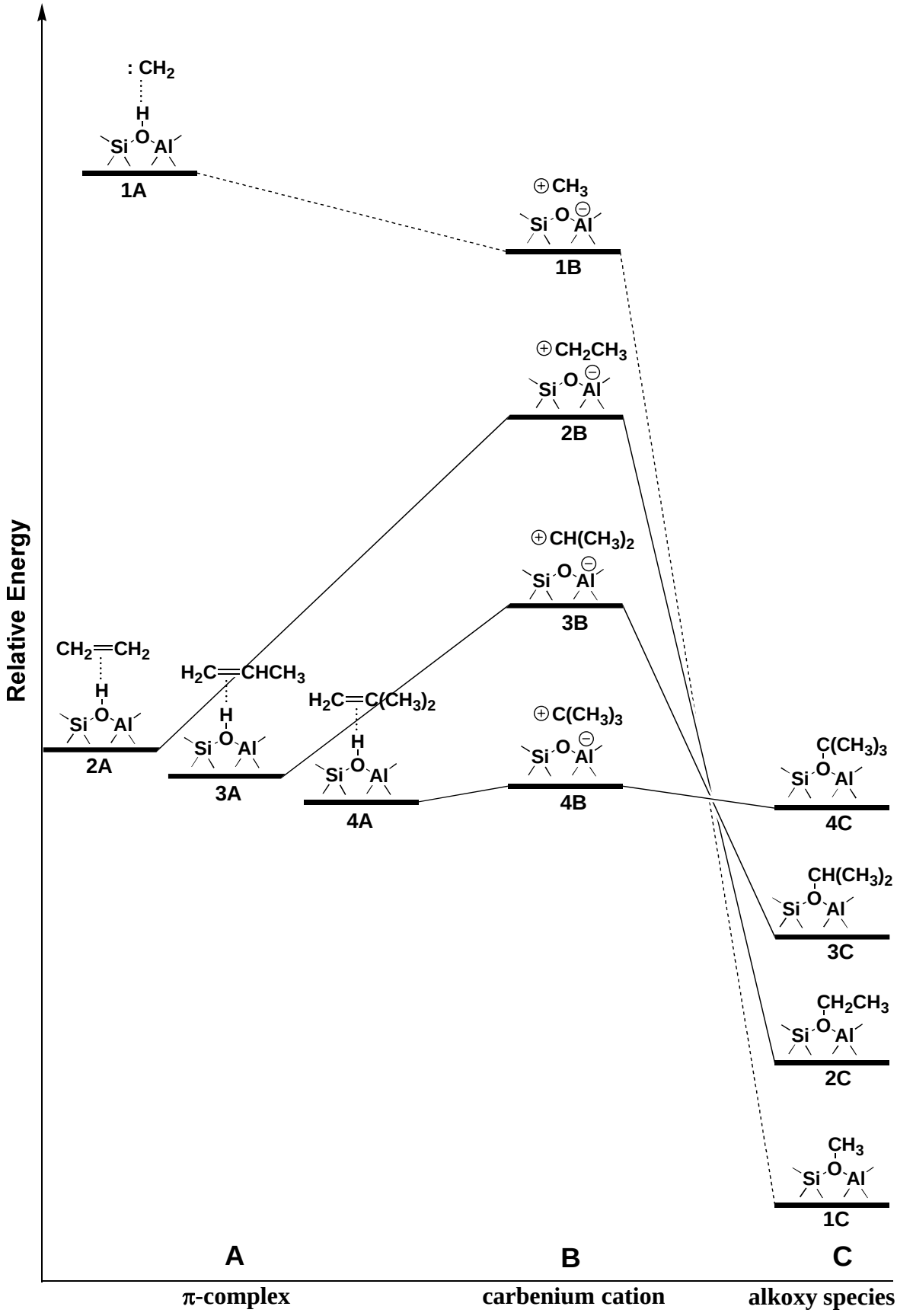

Fig. 8.8 Energy profile for the formation of surface alkoxy species derived from theoretical investigations [122-126].

this case, the presence of reactant molecules does not contribute significantly in the rate-determining step in which the transition state largely resembles free carbenium ions. Therefore, the activation energy in this step should be close to the energy difference between **4C** and **4B** shown in Fig. 8.8.

A further issue is the C–H bond activation of surface methoxy species in the absence of other reactants and at reaction temperatures higher than *ca.* 523 K. This topic is directly related to mechanistic investigations of the first C–C bond formation in the MTO process [4]. Some of experimental observations on the C–H bond activation of surface methoxy species are summarized in Tab. 8.1. For example, Ono and Mori [37] reported the IR evidence for the formation of surface methoxy groups on zeolite H-ZSM-5 from CD_3OH and showed that the desorption of surface methoxy species from the catalyst is accompanied by the cleavage of C–D bonds at temperatures higher than 512 K. By *in situ* IR spectroscopy, Forester and Howe [32] observed that the onset of significant hydrocarbon formation is correlated with the cleavage of C–D bonds in CD_3-ZSM-5 above 523 K. Datka *et al.* [164] found that the decomposition of surface methoxy species on zeolites H-X and H-Y results in the formation of C_2–C_5 olefins and a small amount of alkanes. They proposed that disproportionation of olefins would form alkanes and aromatics (coke, IR bands at 1590 cm^{-1}) [164]. By ^{13}C MAS NMR spectroscopy, it was found that decomposition of surface methoxy species at 523 K and above is responsible for the formation of first hydrocarbons on zeolites H-Y and H-ZSM-5 and on silicoaluminophosphate H-SAPO-34 [31, 128]. A very recent investigation [171] on the conversion of chloromethane on H-SAPO-34 indicated that chloromethane can be efficiently converted to light olefins in the temperature range of 623 to 773 K. The *in situ* IR observations clarified the formation of surface methoxy species as intermediate products [171]. Decomposition of surface methoxy species or coke deposition from incomplete calcination is suggested as possible origins for the formation of the first reaction centers [171].

Concerning the detailed mechanism for the C-H bond activation upon decomposition of surface methoxy species, it has been suggested that reactive intermediates with carbene or ylide nature are very likely formed [4, 39]. Indirect evidence for the existence of carbene as transient species was, for example, obtained by using cyclohexane as a trapping agent during the decomposition of surface methoxy species [31]. The formation of methylcyclohexane implies the transient existence of carbene, which undergoes the typical sp^3 insertion into the

C–H bonds [31]. The oxidation reaction of surface methoxy species in this contribution might be looked upon as an additional evidence for carbene mechanism. According to Hutchings and Hunter [39], the formation of formic acid upon the oxidation of surface methoxy species indicates the existence of carbene, which further reacts with oxygen *via* the Criegee intermediate [172]. Furthermore, Sinclair and Catlow [173] performed DFT calculations to investigate the decomposition of surface methoxy species on acidic zeolites and showed that surface-stabilized carbene (**1A** in Fig. 8.8) could be produced with an activation barrier of 215-232 kJ mol^{-1}. The deprotonation step (from **1C** to **1A** in Fig. 8.8) was, therefore, suggested as the rate-determining step during the conversion of methanol to hydrocarbons. In agreement with the value reported by Sinclair and Catlow [173], Lesthaeghe *et al.* [174] recently calculated a theoretical barrier of 241 kJ mol^{-1} for the deprotonation of surface methoxy species to carbene. Considering this step as a highly activated one, however, they ruled out the deprotonation of methoxy species to carbene as a possible direct route for the first C–C bond formation during methanol conversion [174]. It was recently claimed that [175], in contradiction to a number of previous investigations listed in Tab. 8.1, the C–H bonds of surface methoxy species are not broken at temperatures between 573 and 623 K, supported by the absence of H/D exchange between CH_3-SAPO-34 and CD_3-SAPO-34 coexisting on the catalyst. However, the direct evidence for the failure of C–C bond formation from these surface methoxy species, *i.e.*, the yields of olefin products and the H/D distribution in these olefins was not disclosed therein [175], although GC and GC-MS were applied to analyze the effluent gases.

The *in situ* stopped-flow protocol [30] opens a new approach to the understanding of the nature of surface methoxy species on solid acidic catalysts. On the basis of this development, the main focus of the present work was, therefore, to further investigate the chemical reactivity of surface methoxy species in acidic zeolites. By ^{13}C MAS NMR spectroscopy, the following evidence for the high reactivity of surface methoxy species are obtained for the first time on solid acid catalysts:

i) Surface methoxy species react with ammonia on acidic zeolite H–Y and silicoaluminophosphate H–SAPO-34 at room temperature, by which methylamines and methylammonium cations are formed. On the contrary, methanol and ammonia do not react on acidic zeolites at room temperature. The significant difference in reactivity between surface methoxy species and methanol indicates that surface methoxy species are very reactive in methylating amines on acidic zeolites.

ii) The transformation of surface methoxy species to surface ethoxy species or other alkoxy species can be achieved by the reaction of surface methoxy species and corresponding alkyl halides on acidic zeolites. This new approach may provide a general method for the preparation of surface alkoxy species from surface methoxy species on solid acid catalysts.

iii) Surface methoxy species react readily with hydrochloride, by which methyl chloride is produced as the sole product. These results indicate that surface methoxy species may be involved in methanol hydrochlorination on solid catalysts.

iv) In agreement with the recent work of Iglesia and co-workers [149], the carbonylation of dimethyl ether by carbon monoxide on acidic zeolites is interpreted as similar to the classic Koch-type reaction in solution, where the unstable acylium cation, $CH_3–C^+=O$, is formed by the reaction of surface methoxy species and CO.

v) In accordance with the Ritter-type reaction on solid acid catalysts [150], the formation of N-methyl acetamide was interpreted by further hydrolysis of the intermediate, N-alkylnitrilium cation, after the reaction of surface methoxy species and acetonitrile on acidic zeolites.

vi) Carbon monoxide and carbon dioxide can be produced by the oxidation of surface methoxy species on acid zeolites in the presence of oxygen. The oxidation of surface methoxy species may compete with the thermal decomposition of surface methoxy species. However, oxygen may not play an active role to initiate the formation of primary hydrocarbons in the induction period of the MTO process.

9 Coke Formation during the Methanol-to-olefin Conversion on Acidic Zeolites H-SAPO-34 in the Fixed-bed Reactor Characterized by *In Situ* UV/Vis and MAS NMR Spectroscopy

9.1 Introduction

Nowadays, it is well accepted that the steady state of the methanol-to-olefins process is dominated by the "hydrocarbon-pool" route [45-47]. In this case, methanol is added onto reactive organic species, such as large olefins, methylbenzenes, and cyclic carbenium ions, while light olefins are formed *via* elimination from these species. However, the further development of large organic compounds acting as coke trapped in the cages of acidic zeolite catalysts is the most important origin of catalyst deactivation in industrial processes. Therefore, finding ways to limit catalyst deactivation by coke formation and to regenerate coked catalysts is an important economical objective [29]. Due to the specific effects of the micropore system and catalytically active Broensted sites in zeolites, the investigation of hydrocarbon-pool compounds and coke deposits is obviously a severe and complex task in the field of heterogeneous catalysis [52].

As described in Chapter 5, the development and rigorous application of the complementary *in situ* NMR-UV/Vis spectroscopic technique to study the catalytic solid under real working conditions inside the reactor results in fundamental knowledge about the catalytic process in terms of active sites, reaction intermediates and reaction mechanism. On the other hand, a great restriction for almost industrial application of ^{13}C MAS NMR investigations is to work with enriched reactants, which is so expensive that it is nearly impossible to further utilize as a tool to gather information for a pilot design of the majority processes under working conditions in the field of heterogeneous catalysis. Furthermore, normally a great amount of petrochemical reactions take place at high temperatures. According to the Curie's law [85], the signal-to-noise ratio of ^{13}C MAS NMR spectra at higher temperature become much worse, which causes a troublesome challenge for further evaluation.

Thus, this chapter will focus on the study of coke formation and its regeneration during the methanol conversion on the working acidic zeolite catalyst H-SAPO-34 in a standard fixed-bed reactor by on-line GC and *in situ* UV/Vis spectroscopy under continuous flow

conditions. In this study, the commercial non-enriched methanol was used as the reactant instead of the expensive ^{13}C-enriched material. Therefore, no investigations of the catalytic reaction by *in situ* ^{13}C MAS NMR spectroscopy were performed in this case. In addition, after the deactivation of the catalyst, the coke deposits formed in the fixed-bed reactor were characterized at room temperature by various analysis methods including *ex situ* ^{13}C MAS NMR spectroscopy, C and H elemental composition analysis (CH analysis), and TGA analysis. Among these techniques, semi-quantitative ^{13}C MAS NMR spectra could give the content of aromatic compounds and alkyl groups per aromatic ring under reaction conditions. On the basis of the NMR evaluation, the results of CH and TGA could offer the mean concentration of aromatic compounds and alkyl groups per aromatic ring.

9.2 Experimental Part

9.2.1 Experimental Equipment

In contrast to the equipment shown in Fig. 5.14, a standard fixed-bed reactor equipped with an *in situ* UV/Vis spectroscopy was applied in Fig. 9.1.

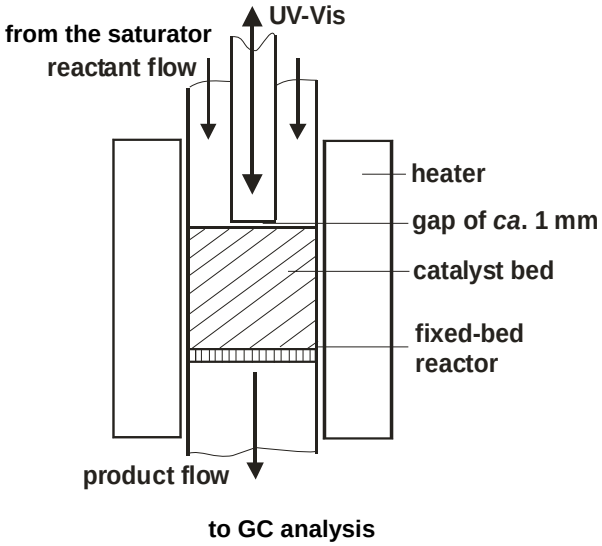

Fig. 9.1 Scheme of the standard fixed-bed reactor equipped with *in situ* UV/Vis spectroscopy at the top with a gap of *ca.* 1 mm between the catalyst bed and the tip of the fiber optics.

The fixed-bed reactor with an inner diameter of 8 mm was filled with 300 mg of dry catalysts. During the catalytic measurements, a flow of methanol according to a modified residence time of W_{cat}/F_{me} = 25 g h/mol loaded by dry nitrogen as the carrier gas was

introduced. The glass fiber optics of the UV/Vis spectrometer was installed on top of the fixed-bed reactor with a gap of *ca.* 1 mm between the catalyst bed and the tip of the fiber optics. *Via* the fiber optics, the catalyst sample inside the standard fixed-bed could be *in situ* investigated by the fiber optics UV/Vis spectrometer. Reference UV/Vis spectra of calcined H-SAPO-34 were recorded at the reaction temperature prior to introducing reactants. UV/Vis measurements between 200 and 600 nm in the diffuse reflection mode were conducted with an HPSUV1000A fiber optic spectrometer, an AvaLight-DH-S deuterium light source, and a glass fiber reflection probe FCR-7UV20-3-SR-S1 by Avantes. Narrow peaks at *ca.* 460 and 500 nm occurring in some of the UV/Vis spectra are caused by the equipment.

9.2.2 Catalytic Reaction Conditions

H-SAPO-34 samples were prepared and characterized as depicted in Chapter 6. Prior to the catalytic investigations, about 300 mg of calcined catalysts were filled into the standard fixed-bed reactor. After transferring the reactor inside the oven, an additional dehydration of the catalyst was performed with a heating rate of 1 K/min up to 673 K under flowing nitrogen (30 ml/min). Then, the catalyst was kept at the respective reaction temperatures for a given reaction time. In some cases, a continuous flow of ^{13}C-enriched methanol with a modified residence time of W_{cat}/F_{me} = 25 g h/mol was subsequently injected into the fixed-bed reactor. The exhaust from the reactor was led to the sampling loop for online GC analysis. Simultaneously, a snapshot of the coke deposits formed on the catalyst bed was taken by *in situ* UV/Vis spectroscopy. The volatile reaction products escaping from the bottom of the fixed-bed reactor were detected *via* an on-line GC HP 5890 (Hewlett Packard) equipped with a Coating Poraplot Q capillary column (Chrompack Plot fused silica, length 50 m, inner diameter 0.32 mm). The exhaust flow containing the volatile reaction products was sampled and analyzed in steps of 15 min. A constant flow of methane (8 ml/min), added to the methanol feed, was used as an internal GC standard and allowed a quantification of the reaction products.

Furthermore, the partially coked catalysts formed in the fixed-bed reactor were transferred to a 7 mm MAS NMR rotor in a glove box without any contact with air for further quantitative *ex situ* ^{13}C MAS NMR measurements, complemented with CH analysis and thermogravimetric analysis (TGA). ^{13}C MAS NMR characterization was performed with a 7 mm Bruker MAS NMR probe on a Bruker MSL 400 spectrometer at the ^{13}C resonance

frequency of 100.6 MHz. ^{13}C HPDEC MAS NMR spectra were recorded after an excitation with a $\pi/2$ pulse and with a repetition time of 5 s. For ^{13}C spin-counting experiments, a repetition time of 30 s and an external intensity standard (dehydrated zeolite H-SAPO-34 loaded with $^{13}CH_3OH$) were applied. The sample spinning rate of *ca.* 3.5 kHz was applied. All ^{13}C MAS NMR spectra were referenced to TMS. The decomposition and simulation of NMR spectra were performed using the Bruker software WINNMR and WINFIT. The elements C and H of the coked catalysts under study were determined by element analysis on an Elementar Vario EL instrument. TGA analysis (SETRAM Setsys 16/18) of the coked samples was performed under the synthetic air flow rate of *ca.* 20 ml/min at a heating rate of 10 K/min up to 873 K.

9.3 Results and Discussion

9.3.1 Study of Coke Formation during the Methanol Conversion on H-SAPO-34 by *In Situ* UV/Vis Spectroscopy and Online GC Analysis

Fig. 9.2 shows stack plots of UV/Vis spectra (a) recorded at 673 K during the methanol conversion under working conditions in the standard fixed-bed reactor as a function of time-on-stream during the first 165 minutes and the yields of ethylene ($C_{2=}$), propylene ($C_{3=}$), butenes($C_{4=}$), and pentenes (($C_{5=}$) as determined by online GC given in wt. %. After the induction period of methanol conversion, the yields of light olefins tend to be stable, which indicates that the reaction reached the steady state. The yields of ethylene, propylene, butene, and pentene were *ca.* 35.0, 43.0, 13.0, and 2.0 %, respectively. With a long time-on-stream at the reaction temperature of 673 K, an increase of ethylene selectivity and a decrease of propylene selectivity took place upon the H-SAPO-34 catalyst approached deactivation. The UV/Vis bands at 245 and 280 nm indicate the presence of non-protonated dienes or aromatics and polyalkylaromatics, respectively [115, 177]. The weak band at 345 nm can be explained by dienylic carbenium ions. The strong band occurring at 400 nm is a hint for the formation of non-protonated polycyclic aromatics. In addition, it was also evidenced that the formation of polycyclic aromatics, which are typical for coke deposits, already started at the reaction temperature of 673 K. It is important to note that the stack plot of UV/Vis spectra also shows slightly separated bands at 385 to 425 nm with increasing time-on-stream. This finding indicates that a more detailed assignment of the bands at 385 to 425 nm is possible.

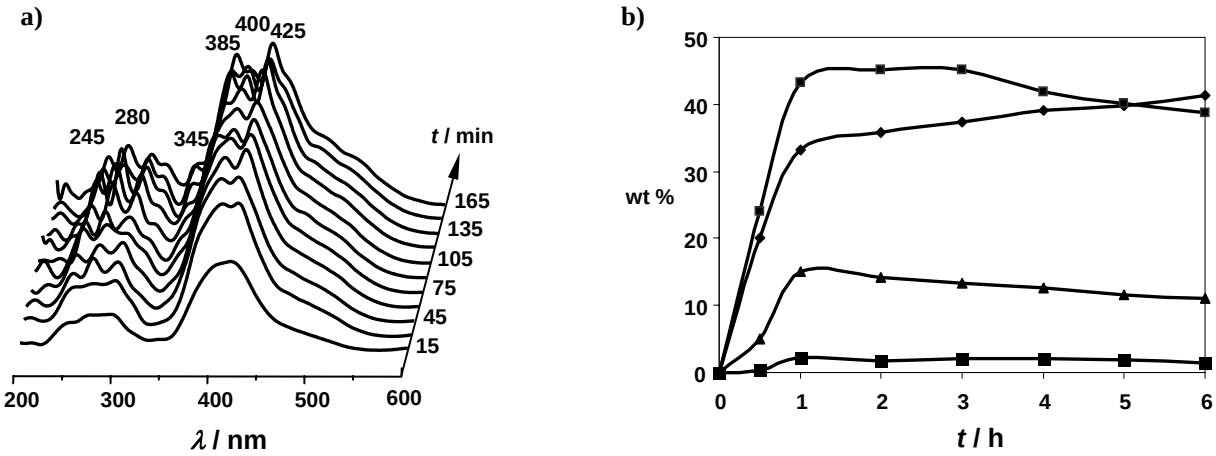

Fig. 9.2 Stack plot of UV/Vis spectra recorded during the first minutes of the methanol conversion (W_{cat}/F_{me} = 25 gh/mol) on H-SAPO-34 at the reaction temperature of 673 K in the standard fixed-bed reactor as a function of the reaction time (a) and the yields of ethylene (—◆— $C_{2=}$), propylene (—■— $C_{3=}$), butenes (—▲— $C_{4=}$), and pentenes (—■— $C_{5=}$) as determined by on-line GC given in wt. % (b).

Fu *et al.* [180] studied the nature of coke deposits formed upon conversion of 50 % by grinding of the catalyst framework, extraction of the carbonaceous compounds, and GC-MS analysis. The authors identified various naphthalenes, phenantrenes, and pyrenes acting as coke deposits. Applying ultraviolet Raman spectroscopy, Chua and Stair [181] investigated the conversion of methanol on H-ZSM-5 at 473 K under *in situ* conditions. The best assignment of the bands of organic deposits, which they observed, was reached by adsorption of pentacene as a reference material. Therefore, the formation of polycyclic aromatics with chain-like topology was suggested by these authors. One of the above-mentioned compounds is anthracene, which was investigated by Stepanenko *et al.* [178] utilizing laser-induced fluorescence spectroscopy. These authors observed well-resolved bands at 385 nm for 9-methylanthracene and at *ca.* 380 and 425 nm for 9,10-dimethylanthracene (9,10-DMA). In the present work, therefore, 9,10-DMA was studied as a reference material upon adsorption on dehydrated siliceous MCM-41. After heating physical mixtures of 9,10-DMA and MCM-41 at 453 K for 0.5 h, the UV/Vis spectra shown in Fig. 9.3 were recorded. At a low loading of MCM-41 with 9,10-DMA (Fig. 9.3a), a broad band at 400 nm occurred, comparable to the UV/Vis bands recorded shown in Fig. 9.2. At a high loading of MCM-41 with 9,10-DMA (Fig. 9.3b), different bands could be identified at *ca.* 370 to 410 nm. Hence, with increasing amounts of anthracene, more distinct UV/Vis bands occur in the spectral range, which is characteristic for the UV/Vis bands of organic deposits in the spectra shown in Fig. 9.2.

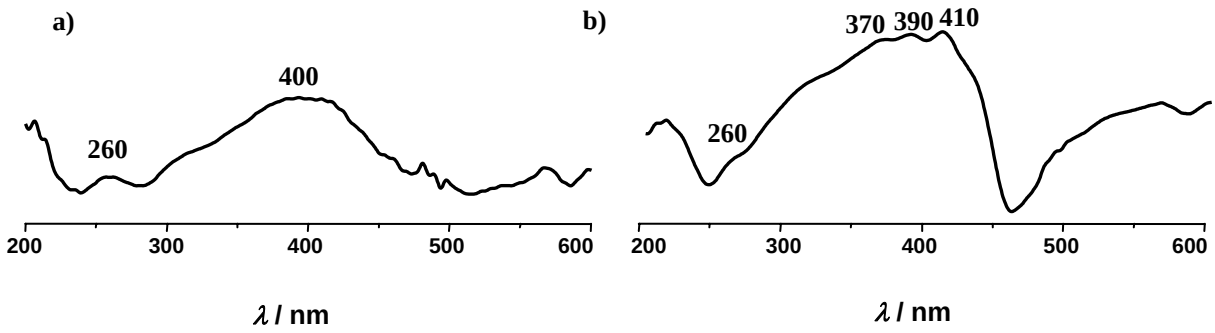

Fig. 9.3 UV/Vis spectra of 9, 10-dimethylanthracene (9,10-DMA) loaded on dehydrated (723 K for 12 h) mesoporous MCM-41 material with weight ratios of m_{DMA}/m_{MCM41} = 0.2:1 (a) and 0.5:1 (b). After adding 9,10-DMA to dehydrated MCM-41, the mixtures were heated at 453 K for 0.5 h.

The effect of the amount of coke deposits on the detailed position and shape of bands at *ca.* 400 nm was studied by *in situ* UV/Vis spectroscopy during the first minutes of the methanol conversion on H-SAPO-34 at 673 K. Only after increasing the time-on-stream up to at least *ca.* 45 minutes, the bands at 400 to 425 nm dominated the UV/Vis spectra and showed a weak splitting. This band splitting was similar to the behavior of the spectra in Fig. 9.3. Hence, the different positions and shapes of UV/Vis bands observed at 385 to 425 nm in the spectra in Fig. 9.2 may be due to different amounts of similar polycyclic aromatics with chain-like topology, such as polymethylanthracenes.

9.3.2 Quantitative Evolution of Coke Deposits Formed during the Methanol Conversion on H-SAPO-34 in the Fixed-bed Reactor

The partially coked catalysts formed in the above-mentioned fixed-bed reactor at the reaction temperature of 673 K for 6 h were transferred to a 7 mm Bruker MAS NMR rotor in a glove box without any contact with air for further quantitative characterization by ^{13}C MAS NMR measurements, which were complemented with CH elemental analysis and TGA analysis. Hereby, it is important to mention that the coked catalysts contain a great amount of non-enriched carbon atoms. Nevertheless, a ^{13}C MAS NMR spectrum with a high resolution was obtained by recording at room temperature as shown in Fig. 9.4a. The spectra are dominated by signals at *ca.* 18 ppm due to ^{13}C atoms of alkyl groups, most of which are methyl groups. The broad resonances from 125 to 133 ppm might be assigned to aromatic compounds. These signals further evidence the formation of polyalkylaromatics on the partially coked H-SAPO-34 catalysts. In Fig. 9.4b, the simulation of the ^{13}C MAS NMR spectrum allows the

quantitative evaluation by the Bruker software WINFIT.

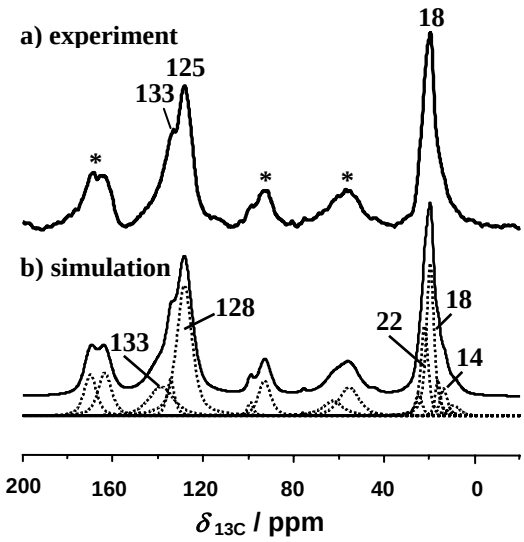

Fig. 9.4 Simulation of the ^{13}C MAS NMR spectrum recorded at room temperature after methanol conversion (W_{cat}/F_{me} = 25 gh/mol) on H-SAPO-34 at the reaction temperature of 673 K for 6 h in the standard fixed-bed reactor with a sample spinning frequency of 3.5 kHz. Asterisks denote spinning sidebands. The simulation was performed with the Bruke software WINFIT.

Table 9.1 gives a summary of the composition of organic deposits on the partially coked H-SAPO-34 catalysts. In column 1 of Tab. 9.1, the percentages of organic components were derived from the simulation of the ^{13}C MAS NMR spectrum in Fig. 9.4. On the other hand, the total amount of organic deposits in the cages was determined by CH and TGA measurements. On the basis of the contents obtained from ^{13}C MAS NMR spectrum, the absolute concentration of alkyl groups and aromatic compounds in column 2 and 3 of Tab. 9.1 were calculated. It was found that the content of methyl groups bound to aromatics is much higher than that of ethyl groups bound to aromatics, which might evidence that polymethylbenzenes act as active hydrocarbon compounds. It is obvious to note that the concentrations, which were obtained by CH element analysis, are slightly higher than those obtained by TGA analysis. It might be indicated that after burning off the coked catalysts by synthetic air at 873 K during TGA analysis, there was still a small amount of remaining organic compounds, which could be parts of the dark coke that cannot be easily removed during the regeneration process with synthetic air.

Tab. 9.1 Quantitative evaluation of organic deposits in the chabazite cages ($T_{12}O_{24}$: 1.38 mmol/g) of H-SAPO-34 upon conversion of non-enriched methanol at 673 K with the residence time of W_{cat}/F_{me} = 25 gh/mol in the standard fixed-bed reactor. The percentages of organic components were derived from the simulation of the ^{13}C MAS NMR spectrum, and the total amounts of organic deposits in the cages were determined by CH and TGA measurements. The assignments of ^{13}C MAS NMR signals were performed according to Ref. [114].

Concentration of organic deposits	Measurement methods		
	NMR (%)	CH (mmol/g)	TGA (mmol/g)
C atoms in methyl groups bound to aromatics	40.06	5.78	5.30
C atoms in ethyl groups bound to aromatics	2.43	0.35	0.32
non-alkylated ring carbons in aromatics	37.36	5.39	4.94
alkylated ring carbons in aromatics	20.15	2.91	2.66

9.3.3 Study of the Isotopic Composition of the Organic Deposits Formed by the Conversion of Non-enriched and ^{13}C-enrichced Methanol on H-SAPO-34 Catalysts

In order to clarify, whether the organic deposits observed by ^{13}C MAS NMR and UV/Vis spectroscopy are spectators of the methanol conversion on H-SAPO-34 or contribute to the formation of olefins, catalytic experiments with subsequent conversion of non-enriched methanol ($^{12}CH_3OH$) and ^{13}C-enriched methanol ($^{13}CH_3OH$) were performed. During the first step, $^{12}CH_3OH$ was converted on H-SAPO-34 in the fixed-bed reactor with a modified residence time of W_{cat}/F_{me} = 25 g h/mol for 6 h at 623 and 673 K. Subsequently, the used catalysts loaded with organic deposits were filled into a MAS NMR-UV/Vis rotor reactor. During the second step, $^{13}CH_3OH$ was converted for 2 h in the MAS NMR rotor reactor with the same residence time at 623 and 673 K. By quantitative ^{13}C MAS NMR spectroscopy, the numbers of ^{13}C atoms contributing to alkyl groups and aromatic compounds were determined (Fig. 9.5a). It was evidenced by *in situ* UV/Vis spectroscopy that no change of the nature of organic deposits occurred between the first and the second step (Figs. 9.5b and 9.5c). The numbers of ^{13}C atoms determined by ^{13}C MAS NMR spectroscopy were compared with those of catalysts, which were obtained after exclusive conversion of $^{13}CH_3OH$ for 2 h. The ^{13}C MAS NMR and UV/Vis spectra recorded upon the methanol conversion on H-SAPO-34 at 673 K are not shown in this dissertation. Table 9.2 gives a summary of the results of these

^{13}C-scrambling experiments.

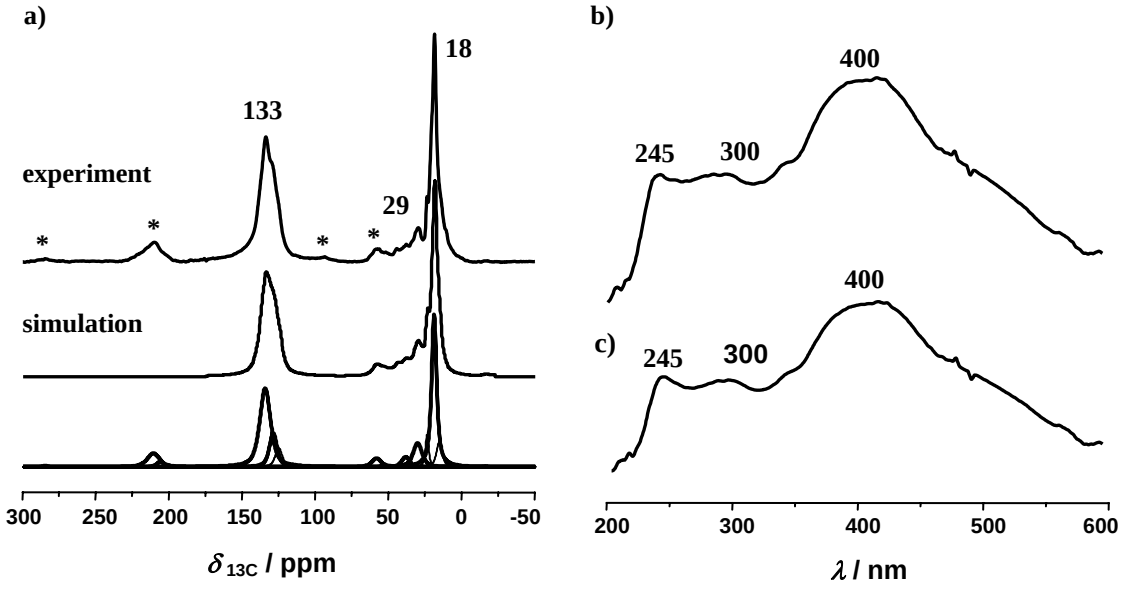

Fig. 9.5 *In situ* ^{13}C MAS NMR (a) and UV/Vis spectra (b, c) recorded upon conversion of $^{12}CH_3OH$ at 623 K for 6 h in the standard fixed-bed reactor (b) and subsequent conversion of $^{13}CH_3OH$ at 623 K for 2 h in the MAS NMR rotor reactor (a, c).

Tab. 9.2 Quantitative evaluation of ^{13}C MAS NMR spectra recorded upon the continuous conversion of $^{13}CH_3OH$ for 2 h (column 2) and sequential conversion of $^{12}CH_3OH$ for 6 h and $^{13}CH_3OH$ for 2 h (column 3) on H-SAPO-34 with W/F = 25 gh/mol. The last column gives the contents of ^{13}C atoms scrambled with the non-enriched coke compounds during conversion of $^{13}CH_3OH$.

Incorporation of ^{13}C atoms	**Number of ^{13}C atoms upon conversion of $^{13}CH_3OH$**	**Number of ^{13}C atoms upon conversion of $^{12}CH_3OH$ and $^{13}CH_3OH$**	**Content of scrambled ^{13}C atoms**
At T = 623 K:			
in alkyl groups	2.74 mmol/g	0.61 mmol/g	22.3 %
in aromatic rings	3.28 mmol/g	1.00 mmol/g	30.5 %
At T = 673 K:			
in alkyl groups	0.69 mmol/g	0.21 mmol/g	30.4 %
in aromatic rings	3.33 mmol/g	0.65 mmol/g	19.5 %

In column 3 of Tab. 9.2, the numbers of ^{13}C atoms are given, which scrambled during the conversion of $^{13}CH_3OH$ on H-SAPO-34 with the non-enriched organic deposits formed *via* conversion of $^{12}CH_3OH$. These values have to be compared with the numbers of ^{13}C atoms in organic deposits formed by exclusive conversion of $^{13}CH_3OH$ on fresh H-SAPO-34 catalysts (column 2). Column 4 of Tab. 9.2 gives the contents of carbon atoms in the organic deposits, which contribute to this $^{12}C/^{13}C$ scrambling process. At the reaction temperature of 623 K, carbon atoms in aromatic rings contribute to the $^{12}C/^{13}C$ scrambling process in the same order

as carbon atoms in alkyl groups. This finding supports the formation of olefins during the MTO process on H-SAPO-34 *via* the paring mechanism [182]. In this case, the aromatic rings of polyalkylaromatics are rearranged to five-ring compounds, while the former ring carbon atoms are added to substituting alkyl groups. Subsequently, these alkyl groups are split off yielding olefinic products, while the five-ring compounds are rearranged back to aromatic compounds upon alkylation by $^{13}CH_3OH$. The rearrangement of the aromatic rings is the reason for the $^{12}C/^{13}C$ scrambling of ring carbon atoms, and *vice versa*. Interestingly, the content of scrambled ring carbon atoms in the organic deposits is slightly lower for methanol conversion at 673 K (19.5 %) in comparison with methanol conversion at 623 K (30.5 %) on the H-SAPO-34 catalyst under study. This result agrees with the higher content of non-active polycyclic aromatics forming coke deposits on H-SAPO-34 at 673 K.

9.4 Conclusions

In the present work, the coke formation during the methanol conversion on the working acidic zeolite catalysts H-SAPO-34 in a standard fixed-bed reactor by on-line GC and *in situ* UV/Vis spectroscopy under continuous-flow conditions was investigated. In addition, the coke deposits formed in the fixed-bed reactor were characterized at room temperature by various analysis methods including ^{13}C MAS NMR spectroscopy, CH elemental analysis and TGA analysis, which allows quantitative studies of the ^{13}C carbon atoms in different chemical environments, such as alkyl groups and aromatic rings, while UV/Vis spectroscopy is sensitive for different aromatic compounds such as polyalkylaromatics and polycyclic aromatics. The most important coke deposits observed by UV/Vis spectroscopy are polycyclic aromatics with chain-like topology, such as polymethylanthracenes. The detailed position and shape of the UV/Vis bands of these compounds were found to depend on the amount of coke deposits.

^{13}C MAS NMR spectroscopic investigations of the $^{13}C/^{12}C$ scrambling between $^{13}CH_3OH$ and non-enriched organic deposits on used H-SAPO-34 support the paring mechanism for the growth of alkyl groups at polyalkylaromatics during the methanol conversion on this catalyst. By UV/Vis spectroscopy it could be evidenced that no change of the nature of organic deposits occurred during the $^{13}C/^{12}C$ scrambling experiments. Generally, the experiments have shown that UV/Vis spectroscopy in the reflection mode is very sensitive

for aromatic deposits on working zeolite catalysts. Therefore, it can be an interesting tool for the *in situ* watching of coke formation on MTO catalysts in industrial processes.

10 *In Situ* MAS NMR-UV/Vis Spectroscopic Study of Hydrocarbon-pool Compounds Formed during the Methanol-to-olefin Conversion on H-SAPO-34 under Continuous-flow Conditions

10.1 Introduction

Since there is still a considerable debate on the mechanism of the MTO reaction, significant efforts were made to elucidate the phenomenon of hydrocarbon formation on zeolite catalysts. Various techniques, such as FT-IR [32], MAS NMR [13], and UV/Vis spectroscopy [74], partially coupled with on-line GC, were employed to obtain more insight into the conditions of the formation of hydrocarbons. It is well known that MAS NMR spectroscopy provides the possibility for the detailed separation and assignment of signals of adsorbates on the surface of solid catalysts [60]. On the other hand, UV/Vis spectroscopy possesses a high sensitivity for compounds absorbing radiation in the UV/Vis region, such as molecules with conjugated double bonds, aromatics, and unsaturated carbenium cations, which are characteristic compounds of the hydrocarbon pool and coke deposits in the MTO conversion [60]. Therefore, the novel *in situ* MAS NMR-UV/Vis technique [72] combined with on-line GC offers an interesting approach for studying the formation of organic deposits under steady-state conditions of the methanol conversion on working catalysts and the regeneration of used catalysts. The present study was complemented by a quantitative evaluation of the ^{13}C MAS NMR experiments giving mean numbers of aromatic compounds and of alkyl groups per aromatic ring under reaction conditions.

10.2 Experimental Part

10.2.1 Experimental Equipment

The experimental set-up of *in situ* MAS NMR-UV/Vis spectroscopy is shown in Fig. 5.14 [71-72]. Before the *in situ* NMR investigations, the non-hydrated catalyst is filled into a 7 mm MAS NMR rotor under the dry nitrogen in a glove box and is carefully shaped to a cylindrical catalyst bed by a special tool. The hole in the MAS NMR cap is blocked by a plug. Subsequently, this rotor with the catalyst bed is transferred into the MAS NMR stator. At the same time, the purging gas on the top of the stator is started. The plug on the cap is removed and the injection tube is quickly inserted into the NMR rotor. Afterwards, the regular *in situ*

MAS NMR experiment can be performed.

^{13}C MAS NMR spectra were recorded when the reaction was carried out under continuous-flow conditions. The spectroscopic investigations were performed with a modified DSI-740 7 mm STD MAS NB NMR probe, Doty Scientific Instruments, Columbia, USA. High-power proton decoupling MAS NMR spectra were recorded on a Bruker MSL 400 spectrometer at the resonance frequency of 100.6 MHz and after an excitation with a $\pi/2$ pulse. Applying an external intensity standard consisting of dehydrated H-SAPO-34 loaded with $^{13}CH_3OH$, ^{13}C spin-counting was performed with the repetition time of 30 s. All ^{13}C MAS NMR spectra were referenced to TMS. The decomposition and simulation of NMR spectra were carried out with the Bruker software WINNMR and WINFIT.

At the bottom of the MAS NMR rotor reactor, a quartz glass window was installed as depicted on the right-hand side in Fig. 5.14 (b). *Via* this quartz glass window and using a glass fiber optics, the catalyst sample inside the rotor could be investigated by a fiber-optic UV/Vis spectrometer. Reference UV/Vis spectra of calcined H-SAPO-34 were recorded at the reaction temperature prior to introducing reactants. UV/Vis measurements between 200 and 600 nm in the diffuse reflection mode were conducted with an HPSUV1000A Fiber Optic spectrometer, an AvaLight-DH-S deuterium light source, and a glass fiber reflection probe FCR-7UV20-3-SR-S1 by Avantes. Narrow peaks at *ca.* 460 and 500 nm occurring in some of the UV/Vis spectra are caused by the equipment. With this technique, a direct NMR investigation of the formation and transformation of surface compounds under steady-state conditions and a simultaneous UV-Vis spectrum and GC analysis can be achieved.

10.2.2 Catalytic Reaction Conditions

Catalyst samples using H-SAPO-34 were prepared and characterized as described in Chapter 6. Prior to the *in situ* NMR-UV/Vis investigations, about 100 mg of the dehydrated catalysts were filled into a 7 mm MAS NMR rotor reactor. An additional *in situ* dehydration of the catalyst was performed with a heating rate of 1 K/min up to 673 K under flowing nitrogen (30 ml/min). Then, the catalyst was kept at the respective reaction temperatures for a given reaction time. Subsequently, a continuous flow of ^{13}C-enriched methanol with a modified residence time of W_{cat}/F_{me} = 25 g h/mol was injected into the fixed-bed reactor. The exhaust from the reactor was led to the sampling loop for on-line GC analysis. Simultaneously, a snapshot of the coke deposits formed on the catalyst bed would be taken by *in situ* UV/Vis

spectroscopy. The volatile reaction products escaping from the bottom of the fixed-bed reactor were detected *via* the on-line GC equipment. The exhaust flow containing volatile products was sampled and analyzed in steps of 15 min. A constant flow of methane (8 ml/min), added to the methanol feed, was used as an internal GC standard and allowed a quantification of the reaction products.

10.3 Results and Discussion

10.3.1 *In situ* CF MAS NMR-UV/Vis Spectroscopy of the Methanol-to-olefin Conversion on H-SAPO-34

Fig. 10.1 shows the *in situ* ^{13}C MAS NMR and UV/Vis spectra recorded during the conversion of ^{13}C-enriched methanol on H-SAPO-34 under continuous-flow conditions (CF) at reaction temperatures of 473 (a) to 673 K (d). The yields of volatile reaction products, such as dimethyl ether (DME), ethylene ($C_{2=}$), propylene ($C_{3=}$), and butenes ($C_{4=}$), were simultaneously analyzed by on-line GC and are given on the left-hand side.

At temperatures of 473 K and 523 K (Figs. 10.1a and 10.1b), the conversion of methanol is dominated by the formation of DME, which is indicated by the on-line GC data and ^{13}C MAS NMR signals of adsorbed methanol (50 ppm) and DME (61 ppm). The simultaneously recorded UV/Vis spectra of organic surface species formed during the methanol conversion are depicted on the right-hand side. Already at 473 K, UV/Vis sensitive species begin to be formed causing the band at 245 nm, which can be assigned to dienes [115, 177]. The concentration of these dienes is too small for their detection by ^{13}C MAS NMR spectroscopy.

After a further increase of the reaction temperature to 573 K (Fig. 10.1c), most of the methanol and DME molecules were converted. New ^{13}C MAS NMR signals appeared in the region of alkyl groups at 10-40 ppm accompanied by broad signals in the aromatic region of 125-135 ppm [114]. These signals indicate the formation of polyalkylaromatics. Simultaneously, a strong increase of the yields of light olefins was observed by on-line GC analysis. The UV/Vis spectrum recorded at 573 K consists of a dominating band at *ca.* 300 nm, probably due to the formation of monoenylic carbenium ions [74, 116]. Additional bands appear as weak shoulders at *ca.* 280 and 345 nm attributed to polyalkylaromatics and dienylic

carbenium ions [74, 116]. These findings indicate that olefinic compounds may react with monoenylic carbenium ions to form dienylic carbenium ions and aromatic compounds. Tab. 10.1 gives a survey on the assignment of UV/Vis bands.

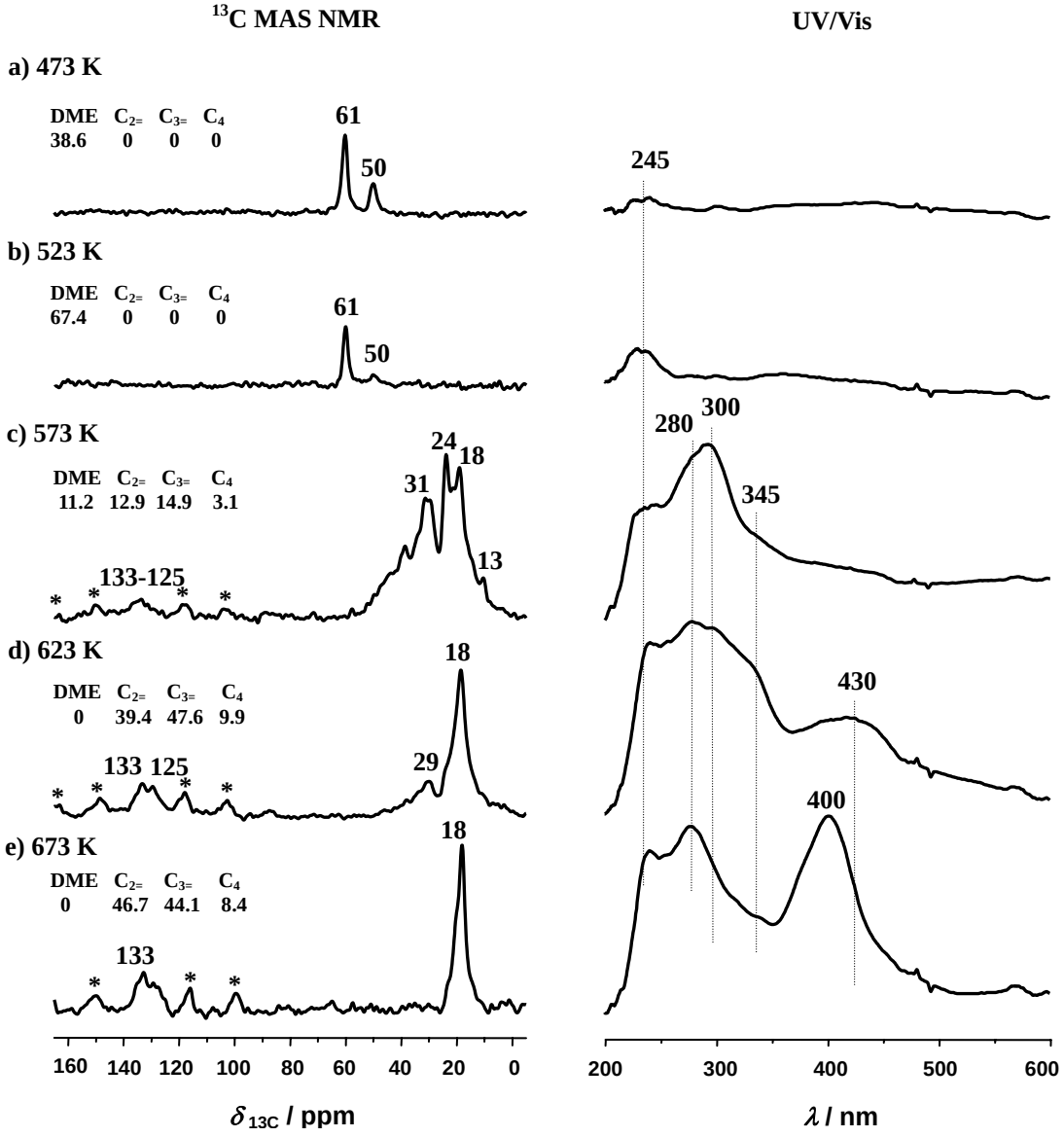

Fig. 10.1 ^{13}C MAS NMR (left) and UV/Vis spectra (right) recorded during the conversion of ^{13}C-enriched methanol (W_{cat}/F_{me} = 25 gh/mol) on H-SAPO-34 at reaction temperatures of 473 (a) to 673 K (d). On the left-hand side, the yields of dimethyl ether (DME), ethene ($C_{2=}$), propene ($C_{3=}$), and butenes ($C_{4=}$) as determined by on-line GC are given in %. Asterisks in the NMR spectra denote spinning sidebands.

Tab. 10.1 Assignments of UV/Vis bands (π-π* transitions) observed during methanol-to-olefins conversion on H-SAPO-34.

Band at ν / nm	Assignments	References
220-245	dienes	[115, 177]
254-280	aromatics and polyalkylaromatics	[115, 177]
270	phenols	[177]
300-320	monoenylic carbenium ions	[74, 116]
345-380	dienylic carbenium ions	[74, 116]
400-410	polycyclic aromatics	[115, 177]
430-470	trienylic carbenium ions	[74, 116]

Upon raising the reaction temperature to 623 K (Fig. 10.1d), a further increase of the yields of light olefins, but no DME were found by on-line GC analysis of the volatile products. The high-field range of the ^{13}C MAS NMR spectrum is dominated by a signal at 18 ppm due to methyl groups bound to aromatics, while most of the other signals in the region of alkyl groups occurring at lower reaction temperatures disappeared. Simultaneously, the intensities of the ^{13}C MAS NMR signals of aromatic compounds at 125-135 ppm increased. The UV/Vis spectrum recorded at 623 K is dominated by the band at 280 nm with shoulders at 300 and 345 nm due to polyalkylaromatics and monoenylic and dienylic carbenium ions, respectively. In addition, a broad band appeared at 430 nm, which is generally explained by trienylic carbenium ions [74, 116].

The *in situ* UV/Vis spectra recorded at 573 to 623 K indicate that a reaction of olefins with reactive carbenium ions occurs on the working catalyst leading to the formation of higher carbenium ions with maximum three conjugated double bonds. Up to the formation of dienylic carbenium ions, this pathway may contribute to the formation of aromatic hydrocarbon-pool compounds. The presence of trienylic carbenium ions, however, is a first indication for the formation of larger organic deposits, such as carbenium ions formed by polycyclic aromatics.

In agreement with the above-mentioned finding, the *in situ* UV/Vis spectrum recorded at 673 K (Fig. 10.1e) shows a strong band at 400 nm due to the non-protonated polycyclic aromatics, such as polymethylanthracenes [178]. The bands of carbenium ions at 345 and 430 nm are decreased, and at low wavelengths exclusively bands of dienes and polyalkylaromatics appear at 245 and 280 nm, respectively. Fig. 10.2 is a stack plot of *in situ* UV/Vis spectra recorded in steps of 15 min during the conversion of methanol on H-SAPO-34 at 673 K. In

this stack plot, the systematic decrease of the UV/Vis bands of dienylic and trienylic carbenium ions at 345 and 430 nm, respectively, can be observed as a function of the reaction time. The absence of UV/Vis bands of carbenium ions after a reaction time of *ca.* 75 min may indicate that the formation of reactive hydrocarbon pool compounds was finished. At the same time on stream, the band at 400 nm due to polycyclic aromatics starts to grow. The simultaneously recorded ^{13}C MAS NMR spectrum shows signals at 18 and *ca.* 135 ppm (Fig. 10.1e, left), which can be explained by polymethylaromatics [114]. In agreement with the results of UV/Vis spectroscopy, the broad ^{13}C MAS NMR signal at *ca.* 125 ppm indicates the formation of polycyclic aromatics.

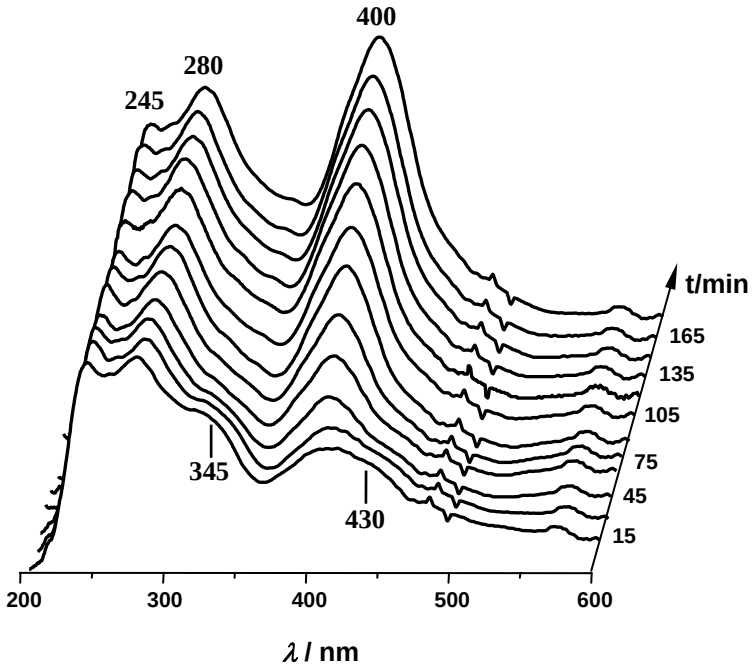

Fig. 10.2 Stack plot of UV/Vis spectra of H-SAPO-34 recorded during the conversion of methanol (W_{cat}/F_{me} = 25 gh/mol) at 673 K as a function of the reaction time.

Considering the yields of volatile reaction products as determined by on-line GC analysis, a continuous increase of the formation of propylene occurred up to the reaction temperature of 623 K (Figs. 10.1c and 10.1d, left-hand side). At this temperature, the yield of propylene (47.6 %) was higher than the yield of ethylene (39.4 %). At 673 K (Fig. 10.1e, left-hand side), however, the yield of ethylene (46.7 %) became higher in comparison with the yield of propylene (44.1 %). This change of the product selectivity has to be considered in the connection with the occurrence of the strong UV/Vis band at 400 nm due to polycyclic aromatics, which indicates that the catalyst deactivation has started.

Song *et al.* [179] and Sassi *et al.* [168] found that hydrocarbon-pool compounds

consisting of polyalkylaromatics with low numbers of methyl groups (*ca.* 2-3) prefer the formation of ethylene. Therefore, it was the aim of the following quantitative ^{13}C MAS NMR studies to clarify whether catalyst deactivation, which started at the reaction temperature of 673 K, was accompanied by a decrease of the mean number of alkyl groups per aromatic ring of the hydrocarbon-pool compounds.

10.3.2 Quantitative ^{13}C MAS NMR Investigation of Hydrocarbon-pool Compounds on H-SAPO-34 Formed under Continuous-flow Conditions

As an example, Fig. 10.3a, left, presents the ^{13}C MAS NMR spectrum of the used H-SAPO-34 catalysts obtained at room temperature after methanol-to-olefin conversion at 673 K for 3 h. The concentration of organic deposits in the chabazite cages ($T_{12}O_{24}$: 1.38 mmol/g) of H-SAPO-34 was determined by the simulation of the spectral range of ^{13}C MAS NMR signals due to ^{13}C atoms in alkyl groups and aromatic rings and the comparison of ^{13}C MAS NMR intensities with that of an external intensity standard (dehydrated H-SAPO-34 loaded with $^{13}CH_3OH$).

Columns 1 and 2 of Tab. 10.2 give a summary on the chemical shift ranges and assignments of ^{13}C MAS NMR signals occurring in the spectra of the used H-SAPO-34 catalyst. In columns 3 and 4 of Tab. 10.2, the concentration of ^{13}C atoms contributing to alkyl groups and aromatic rings are given for the organic deposits formed on the H-SAPO-34 catalyst at 623 and 673 K. The number of methyl groups bound to aromatics is significantly higher than those of ethyl and isopropyl groups. In agreement with former studies [13], this finding shows that polymethylbenzene molecules are the most important hydrocarbon-pool compounds formed during the methanol conversion on H-SAPO-34. Upon methanol conversion at 623 K, aromatic compounds with 3.28 mmol ^{13}C atoms or 0.55 mmol aromatic rings per gram were formed corresponding to *ca.* 0.4 benzene rings per chabazite cage. These aromatic compounds are alkylated by a mean number of 2.23 mmol methyl, ethyl, and propyl groups per gram corresponding to *ca.* 4.1 alkyl groups per aromatic ring.

After increasing the reaction temperature to 673 K, a strong decrease of the mean number of alkyl groups to 0.61 mmol g^{-1} corresponding to 1.1 alkyl groups per aromatic ring occurred, while the number of aromatic rings per cage is nearly constant (column of Tab. 10.2). In agreement with Song *et al.* [179], the decrease of the yield of propylene at the

reaction temperature of 673 K observed in the present study can be explained by the lower number of methyl groups per aromatic ring of the hydrocarbon-pool compounds in comparison with the hydrocarbon-pool compounds present at 623 K. In addition, the composition of the organic deposits changes to that of typical coke compounds as indicated by the strong UV/Vis band at 400 nm due to polycyclic aromatics (Fig. 10.3a, right).

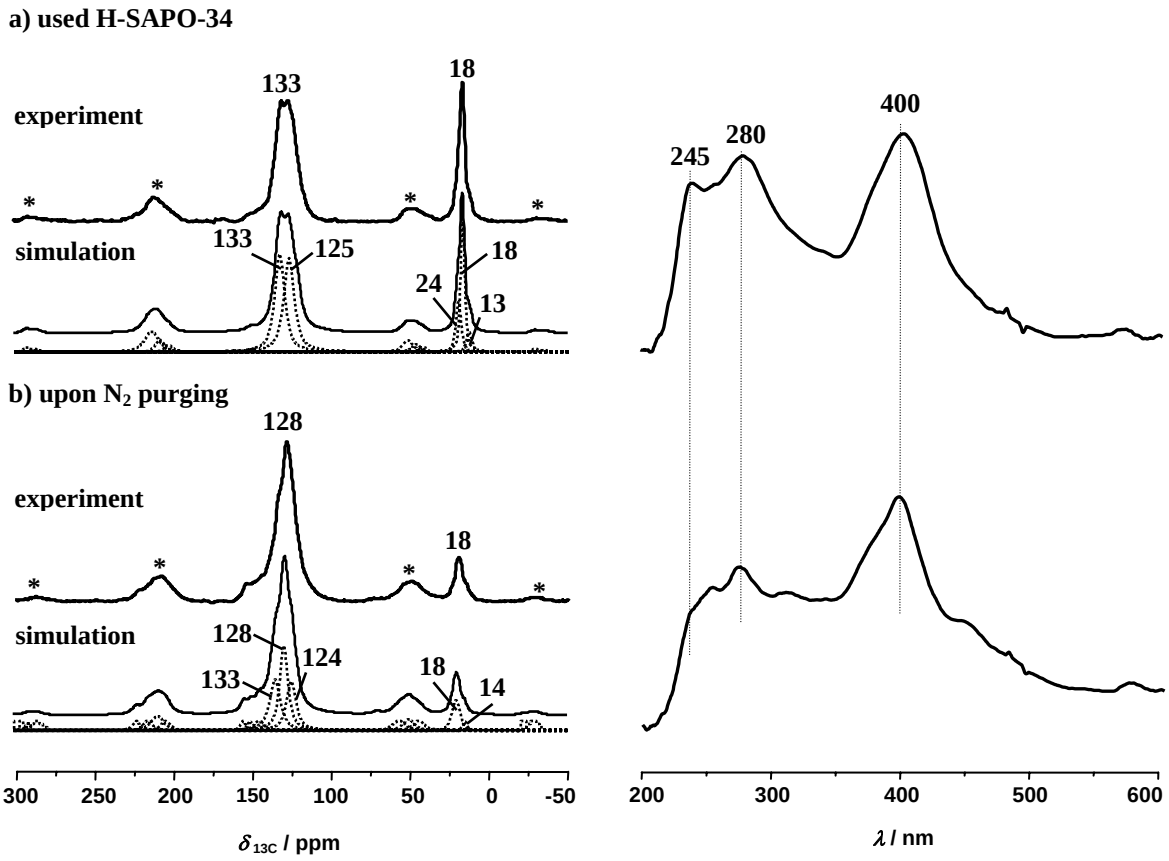

Fig. 10.3 ^{13}C MAS NMR (left) and UV/Vis spectra (right) of H-SAPO-34 recorded at room temperature after methanol conversion at 673 K (a) and subsequent purging with nitrogen (30 ml/min) at 673 K (b). Asterisks in the NMR spectra denote spinning sidebands.

In order to study the thermal stability of the organic deposits formed on H-SAPO-34 at 673 K, the methanol flow was stopped and the used catalyst was purged by dry nitrogen at 673 K for 2 h. Fig. 10.3b, left, shows the ^{13}C MAS NMR spectrum of this catalyst subsequently recorded at room temperature for quantitative evaluation. The results of the evaluation are summarized in column 5 of Tab. 10.2. As indicated by these values, the number of ^{13}C atoms in aromatic compounds decreased slightly to 2.45 mmol g^{-1} corresponding to *ca.* 0.3 aromatic rings per chabasite cage. Also the number of alkyl groups decreased to 0.34 mmol g^{-1} corresponding to 0.8 alkyl groups per aromatic ring. This is a decrease of

organic deposits by 25 to 27 % in comparison with the used catalyst before purging with dry nitrogen at 673 K.

Tab. 10.2 Quantitative evaluation of the ^{13}C MAS NMR signals of organic deposits in the chabasite cages ($T_{12}O_{24}$: 1.38 mmol/g) of H-SAPO-34 upon conversion of ^{13}C-enriched methanol at 623 and 673 K under continuous-flow conditions with the residence time of W_{cat}/F_{me} = 25 gh/mol, subsequent purging by dry nitrogen (30 ml/min) at 673 K for 2 h or regeneration by synthetic air (syn. air, 20 vol. % O_2, 30 ml/min) at 673 and 773 K for 2 h. The assignments of ^{13}C MAS NMR signals were performed according to Ref. [114].

Signal at δ_{13C} /ppm	**Assignments**	**Concentration of ^{13}C atoms / mmol g^{-1}**				
		***in situ* CF at 623 K**	***in situ* CF at 673 K**	**N_2 at 673 K**	**syn. air at 673 K**	**syn. air at 773 K**
16-21	in methyl groups bound to aromatics	1.87	0.53	0.31	-	-
14-15 and 22-29	in ethyl groups bound to aromatics	0.42	0.16	0.06	-	-
23-24 and 33-37	in isopropyl groups bound to aromatics	0.45	-	-	-	-
125-135	in alkylated and non-alkylated aromatics	3.28	3.33	2.45	1.04	0.31
145-155	at ring positions of aromatics bound to hydroxyl groups	-	-	-	0.45	0.13

In the UV/Vis spectra of the used H-SAPO-34 catalyst recorded upon purging with dry nitrogen at 673 K, mainly the UV bands of polyalkylaromatics at 280 nm and the shoulder at 245 nm due to dienes are decreased (compare Figs. 10.3a and 10.3b, right). This behavior corresponds to the smaller number of polyalkylaromatics observed by ^{13}C MAS NMR spectroscopy. On the other hand, the large band at 400 nm indicates that polycyclic aromatics occurring as coke compounds on the used H-SAPO-34 catalyst exhibit a high thermal stability and are not affected by purging with nitrogen (Fig. 10.3b, right). Their removal by thermal treatments requires more severe conditions, such as purging with oxygen.

10.3.3 MAS NMR-UV/Vis Investigation of the Regeneration of the Used H-SAPO-34 Catalysts by Purging with Synthetic Air

In industrial processes, catalysts deactivated by coke are commonly regenerated by burning

off the organic deposits in the presence of oxygen [29]. In the present study, the used H-SAPO-34 catalyst obtained after methanol conversion at 673 K, therefore, was treated with synthetic air (20 vol. % O_2,) at 673 and 773 K for 2 h. The effect of this treatment on the organic deposits was investigated by ^{13}C MAS NMR-UV/Vis spectroscopy. Fig. 10.4, left, shows the ^{13}C MAS NMR spectra of the used H-SAPO-34 catalyst recorded upon purging with synthetic air for 2 h.

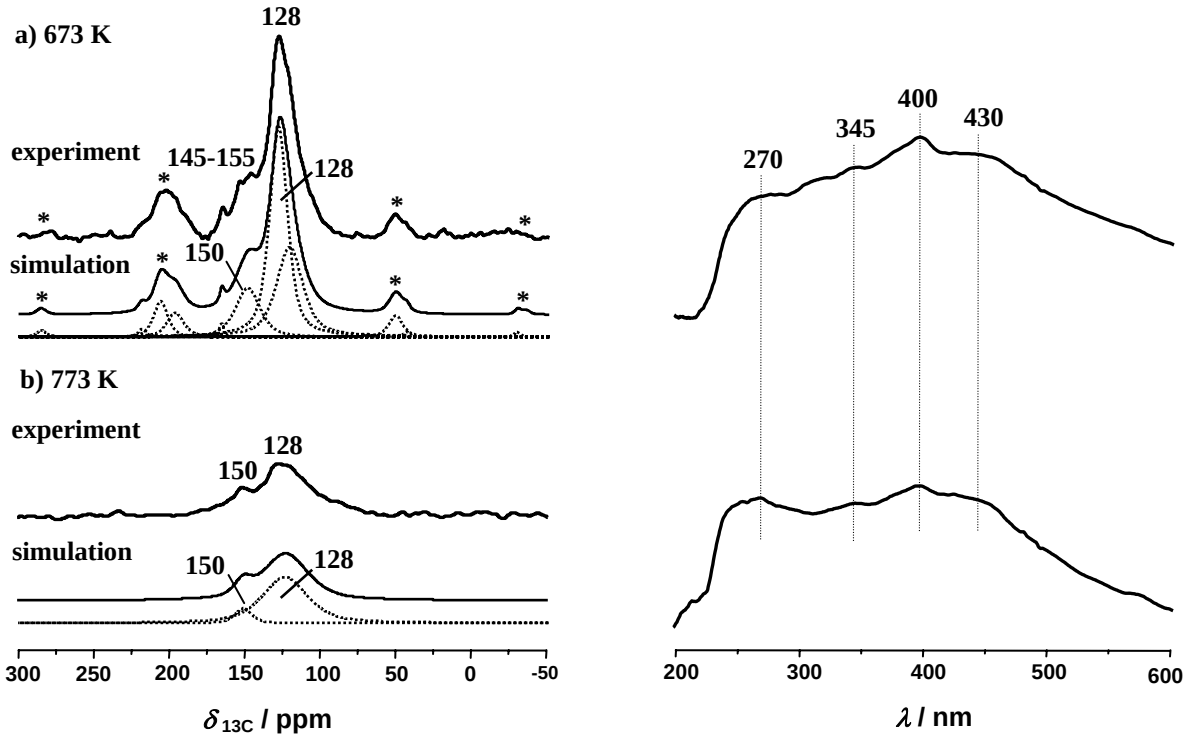

Fig. 10.4 ^{13}C MAS NMR (left) and UV/Vis spectra (right) of H-SAPO-34 recorded at room temperature after the methanol conversion at 673 K and subsequent purging with synthetic air (20 vol.% O_2, 30 ml/min) at 673 K (a) and 773 K (b). Asterisks in the NMR spectra denote spinning sidebands.

Upon the treatment at 673 K, a significant removal of all polyalkylaromatics occurred (Fig. 10.4a, left, and column 6 of Tab. 10.2). In comparison with the used H-SAPO-34 catalyst, which was not treated with synthetic air (column 4 of Tab. 10.2), the number of ^{13}C atoms in aromatic rings of the organic deposits was decreased by *ca.* 69 %. This is accompanied by a strong decrease of the UV/Vis band of polycyclic aromatics (400 nm) acting as coke deposits (Fig. 10.4b, right). In addition, the UV/Vis band of polyalkylaromatics (280 nm) disappeared totally, which agrees with the above-mentioned results of ^{13}C MAS NMR spectroscopy. Interestingly, new ^{13}C MAS NMR signals can be observed at 145-155 ppm. These signals are a hint for the hydroxylation of remaining aromatic compounds during the treatment with synthetic air. In the UV/Vis spectra shown in Fig. 10.4, right, these

phenolic species are responsible for the new band at *ca.* 270 nm [177].

Upon raising the regeneration temperature to 773 K, a decrease of the number of ^{13}C atoms in aromatic rings of organic deposits by 90 % in comparison with the non-purged H-SAPO-34 catalyst occurred (Fig. 10.4b, left and column 7 of Tab. 10.2). Likewise, the UV/Vis band of neutral polycyclic aromatics at 400 nm became weaker (Fig. 10.4b, right). Interestingly, the bands at 345 and 430 nm are pronounced in the UV/Vis spectrum. This finding indicates that the organic deposits remaining on the H-SAPO-34 catalyst regenerated at 773 K partially consist of dienylic and trienylic carbenium ions, *i.e.*, of chemically reactive compounds.

10.4 Conclusions

Applying *in situ* MAS NMR-UV/Vis spectroscopy under continuous-flow conditions, an investigation of organic deposits formed during the methanol-to-olefin conversion on H-SAPO-34 under steady-state conditions was performed. By simultaneous on-line GC analysis of the volatile products, the relationship between the product selectivity and the nature of organic deposits formed on the working catalyst could be studied.

At reaction temperatures of 573 and 623 K, ^{13}C MAS NMR signals of polyalkylaromatics (18, 125-135 ppm) accompanied by UV/Vis bands of monoenylic (300 nm), dienylic (345 nm), and trienylic carbenium ions (430 nm) were observed. Under these conditions, a higher yield of propylene than of ethylene was obtained. At 673 K, the appearance of a strong UV/Vis band of polycyclic aromatics, such as polymethylanthracenes (400 nm), was accompanied by a decrease of the yield of propylene. Based on these results, a stepwise reaction of olefins with carbenium ions leading to the formation of aromatic deposits was suggested. The UV/Vis bands of trienylic carbenium ions and polycyclic aromatics indicate the formation of coke deposits responsible for the deactivation of H-SAPO-34, which started already at 673 K. While the formation of polyalkylaromatics in the chabasite cages of H-SAPO-34 used as MTO catalysts was well accepted [24], the formation of polycyclic aromatics, such as polymethylanthracenes, occurred in neighboring chabasite cages or at the outer surface of the catalyst particles.

It could be shown by quantitative evaluation of the *in situ* ^{13}C MAS NMR spectra that

the catalyst deactivation was accompanied by a decrease of the mean number of methyl groups per aromatic ring. This finding explained, in agreement with previous studies of other groups, the observed change of the product selectivity from propylene to ethylene.

Purging of the used catalyst at reaction temperature with nitrogen led to a decrease of the number of polyalkylaromatics by 25-27 % only, but not to a decrease of the polycyclic aromatics acting as coke deposits. Upon thermal treatment of the used H-SAPO-34 catalyst with synthetic air at 673 and 773 K, however, all polyalkylaromatics and most of the polycyclic aromatics were removed. As indicated by ^{13}C MAS NMR and UV/Vis spectroscopy, the residual organic deposits partially consist of phenolic compounds and reactive dienylic and trienylic carbenium ions.

Literatures

[1] G.A. Olah, A. Goeppert, G.K.S. Prakash, *Beyond Oil and Gas: The Methanol Economy*, WILEY-VCH, Weinheim, 2006.

[2] Special Report: 2004 Worldwide EOR Survey, *Oil. Gas. J.* Apr. 12, 2004.

[3] P.M.M. Blauwhoff, J.W. Gosselink, E.P. Kieffer, S.T. Sie, W.H.J. Stork, *Zeolites as Catalysts in Industrial Processes*, in: J. Weitkamp, L. Puppe (eds.), *Catalysis and Zeolites: Fundamentals and Applications*, Springer-Verlag, Berlin, Heidelberg, New York, 1999, p.437.

[4] M. Stoecker, *Microporous Mesoporous Mater.* 29 (1999) 3-48.

[5] A.V. Grosse, J.C. Snyder, U.S. Patent 2 492 984, 1950.

[6] L. Kim, M.M. Wald, S.G. Brandengerger, *J. Org. Chem.* 43 (1978) 3432-3434.

[7] D.C. Hargis, L.J. Kehoe, U.S. Patent 4 072 732, 1978.

[8] D.E. Pearson, *J.C.S. Chem. Commun.* (1974) 397-397.

[9] C.D. Chang, A.J. Silvestri, *Chemtech.* 10 (1987) 624-631.

[10] C.D. Chang, *Catal. Rev.-Sci. Eng.* 25 (1983) 1-118.

[11] C.D. Chang, *Catal. Rev.-Sci. Eng.* 26 (1984) 323-345.

[12] H.G. Karge, M. Hunger, H.K. Beyer, *Characterization of Zeolites*, in: J. Weitkamp, L. Puppe (eds.), *Catalysis and Zeolites: Fundamentals and Applications*, Springer-Verlag, Berlin, Heidelberg, New York, 1999, p.198.

[13] J.F. Haw, W. Song, D.M. Marcus, J.B. Nicholas, *Acc. Chem. Res.* 36 (2003) 317-326.

[14] B.M. Lok, C.A. Messina, R.L. Patton, R.T. Gajek, T.R. Cannan, E.M. Flanigen, U.S. Patent 4 440 871, 1984.

[15] J.F. Haw, D.M. Marcus, *Top. Catal.* 34 (2005) 41-48.

[16] J. Chen, J.M. Thomas, P.A. Wright, R.P. Townsend, *Catal. Lett.* 28 (1994) 241-248.

[17] J. Chen, P.A. Wright, J.M. Thomas, S. Natarajan, L. Marchese, S.M. Bradley, G. Sankar, C.R.A. Catlow, *J. Phys. Chem.* 98 (1994) 10216-10224.

[18] C.D. Chang, W.H. Lang, A.J. Silvestri, U.S. Patent 4 062 905, 1977.

[19] C.D. Chang, A.J. Silvestri, *J. Catal.* 47 (1977) 249-259.

[20] E.G. Derouane, P. Dejaifve, Z. Gabelica, *Faraday Disc. Chem. Soc.* 82 (1981) 331-344.

[21] G.F. Froment, W.J.H. Dehertog, A.J. Marchi, *Catalysis* 9 (1992) 1-64.

[22] M.A. Aramendia, V. Borau, C. Jimenez, J.M. Marinas, R. Roldan, F.J. Romero, F.J. Urbano, *Chem. Lett.* 7 (2002) 672-673.

[23] http://www.iza-structure.org/.

[24] C.D. Chang, *Methanol to Hydrocarbons*, in: G. Ertl, K. Knoezinger, J. Weitkamp (eds.), *Handbook of Heterogeneous Catalysis*, Wiley-VCH, Weinheim, Germany, 1997, p.1894.

[25] B.M. Lok, C.A. Messina, R.L. Patton, R.T. Gajek, T.R. Cannan, E.M. Flanigen, *J. Am. Chem. Soc.* 106 (1984) 6092-6093.

[26] V.D.M. Marcus, W. G. Song, L.L. Ng, Jame F. Haw, *Langmuir* 18 (2002) 8386-8391.

[27] P. Salvador, J.J. Fripiat, *J. Phys. Chem.* 79 (1975) 1842-1849.

[28] H. Klein, C. Kirschhock, H. Fuess, *J. Phys. Chem.* 98 (1994) 12345-12360.

[29] H. Schulz, M. Wei, *Microporous Mesoporous Mater.* 29 (1999) 205-218.

[30] W. Wang, M. Seiler, M. Hunger, *J. Phys. Chem. B*, 105 (2001) 12553-12558.

[31] W. Wang, A. Buchholz, M. Seiler, M. Hunger, *J. Am. Chem. Soc.* 125 (2003) 15260-15267.

[32] T.R. Forester, R.F. Howe, *J. Am. Chem. Soc.* 109 (1987) 5076-5082.

[33] J.P. van den Berg, J.P. Wolthuizen, J.H.C. van Hooff, in: L.V. Rees (eds.), *Proceedings 5th International Zeolite Conference* (Naples), Heyden, London, 1980, p.649.

[34] G.A. Olah, H. Doggweiler, J.D. Felberg, S. Frohlich, M.J. Grdina, R. Karpeles, T. Keumi, S. Inaba, W.M. Ip, K. Lammertsma, *J. Am. Chem. Soc.* 106 (1984) 2143-2149.

[35] R. Hunter, G.J. Hutchings, *J. Chem. Soc. Chem. Comm.* (1985) 886-887.

[36] E.A. Swabb, B.C. Gates, *Ind. Eng Chem. Fundam.* 11 (1972) 540-545.

[37] Y. Ono, T. Mori, *J. Chem. Soc. Faraday Trans.* I, 77 (1981) 2209-2221.

[38] C.D. Chang, S.D. Hellring, J.A. Pearson, *J. Catal.* 115 (1989) 282-285.

[39] G. J. Hutchings, R. Hunter, *Catal. Today* 6 (1990) 279-306.

[40] W. Song, D.M. Marcus, H. Fu, J.O. Ehresmann, J.F. Haw, *J. Am. Chem. Soc.* 124 (2002) 3844-3845.

[41] D.M. Marcus, K.A. Mclachlan, M.A. Wildman, J.O. Ehresmann, P.W. Kletnieks, J.F. Haw, *Angew. Chem. Int. Ed.* 45 (2006) 3133-3136.

[42] W. Hoelderich, H. Eichhorn, R. Lehnert, L. Marosi, W. Mross, R. Reinke, W. Ruppel, H. Schlimper, in: R.A. Bisio, D.G. Olson (eds.), *Proceedings of the 6th International Zeolite Conference*, Reno, USA, 1983, Butterworths, Guildford, 1984, p.545.

[43] R.M. Dessau, *J. Catal*. 99 (1986) 111-116.

[44] S. Kolboe, *Acta Chem. Scand*. A 40 (1986) 711-713.

[45] I.M. Dahl, S. Kolboe, *Catal. Lett*. 20 (1993) 329-336.

[46] I.M. Dahl, S. Kolboe, *J. Catal.* 149 (1994) 458-464.

[47] I.M. Dahl, S. Kolboe, *J. Catal.* 161 (1996) 304-309.

[48] P.W. Goguen, T. Xu, D.H. Barich, T.W. Skloss, W. Song, Z. Wang, J.B. Nicholas, J.F. Haw, *J. Am. Chem. Soc.* 120 (1998) 2650-2651.

[49] W. Song, J.F. Haw, J.B. Nicholas, C.S. Heneghan, *J. Am. Chem. Soc.* 122 (2000) 10726-10727.

[50] M. Hunger, M. Seiler, A. Buchholz, *Catal. Lett.* 74 (2001) 61-68.

[51] E. E Wolf, F. Alfani, *Catal. Rev. Sci. Eng.* 24 (1982) 329-371.

[52] M. Guisnet, P. Magnoux, *Appl. Catal. A: General.* 212 (2001) 83-96.

[53] K.G. Allum, A.R. Williams, in: D.M. Bibby, C.D. Chang, R.W. Howe, S. Yurchak (eds.), *Methane Conversion, Stud. Surf. Sci. Catal.* Vol. 36, Elsevier, Amsterdam, 1988, p.691.

[54] C.D. Chang, *Catal. Today* 13 (1992) 103-111.

[55] F.J. Keil, *Microporous Mesoporous Mater.* 29 (1999) 49-66.

[56] J.M. Thomas, *Angew. Chem. Int. Ed.* Engl. 33 (1994) 913-937.

[57] J.M. Thomas, R. Raja, *Chem. Commun*. (2001) 675-687.

[58] B.M. Weckhuysen, *Chem. Commun*. (2002) 97-110.

[59] B.M. Weckhuysen, P. Van der Voort, G. Catana (eds.), *Spectroscopy of Transition Metal Ions on Surfaces*, Leuven University Press, Leuven, 2000.

[60] M. Hunger, *Microporous Mesoporous Mater.* 82 (2005) 241-255.

[61] J.A. Lercher, V. Veefkind, K. Vajerwerg, *Vib. Spectrosc.* 19 (1999) 107-121.

[62] I.A. Fischer, A.T. Bell, *J. Catal.* 178 (1998) 153-173.

[63] M.W. Anderson, J. Dwyer, G.J. Hutchings, D.F. Lee, M. Makarova, B. Zibrowius, *Catal. Lett.* 31 (1995) 377-393.

[64] S. Kuba, H. Knözinger, *J. Raman. Spectrosc.* 33 (2002) 325-332.

[65] C. Li, *J. Catal.* 216 (2003) 203-212.

[66] D.C. Koningsberger, B.L. Mojet, G.E. van Dorssen, D.E. Ramaker, *Top. Catal.* 10 (2000) 143-155.

[67] A. Knop-Gericke, M. Hävecker, Th. Schedel-Niedrig, R. Schlögl, *Top. Catal.* 10 (2000) 187-198.

[68] J.A. van Bokhoven, C. Louis, T.M. Jeffrey, M. Tromp, O.V. Safonova, P. Glatzel, *Angew. Chem. Int. Ed.* 45 (2006) 4651-4654.

[69] J.F. Haw (eds.), *In-situ Spectroscopy in Heterogeneous Catalysis*, Wiley-VCH, Weinheim, 2002.

[70] J.F. Haw, P.W. Goguen, T. Xu, T.W. Skloss, W.G. Song, Z.K. Wang, *Angew. Chem. Int.*

Ed. 37 (1998) 948-949.

[71] M. Hunger, M. Seiler, T. Horvath, *Catal. Lett.* 57 (1999) 199-204.

[72] M. Hunger, W. Wang, *Chem. Commun*. (2002) 584-585.

[73] B.M. Weckhuysen (ed.), *In-situ Spectroscopy of Catalysts*, American Scientific Publishers, California, 2004.

[74] R. Ahmad, J. Melsheimer, F.C. Jentoft, R. Schlögl, *J. Catal.* 218 (2003) 365-374.

[75] M.D. Argyle, K.D. Chen, C. Krebs, A.T. Bell, E. Iglesia, *Chem. Commun*. (2003) 2082-2083.

[76] J.W. Niemantsverdriet, W.N. Delgass, *Top. Catal.* 8 (1999) 133-140.

[77] A. Brückner, *Top. Catal.* 38 (2006) 133-139.

[78] A. Panchenko, H. Dilger, J. Kerres, M. Hein, A. Ullrich, T. Kaz, E. Roduner, *Phys. Chem. Chem. Phys.* 6 (2004) 2891-2894.

[79] C.P. Slichter, *Pricinples of Magnetic Resonance* (3rd), Springer-Verlag, Heidelberg, 1990.

[80] E.O. Stejskal, J.D. Memory, *High Resolution NMR in the Solid State*, Oxford University Press, New York, 1994.

[81] J.M. Thomas, J. Klinowski, *Adv. Catal.* 33 (1985) 199-374.

[82] E.R. Andrew, A. Bradbury, R.G. Eades, *Nature* 182 (1958) 1659-1659.

[83] E.R. Andrew, A. Bradbury, R.G. Eades, *Nature* 183 (1959) 1802-1803.

[84] I.J. Lowe, *Phys. Rev. Lett.* 2 (1959) 285-287.

[85] E.R. Andrew, in: D.M. Grant, R.K. Harris (eds.), *Encyclopedia of Nuclear Magnetic Resonance*, John Wiley & Sons, Chichester, 1996, p. 2891.

[86] M. Hunger, E. Brunner, *Mol. Sieves* 4 (2004) 201-293.

[87] M. Mehring, *Principles of high-resolution NMR in solids* (2nd), Springer, Berlin, 1983.

[88] S.R. Hartmann, E.L. Hahn, *Phys. Rev.* 128 (1962) 2042-2053.

[89] C.A. Fyfe, K.T. Mueller, K.C. Wong-Moon, *Cross-polarization Processes Involving Less Common Pairs of Nuclei*, in: G.E. Maciel (eds.), *Nuclear Magnetic Resonance in Modern Technology*, NATO ASI Series, Series C, vol. 447, Kluwer Academic Publishers, Dordrecht, 1994, p. 447-482.

[90] D. Schulze, H. Ernst, D. Fenzke, W. Meiler, H. Pfeifer, *J. Phys. Chem.* 94 (1990) 3499-3502.

[91] M. ChE, F. Bozon-Verduraz, *UV-Vis-NIR and EPR Spectroscopies*, in: G. Ertl, K. Knözinger, J. Weitkamp (ed.), *Handbook of Heterogeneous Catalysis*, Vol.2, Wiley-VCH, Weinheim, 1997, p. 641-652.

[92] M. Kang, T. Inui, *J. Mol. Catal. A: Chemical* 140 (1999) 55-63.

[93] A. Buchholz, W. Wang, M. Xu, A. Arnold, M. Hunger, *Microporous Mesoporous Mater.* 57 (2003) 157-168.

[94] S.T. Wilson, B.M. Lok, E.M. Flaigen, US patent 4 310 440, 1982.

[95] M. Hunger, *Solid State Nucl. Magn. Reson.* 6 (1996) 1-29.

[96] Z. Luan, C.F. Cheng, W. Zhou, J. Klinowski, *J. Phys. Chem.* 99 (1995) 1018-102.

[97] B. Zibrowius, E. Loeffler, M. Hunger, *Zeolites* 12 (1992) 167-174.

[98] E.G. Derouane, J.P. Gilson, J.B. Nagy, *Zeolites* 2(1982) 42-46.

[99] C.E. Bronnimann, G.E. Maciel, *J. Am. Chem. Soc*. 108 (1986) 7154-7159.

[100] D.K. Murray, J.W. Chang, J.F. Haw, *J. Am. Chem. Soc*. 115 (1993) 4732-4741.

[101] V. Bosacek, *J. Phys. Chem.* 97 (1993) 10732-10737.

[102] V. Bosacek, H. Ernst, D. Freude, T. Mildner, *Zeolites* 18 (1997) 196-199.

[103] V. Bosacek, R. Klik, F. Genoni, G. Spano, F. Rivetti, F. Figueras, *Magn. Reson. Chem.* 37 (1999) S135-S141.

[104] J. Novakova, L. Kubelkova, K. Habersberger, Z. Dolejsek, *J.C.S. Faraday Trans. I* 80 (1984) 1457-1465.

[105] S.R. Blaszkowski, R.A. van Santen, *J. Am. Chem. Soc*. 119 (1997) 5020-5027.

[106] B. Arstad, J.B. Nicholas, J.F. Haw, *J. Am. Chem. Soc*. 119 (1997) 5020-5027.

[107] S. Svelle, B. Arstad, S. Kolboe, O. Swang, *J. Phys. Chem. B* 107 (2003) 9281-9289.

[108] B.E. Langner, *Appl. Catal.* 2 (1982) 289-302.

[109] E. Fiedler, G. Grossmann, B. Kersebohm, G. Weiss, C. Witte, in: B. Elvers, S. Hawkins, G. Schulz (eds.), *Ullmann's Encyclopedia of Industrial Chemistry*, 5th Completely Revised Version, Vol. A 16, VCH, Weinheim, Basel, Cambridge, New York, 1990, p. 477.

[110] A.M. Beale, A.M.J. van der Eerden, K. Kervinen, M.A. Newton, B.M. Weckhuysen, *Chem. Commun.* (2005) 3015-3017.

[111] A. Brueckner, *Chem. Commun.* (2005) 1761-1763.

[112] M.A. Newton, B. Jyoti, A.J. Dent, S.G. Fiddy, J. Evans, *Chem. Commun.* (2004) 2382-2383.

[113] F. Salehirad, M.W. Anderson, *J. Catal.* 164 (1996) 301-314.

[114] H. Kalinowski, S. Berger, S. Braun, *^{13}C-NMR-Spektroskopie*, Georg Thieme Verlag Stuttgart, New York, 1984, p. 447.

[115] H.G. Karge, M. Laniecki, M. Ziolek, G. Onyestyak, A. Kiss, P. Kleinschmit, M. Siray, in: P.A. Jacobs, R.A. van Santen (eds.), *Proceedings of the 8th International Zeolite Conference*, Amsterdam, 1989, Elsevier, Amsterdam, 1989, p. 1327-1337.

[116] I. Kiricsi, H. Foerster, G. Tasi, J.B. Nagy, *Chem. Rev.* 99 (1999) 2085-2114.

[117] G.A. Olah, G.K.S. Prakash, J. Sommer, *Superacids*, Wiley-Interscience, New York, 1985.

[118] H. Noguchi, E. Yoda, N. Ishizawa, J.N. Kondo, A. Wada, H. Kobayashi, K. Domen, *J. Phys. Chem. B* 109 (2005) 17217-17223.

[119] M.T. Aronson, R.J. Gorte, W.E. Farneth, D. White, *J. Am. Chem. Soc*. 111 (1989) 840-846.

[120] A.G. Stepanov, V.N. Romannikov, K.I. Zamaraev, *Catal. Lett*. 13 (1992) 395-405.

[121] J.F. Haw, B.R. Richardson, I.S. Oshiro, N.D. Lazo, J.A. Speed, *J. Am. Chem. Soc*. 111 (1989) 2052-2058.

[122] V.B. Kazansky, *Catal. Today* 51 (1999) 419-434.

[123] C. Tuma, J. Sauer, *Angew. Chem. Int. Ed*. 44 (2005) 4769-4771.

[124] M. Boronat, P.M. Viruela, A. Corma, *J. Am. Chem. Soc*. 126 (2004) 3300-3309.

[125] X. Rozanska, L.A.M.M. Barbosa, R.A. van Santen, *J. Phys. Chem. B* 109 (2005) 2203-2211.

[126] S. Svelle, S. Kolboe, O. Swang, U. Olsbye, *J. Phys. Chem. B* 109 (2005) 12874-12878.

[127] W. Wang, J. Jiao, Y. Jiang, S.S. Ray, M. Hunger, *ChemPhysChem* 6 (2005) 1467-1469.

[128] Y.J. Jiang, W. Wang, V.R.R. Marthala, J. Huang, B. Sulikowski, M. Hunger, *J. Catal.* 238 (2006) 21-27.

[129] Y.J. Jiang, M. Hunger, W. Wang, *J. Am. Chem. Soc*. 128 (2006) 11679-11692.

[130] D.R. Corbin, S. Schwarz, G.C. Sonnichsen, *Catal. Today* 37 (1997) 71-102.

[131] V.A. Veefkind, J.A. Lercher, *Appl. Catal. A: General* 181 (1999) 245-255.

[132] D.T. Chen, L. Zhang, C. Yi, J.A. Dumesic, *J. Catal*. 146 (1994) 257-267.

[133] I.I. Ivanova, E.B. Pomakhina, A.I. Rebrov, M. Hunger, Y.G. Kolyagin, J. Weitkamp, *J. Catal*. 203 (2001) 375-381.

[134] W. Wang, M. Seiler, I.I. Ivanova, U. Sternberg, J. Weitkamp, M. Hunger, *J. Am. Chem. Soc*. 124 (2002) 7548-7554.

[135] A. Thursfield, M.W. Anderson, J. Dwyer, G.J. Hutchings, D. Lee, *J. Chem. Soc., Faraday Trans*. 94 (1998) 1119-1122.

[136] H. Ernst, H. Pfeifer, *J. Catal*. 136 (1992) 202-208.

[137] V.A. Makhlin, S.I. Ivanov, *Kinet. Catal*. 38 (1997) 864-867.

[138] A.M. Becerra, A.E.C. Luna, D.E. Ardissone, M.I. Ponzi, *Ind. Eng. Chem. Res*. 31 (1992) 1045-1050.

[139] A.R. McInroy, D.T. Lundie, J.M. Winfield, C.C. Dudman, P. Jones, S.F. Parker, J.W. Taylor, D. Lennon, *Phys. Chem. Chem. Phys*. 7 (2005) 3093-3101.

[140] A.R. McInroy, D.T. Lundie, J.M. Winfield, C.C. Dudman, P. Jones, D. Lennon, *Langmuir* 21 (2005) 11092-11098.

[141] K. Weissermel, H.J. Arpe, *Industrial Organic Chemistry* (3rd), Wiley-VCH, Weinheim, 1997.

[142] H. Bahrmann, *Koch Reactions*, in: J. Falbe (eds.), *New Syntheses with Carbon Monoxide*, Springer-Verlag, Berlin, 1980, p. 372.

[143] A.G.. Stepanov, M.V. Luzgin, V.N. Romannikov, K.I. Zamaraev, *J. Am. Chem. Soc*. 117 (1995) 3615-3616.

[144] T. Li, N. Tsumori, Y. Souma, Q. Xu, *Chem. Commun*. (2003) 2070-2071.

[145] N. Tsumori, Q. Xu, Y. Souma, H. Mori, *J. Mol. Catal. A: Chemical* 179 (2002) 271-277.

[146] M.V. Luzgin, V.N. Romannikov, A.G. Stepanov, K.I. Zamaraev, *J. Am. Chem. Soc*. 118 (1996) 10890-10891.

[147] A.G. Stepanov, M.V. Luzgin, V. N. Romannikov, V.N. Sidelnikov, E.A. Paukshtis, *J. Catal*. 178 (1998) 466-477.

[148] K. Fujimoto, T. Shikada, K. Omata, H. Tominaga, *Chem. Lett*. (1984) 2047-2050.

[149] P.C. Cheung, A. Bhan, G.L. Sunley, E. Iglesia, *Angew. Chem. Int. Ed*. 45 (2006) 1617-1620.

[150] O. Kresnawahjuesa, R.J. Gorte, D. White, *J. Mol. Catal. A: Chemical* 208 (2004) 175-185.

[151] A.G. Stepanov, M.V. Luzgin, *Chem. Eur. J*. 3 (1997) 47-56.

[152] A. Naito, S. Ganapathy, C.A. McDowell, *J. Chem. Phys*. 74 (1981) 5393-5397.

[153] E.J. Munson, N.D. Lazo, M.E. Moellenhoff, J.F. Haw, *J. Am. Chem. Soc*. 113 (1991) 2783-2784.

[154] W.E. Farneth, R. Gorte, *J. Chem. Rev.* 95 (1995) 615-635.

[155] R.A. van Santen, *Chem. Rev.* 95 (1995) 637-660.

[156] M. Hunger, W. Wang, *Adv. Catal*. 50 (2006) 149-225.

[157] F. Geobaldo, G. Spoto, S. Bordiga, C. Lamberti, A. Zecchina, *J. Chem. Soc.*, *Faraday Trans.* 93 (1997) 1243-1249.

[158] J.N. Kondo, K. Ito, E. Yoda, F. Wakabayashi, K. Domen, *J. Phys. Chem. B* 109 (2005) 10969-10972.

[159] J. Rakoczy, T. Romotowski, *Zeolites* 13 (1993) 256-260.

[160] J. Novakova, L. Kubelkova, Z. Dolejsek, *J. Catal.* 108 (1987) 208-213.

[161] P.E. Sinclair, A. de Vries, P. Sherwood, C.R.A. Catlow, R.A. van Santen, *J. Chem. Soc., Faraday Trans*. 94 (1998) 3401-3408.

[162] P.L. Benito, A.G. Gayubo, A.T. Aguayo, M. Olazar, J. Bilbao, *J. Chem. Technol. Biotechnol.* 66 (1996) 183-191.

[163] F. Wakabayashi, J.N. Kondo, C. Hirose, K. Domen, in: M.M. J. Treacy, B.K. Marcus, M.E. Bisher, J.B. Higgins (eds.), *Proceedings of the 12th International Zeolite Conference*, Baltimore, 1998, Materials Research Society, Warrendale, 1999 p. 2577.

[164] J. Datka, J. Rakoczy, G. Zadrozna, in: M.M. J. Treacy, B.K. Marcus, M.E. Bisher, J.B. Higgins (eds.), *Proceedings of the 12th International Zeolite Conference*, Baltimore, 1998, Materials Research Society, Warrendale, 1999, p. 2601.

[165] E.G. Derouane, J.P. Gilson, J.B. Nagy, *Zeolites* 2 (1982) 42-46.

[166] F. Salehirad, M.W. Anderson, *J. Catal.* 177 (1998) 189-207.

[167] F. Salehirad, M.W. Anderson, *J. Chem. Soc. Faraday Trans.* 94 (1998) 2857-2866.

[168] A. Sassi, W. Song, M.A. Wildman, J.F. Haw, *Catal. Lett.* 81 (2002) 101-105.

[169] G.S. Hammond, *J. Am. Chem. Soc*. 77 (1955) 334-338.

[170] V. Nieminen, M. Sierka, D.Y. Murzin, J. Sauer, *J. Catal.* 231 (2005) 393-404.

[171] Y. Wei, D. Zhang, Z. Liu, B. Su, *J. Catal*. 238 (2006) 46-57.

[172] W.H. Bunnelle, *Chem. Rev.* 91 (1991) 335-362.

[173] P.E. Sinclair, C.R.A. Catlow, *J. Phys. Chem. B* 101 (1997) 295-298.

[174] D. Lesthaeghe, V.Van Speybroeck, G.B. Marin, M. Waroquier, *Angew. Chem. Int. Ed*. 45 (2006) 1714-1719.

[175] D.M. Marcus, K.A. McLachlan, M.A. Wildman, J.O. Ehresmann, P.W. Kletnieks, J.F. Haw, *Angew. Chem. Int. Ed*. 45 (2006) 3133-3136.

[176] M. Bjørgen, F. Bonino, S. Kolboe, K.P. Lillerud, A. Zecchina, S. Bordiga, *J. Am. Chem. Soc.* 125 (2003) 15863-15868.

[177] J. Mohan, *Organic Spectroscopy Principles and Applications*, Alpha Science International Ltd., Harrow, 2002, p. 128 and p. 137.

[178] Y. Stepanenko, A.L. Sobolewski, A. Mordzinski, *J. Mol. Spectrosc.* 233 (2005) 15-22.

[179] W. Song, H. Fu, J.F. Haw, *J. Am. Chem. Soc.* 123 (2001) 4749-4754.

[180] H. Fu, W. Song, J.F. Haw, *Catal. Lett.* 76 (2001) 89-94.

[181] Y.T. Chua, P.C. Stair, *J. Catal.* 213 (2003) 39-46.

[182] M. Bjørgen, U. Olsbye, D. Petersen, S. Kolboe, *J. Catal.* 221 (2004) 1-10.

Publications

Y.J. Jiang, J. Huang, V.R.R. Marthala, Y.S. Ooi, J. Weitkamp, M. Hunger, *In situ MAS NMR-UV/Vis investigation of H-SAPO-34 catalysts partially coked in the methanol-to-olefin conversion under continuous-flow conditions and of their regeneration*, Microporous Mesoporous Mater. 105(2007) 132-139.

Y.J. Jiang, J. Huang, J. Weitkamp, M. Hunger, *In situ MAS NMR and UV/Vis spectroscopic studies of hydrocarbon pool compounds and coke deposits formed in the methanol-to-olefin conversion on H-SAPO-34*, Stud. Surf. Sci. Catal.170 (2007) 1137-1144.

Y.J. Jiang, J. Huang, W. Wang, M. Hunger, *Formation of methylamines by reaction of ammonia with surface methoxy species on zeolites H-Y and the silicoaluminophosphate H-SAPO-34*, Stud. Surf. Sci. Catal. 170 (2007) 1331-1337.

J. Huang, **Y.J. Jiang**, M. Hunger, *Influence of the lanthanum exchange degree on the concentration and acid strength of bridging hydroxyl groups in zeolites La,Na-X*, Stud. Surf. Sci. Catal. 170 (2007) 622-628.

J. Huang, **Y.J. Jiang**, V.R.R. Marthala, Y.S. Ooi, J. Weitkamp, M. Hunger, *Concentration and acid strength of hydroxyl groups in zeolites La,Na-X and La,Na-Y with different lanthanum exchange degrees studied by solid-state NMR spectroscopy*, Microporous Mesoporous Mater. 10 (2007) 129-136.

J. Huang, **Y.J. Jiang**, V.R.R. Marthala, W. Wang, B. Sulikowski, M. Hunger, *In stiu ^{1}H MAS NMR investigation of the H/D exchange of alkylaromatic hydrocarbons on zeolites H-Y, La, Na-Y, and H-ZSM-5*, Microporous Mesoporous Mater. 99 (2007) 86-90.

V.R.R. Marthala, W. Wang, J. Jiao, **Y.J. Jiang**, J. Huang, M. Hunger, *Effect of probe molecules with different proton affinities on the coordination of boron atoms in dehydrated zeolite H-[B]ZSM-5*, Microporous Mesoporous Mater. 99 (2007) 91-97.

V.R.R. Marthala, **Y.J. Jiang**, J. Huang, W. Wang, R. Glaser, M. Hunger, *Beckmann rearrangement of ^{15}N-cyclohexanone oxime on zeolites silicalite-1, H-ZSM-5, and H-[B]ZSM-5 studied by solid-state NMR spectroscopy*, J. Am. Chem. Soc. 128 (2006) 14812-14813.

Y.J. Jiang, W. Wang, V.R.R. Marthala, J. Huang, B. Sulikowski, M. Hunger, *Response to comments on the paper: 'Effect of organic impurities on the hydrocarbon formation via the decomposition of surface methoxy groups on acidic zeolite catalysts'*, J. Catal. 244 (2006) 134-136.

Y.J. Jiang, M. Hunger, W. Wang, *On the reactivity of surface methoxy species in acidic zeolites*, J. Am. Chem. Soc. 128 (2006) 11679-11692.

J. Jiao, J. Kanellopoulos, B. Behera, **Y.J. Jiang**, J. Huang, V.R.R. Marthala, S.S. Ray, W. Wang, M. Hunger, *Effects of adsorbate molecules on the quadrupolar interaction of framework aluminum atoms in dehydrated zeolite H, Na-Y*, J. Phys. Chem. B 110 (2006) 13812-13818.

W. Wang, **Y.J. Jiang**, M. Hunger, *Mechanistic investigations of the methanol-to-olefin (MTO) process on acidic zeolite catalysts by in situ solid-state NMR spectroscopy*, Catal. Today, 113 (2006) 102-114.

Y.J. Jiang, W. Wang, V.R.R. Marthala, J. Huang, B. Sulikowski, M. Hunger, *Effect of organic impurities on the hydrocarbon formation via the decomposition of surface methoxy groups on acidic zeolite catalysts*, J. Catal. 238 (2006) 21-27.

W. Wang, J. Jiao, **Y.J. Jiang,** S.S. Ray, M. Hunger, *Formation and decomposition of surface ethoxy species on acidic zeolite Y* , ChemPhysChem, 6 (2005) 1467-1469.

Presentations:

Y.J. Jiang, W. Wang, M. Hunger, *Formation of methylamines by reaction of ammonia with surface methoxy species on acidic zeolites*, Poster, 15th International Zeolite Conference, Beijing, China, August 12-17, 2007, Poster presentation.

Y.J. **Jiang**, M. Hunger, *Ex situ and in situ MAS NMR-UV/Vis spectroscopic study of hydrocarbon pool compounds and coke deposits formed by methanol conversion on H-SAPO-34*, Poster, 40. Jahrestreffen Deutscher Katalytiker, Weimar, Germany, March 14-16, 2007.

Y.J. **Jiang**, M. Hunger, *Studien an Kohlenwasserstoffen, die durch Methanol-umsetzung an Zeolithkatalysatoren gewonnen warden, durch in-situ Festkörper-NMR-UV/Vis Spektroskopie*, Oral, Festkörper NMR-Methoden und Anwendungen in der Materialforschung, Oberjoch, Germany, July 30-August 3, 2006.

W. Wang, J. Jiao, **Y.J. Jiang**, M. Hunger, *Formation and decomposition of surface ethoxy groups on acidic zeolite Y studied be the in situ MAS NMR-UV/Vis spectroscopy*, Poster, 47th Rocky Mountain Conference on Analytical Chemistry, Denver, USA, July 31-August 4, 2006.

Y.J.**Jiang,** M. Hunger, *In situ solid-state NMR-UV/Vis investigations of the hydrocarbon pool formed by methanol conversion on zeolite catalysts*, Oral, 11th Stuttgarter Tag der Magnetischen Resonanz, Stuttgart, Germany, March 23, 2006.

Y.J. **Jiang**, V.R.R. Marthala, W. Wang, M. Hunger, *Effect of organic impurities in the hydrocarbon formation via the decomposition of surface methoxy groups on solid acid catalysts*, Poster, 18th Deutsche Zeolith-Tagung, Hannover, Germany, March 1-3, 2006.

W. Wang, **Y.J. Jiang,** M. Hunger, *Formation and decompostion of surface ethoxy species on acidic zeolite Y investigated by the in situ MAS NMR/UV-Vis technique", oral presentation*, 17th Deutsche Zeolith-Tagung, Gießen, Germany, March 2-4, 2005.

Workshops:

Y.J. Jiang, M. Hunger, *Ex situ and in situ MAS NMR-UV/Vis spectroscopic study of hydrocarbon pool compounds and coke deposits formed by methanol conversion on H-SAPO-34*, Poster, AMPERE NMR School, Bukowina, Poland, June 24-30, 2007.

Y.J. Jiang, M. Hunger, *Study on the reactivity of surface methoxy species in acidic zeolites by solid state MAS NMR*, Oral, Workshop "New Developments in Magnetic Resonance Techniques", Blaubeuren, Germany, September 6-7, 2006.

Y.J. Jiang, M. Hunger, *Study on the initiation mechanism of the methanol-to-olefin process by in situ MAS NMR-UV/Vis spectroscopy*, Oral, Workshop "Recent Progress in Magnetic Resonance Methods", Hirschegg, Austria, September 18-21, 2005.

Curriculum Vitae

Personal data

Name: Yijiao Jiang

Born: October 12, 1977 in Zhe'jiang, P.R. China

Nationality: Chinese

Education

1984-1990 Elementary school in Long'you, Zhe'Jiang, P.R. China.

1990-1996 Middle School in Long'you, Zhe'Jiang, P.R. China

1996-2000 Study at the Department of Chemical and Environmental Engineering, Kunming University of Science and Technology, Kunming, P.R. China (B. Eng.).

2000-2003 Study at the Department of Chemical and Environmental Engineering, Kunming University of Science and Technology, Kunming, P.R. China, supervised by Prof. Dr.-Ing Ping Ning (M. Eng).

2004-2007 Study at the Institute of Chemical Technology, University of Stuttgart, Germany, supervised by Prof. Dr Michael Hunger (Ph. D.).

Employment

2003-2004 Research Associate in the Department of Environmental Science, Yunnan University, Kunming, P.R. China.